# The Application of Intelligent Tires and Model Based Estimation Algorithms in Tire-Road Contact Characterization

Seyedmeysam Khaleghian

Dissertation submitted to the faculty of the Virginia Polytechnic Institute and State University in partial fulfillment of the requirements for the degree of

Doctor of Philosophy

In

Engineering Mechanics

Saied Taheri, Chair

Mehdi Ahmadian

Gerardo W. Flintsch

Sunghwan Jung

Ronald H. Kennedy

January 18, 2017

Blacksburg, VA

Keywords: Intelligent Tire, Tire-Road Contact, Friction Coefficient Estimation, Model-based Algorithm, Kalman Filter

# The Application of Intelligent Tires and Model Based Estimation Algorithms in Tire-Road Contact Characterization

Seyedmeysam Khaleghian

## ABSTRACT

Lack of driver's knowledge about the abrupt changes in pavement friction and poor performance of the vehicle stability, traction and ABS controllers on the low friction surfaces are the most important factors affecting car crashes. Due to its direct relation to vehicle stability, accurate estimation of tire-road characteristics is of interest to all vehicle and tire companies. Many studies have been conducted in this field and researchers have used different tools and have proposed different algorithms. One such concept is the Intelligent Tire. The application of intelligent tire in tire-road characterization is investigated in this study.

Three different test setups were used in this research to study the application of the intelligent tires to improve mobility; first, a wheeled ground robot was designed and built. A Fuzzy Logic algorithm was developed and validated using the robot for classifying different road surfaces such as asphalt, concrete, grass, and soil. The second test setup is a portable tire testing trailer, which is a quarter car test rig installed in a trailer and towed by a truck. The trailer was equipped with different sensors including an accelerometer attached to the center of the tire inner-liner. Using the trailer, acceleration data was collected under varying conditions and a Neural Network (NN) algorithm was developed and trained to estimate the contact patch length, effective tire rolling radius and tire normal load.

The third test setup developed for this study was an instrumented Volkswagen Jetta. Different sensors were installed to measure vehicle dynamic response. Additionally, one front and one rear tire was instrumented with an accelerometer attached to their inner-liner. Two intelligent tire based algorithms, a tire pressure estimation algorithm and a road condition monitoring algorithm, were developed and trained using the experimental data from the instrumented VW Jetta. The two-step pressure monitoring algorithm uses the acceleration signal from the intelligent tire and the wheel angular velocity to monitor the tire pressure. Also, wet and dry surfaces are distinguished using the acceleration signal from the intelligent tire and the wheel angular velocity through the surface monitoring algorithm.

Some of the model based tire-road friction estimation algorithms, which are widely used for tire-road friction estimation, were also introduced in this study and the performance of each algorithm was evaluated in high slip and low slip maneuvers. Finally a new friction estimation algorithm was developed, which is a combination of experiment based and vehicle dynamic based approaches and its performance was also investigated.

# The Application of Intelligent Tires and Model Based Estimation Algorithms in Tire-Road Contact Characterization

Seyedmeysam Khaleghian

## GENERAL AUDIENCE ABSTRACT

Lack of driver's knowledge about the abrupt changes in pavement friction and poor performance of the vehicle stability, traction and ABS controllers on the low friction surfaces are the most important factors affecting car crashes. Due to its direct relation to vehicle stability, accurate estimation of tire-road characteristics is of interest to all vehicle and tire companies. Many studies have been conducted in this field and researchers have used different tools and have proposed different algorithms. One such concept is the Intelligent Tire. The application of intelligent tire in tire-road characterization is investigated in this study.

Five main algorithms are developed in this study. First a fuzzy-logic terrain classification algorithm is developed for the small wheeled ground robot that classifies all different surfaces into four known categories; asphalt, concrete, sand and grass. A six-wheel grand robot was designed and built for this study and instrumented with intelligent tire, a tri-axial accelerometer embedded to the tire inner-liner, and other appropriate sensors. The input of the terrain classification algorithm are the intelligent tire signal, the slip ratio at the beginning of the motion and the wheel speed. The second algorithm is an intelligent tire based algorithm to estimate the tire normal load. A portable tire testing trailer, which is a quarter car test rig attached to the back of the trailer and towed by a truck was used for this part of the project. The trailer test setup was instrumented with different sensors and the tire normal load was controlled through a pneumatic force transducer and

an air-spring system. A Neural Network algorithm was then trained that estimates the tire normal load using intelligent tire signal, the tire pressure and the wheel speed.

The third and fourth algorithm are intelligent tire based algorithms to monitor the tire pressure and the road surface condition respectively. An instrumented vehicle, which was a Volkswagen Jetta 2003, was prepared and used for this part of the project. The inputs of these algorithms were the intelligent tire signal and the wheel speed and the outputs were the tire pressure condition and road surface condition (dry/ wet) respectively. The last algorithm is a new friction estimation algorithm, which is a combination of experiment based (intelligent tire) and vehicle dynamic based approaches. The algorithm is validated with the experimental data collected using the trailer test setup.

*To my family and my love "Anahita"*

**ACKNOWLEDGMENTS**

I would like to thank my advisor, Professor Saied Taheri, for his advice and support during this study. I would like to thank you for encouraging my research and for allowing me to grow as a research scientist. Your advice on both research as well as on my career have been priceless.

I would also like to thank the members of my committee, Dr. Mehdi Ahmadian, Dr. Gerardo Flintsch, Dr. Sunghwan Jung, and Dr. Ronald Kennedy for their advice and for being kind enough to serve on my graduate committee.

I am sincerely thankful to the CenTiRe (Center for Tire Research) family; my dear friends and colleagues; without their helps and support this study could not be completed.

I would like to thank my family for their great support and care in my entire life, without whom I would never achieve anything I have achieved.

And finally I would like to thanks my fiancé, Anahita who has been with me during all ups and downs of my challenging journey and for the meaning she adds to my life. Thank you all for everything.

Seyedmeysam Khaleghian

January 2017

Blacksburg, VA

## Contents

## List of Figures

## List of Tables

# 1 Introduction and literature review

Approximately 120,000 people were killed on US roadways between 2010-2013 [1-3]. Even in the case of non-fatal crashes, the economic costs are undeniably high [4-5]. Due to the large number of fatalities and the high economic costs, different studies have been conducted on the effects of different factors on car crashes [6-7].

Twenty-four percent of all crashes are weather related, which occur on icy, snowy, or wet pavements or in the presence of rain, sleet, fog and snow [8]. Several studies have been conducted on crashes during rainfall and snowfall [9-12]. It was observed in a study on crashes before and after rain in Calgary and Edmonton that the crash rate is 70% higher on the wet pavements [13]. In a similar study, it was shown that the crash frequency on wet roads is twice the rate of the crashes on dry pavements [14]. This high rate of weather related crashes is mainly attributed to the drivers overestimating the pavement friction, and the effect of bad weather condition on the vehicle stability and stability controllers.

Tire-Road friction estimation is one of the most important problems for both vehicle and tire industries that can decrease the number of weather related crashes dramatically. The effect of tire-road friction force on vehicle performance and stability and on the performance of traction and ABS controllers is undeniable [15-19]. Different studies have developed and used different algorithms to estimate the tire-road friction. Based on the approaches that they have followed, all of the related research can be divided into the following two categories:

1- Experiment-based

2- Model-based

In experiment-based approaches, it is attempted to find the correlation between the sensor data (acoustic sensors, temperature sensor, etc.) and tire-road friction-related parameters. The model-based approaches try to estimate the friction using simplified mathematical models, which can be divided into three sub-categories; wheel and vehicle dynamic based approaches, slip based approaches and tire model based approaches.

In vehicle dynamics based approaches, different dynamic models (single wheel model, bicycle model, planar model, etc.) are used along with an estimation algorithm (recursive least square, steady state and extended Kalman filter, sliding mode observer, etc.) to estimate the tire-road friction force and other friction-related parameters such as slip ratio, slip angle, etc. Tire model based approaches use the friction force and slip data along with a tire model (Magic formula, Brush model, LuGre model, etc.) to estimate the maximum tire road friction coefficient. In slip based approaches, it is assumed that the value of friction in the saturated area of $\mu - slip$ curve can be estimated based on the slope of the curve in low slip region (linear region).

### 1.1 Problem Statement:

Currently the tire-road contact parameters are mostly addressed indirectly using vehicle dynamic based observers. Although these methods provide respectively accurate estimation, most of them fail during abrupt change in pavement or weather condition. To address this problem, intelligent tire, also called smart tire, was developed. The intelligent tire is a tire with some contact sensors, mostly accelerometers and piezoelectric strain sensors, embedded to its inner-liner to monitor the interaction between the tire and different surfaces.

It is believed that tire-road contact parameters estimation will be improved using a combination of so called intelligent tire and vehicle dynamic based observers, which leads to a new generation of

vehicle stability, ABS and traction controllers. Also, using the information directly from the interface between tire and road will reduce the risk of accidents.

### 1.2 Objective:

This study will answer following questions:

- How intelligent tire technology can be used in small ground robots to improve their mobility
- How intelligent tire technology can be used to estimate the tire normal load
- How this technology can be used to monitor the tire pressure and tire-road conditions
- How intelligent tire technology can be integrated with vehicle dynamic based observers to estimate the tire-road contact friction

### 1.3 Contributions:

The specific contributions of this study include the following:

1- Analytical

- Developed a Fuzzy Logic based terrain classification algorithm for the small ground robot which uses the robot's longitudinal speed, wheel slip ratio and tire acceleration as inputs and classifies different surfaces into four known categories of asphalt, concrete, grass and soil.
- Developed an intelligent tire based Neural Network algorithm to estimate the tire normal load.
- Developed an intelligent tire based algorithm to monitor the tire pressure.
- Developed an intelligent tire based algorithm to estimate the road surface conditions.
- Developed a new friction estimation algorithm which uses a combination of experimental and vehicle dynamic based approaches to estimate the tire road friction

2- Experimental

- Designed and built a six-wheel ground robot, instrumented with different sensors, intelligent tire and a data collection system developed in LabVIEW that synchronizes and acquires the data of all the sensors with the same sampling rate.

- ❖ Upgraded the portable tire test setup with new sensors, synchronized data collection system, brake system, and loading mechanism.
- ❖ Developed an instrumented vehicle; uses intelligent tire, 6 axis Inertial Measurement Unit (IMU), instrumented steering system, and encoders and developed a synchronized data collection system.

### 1.4 Organization of the dissertation:

This dissertation contains five chapters; the first chapter, "Introduction", is the comprehensive review of different algorithms which are mostly used to estimate the tire-road friction or other friction related parameters.

The second chapter is "Experimental Test Setup" that explains different test setups which are used in this study, different sensors which were used in these setups and the data collecting routines that developed for them. Three test setups were used for this study; a six-wheel ground robot, a portable tire test setup and an instrumented Volkswagen Jetta.

The Third chapter is "Theory", where the algorithms used for this study are developed. Five algorithms were developed, first a Fuzzy Logic algorithm used in the robot for terrain classification. Second, a Neural Network algorithm to estimate the tire normal load and third, an intelligent tire based algorithm to monitor the tire pressure. The forth algorithm is another intelligent tire based algorithm to classify the road surface condition into wet and dry and finally the fifth, a friction estimation algorithm that uses a combination of experiment-based and vehicle dynamic based observer to estimate the tire-road friction.

Chapter Four and Chapter Five present the experimental results and conclusions and future work, respectively.

## 1.5 Literature Survey:

This section presents a technical survey of tire-road friction estimation research. For each of the different friction estimation approaches, first, the method is explained briefly and then the review of the literature on the subject is presented. The rest of the chapter is organized as follows: first, the tire-road friction force and aligning moment are introduced; the experiment-based friction estimation approaches are discussed in the second section. The model based friction estimation algorithms are reviewed in the third section followed by the conclusions in the last section.

### 1.5.1 Tire-Road Friction Coefficient and Self-Aligning Moment:

In order to start with different friction estimation approaches, it is required to define the tire forces, aligning moment, and friction coefficient. Free body diagram of a single wheel is shown in Figure 1-1, where $F_x, F_y, F_z$ are longitudinal, lateral, and normal tire forces, respectively. The normalized tire traction force is defined as [20]:

$$\rho = \frac{\sqrt{F_x^{\,2} + F_y^{\,2}}}{F_z} \tag{1}$$

its maximum value is called the friction coefficient $(\mu)$. The wheel aligning moment is defined as the tendency to align the wheel plane with the direction of wheel travel, which is caused by steering geometry and side deformation of a tire, which moves forward and has nonzero slip angle.

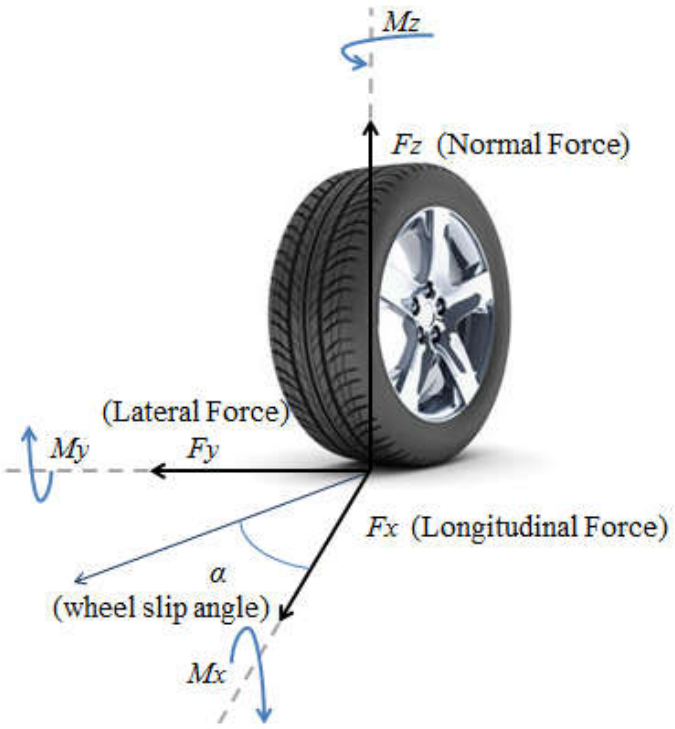


Figure 1-1 free body diagram of a single wheel

### 1.6 Experiment-based:

Figure 1-2 demonstrates the main philosophy behind experiment-based approaches. As it is shown in Figure 1-2, most of the experiment-based methods use sensor measurements of the friction-related parameters (tire noise, tire longitudinal or lateral deformation, etc.) and try to correlate these parameters to tire-road friction [21, 22].

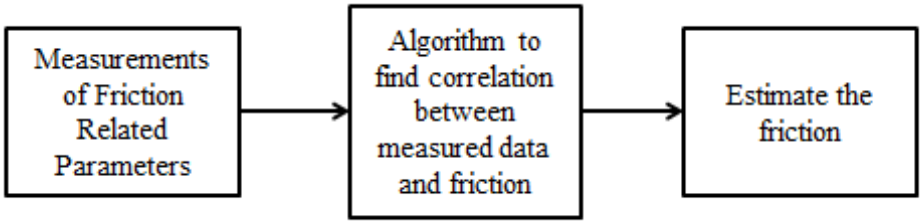


Figure 1-2 experiment-based flowchart diagram

Based on the sensor type and the parameter which is used for this estimation, experiment-based approaches can be categorized as follows:

### 1.6.1 Optical sensors and cameras:

Optical sensors and cameras are used to detect surface properties related to friction. Using optical sensors to measure infrared light at different wavelengths reflected from different roads, the surface type (dry, wet, icy, snowy, etc.) can be identified. The principal of road-eye sensors is shown in Figure 1-3[23]. The other use of optical sensors is to estimate the sidewall deformation and correlate it with friction [24-26].

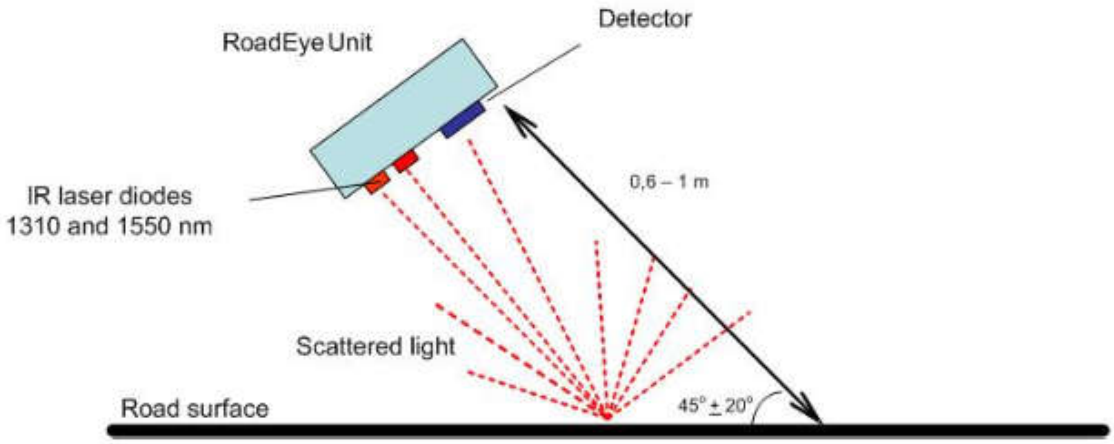


Figure 1-3 the schematic of using optimal sensor to identify different surfaces[23]

Cameras are also used to identify the texture of different surfaces. Once the texture is evaluated, a neural network can be trained to estimate the surface friction [27]. The conventional methods of detecting road conditions are [28]:

- Detection by color difference: It uses the ratios of color signals (R, G and B) to detect road condition.
- Detection by pattern matching: This technique uses geometrical features along with pixel density to estimate the condition of the road.

- Detection by infrared rays: Infrared can be used to detect the presence of water as water has a relatively large absorption band in the infrared range.
- Detection by difference in polarized level: It uses a difference between horizontal and vertical polarization to detect road condition.

What follows is the review of the papers that have used optical sensors for friction estimation. Holzmann et al. [29] used cameras and microphones for estimating the friction coefficient. The image captured by the camera was analyzed for the luminance and neighborhood of pixels. Microphone was used as a reactive measurement to improve the accuracy of the estimation; the frequency range of 100-600 Hz was analyzed. Kuno et al. [28] used a CCD camera to detect the road condition. They detected the distribution of gloss on road surface due to presence of water using the high and low levels of luminance signals. Jokela et al. [30] used two methods of measurement: polarization change and graininess analysis. The amount of vertical and horizontal polarized light reflecting from the surface was used to detect the road surface condition. Graininess analysis is done by using a low pass filter on the image making it blurry and comparing the contrast with the original image.

### 1.6.2 Acoustic Sensor:

Acoustic sensors are used to classify the road surface type/condition (asphalt, concrete, wet, dry, etc.) based on the tire noise. In some of the studies, the acoustic sensors were attached to the vehicle's chassis [31]. Figure 1-4 demonstrates the algorithm, which uses Support Vector Machine (SVM) to classify different surfaces based on tire noise.

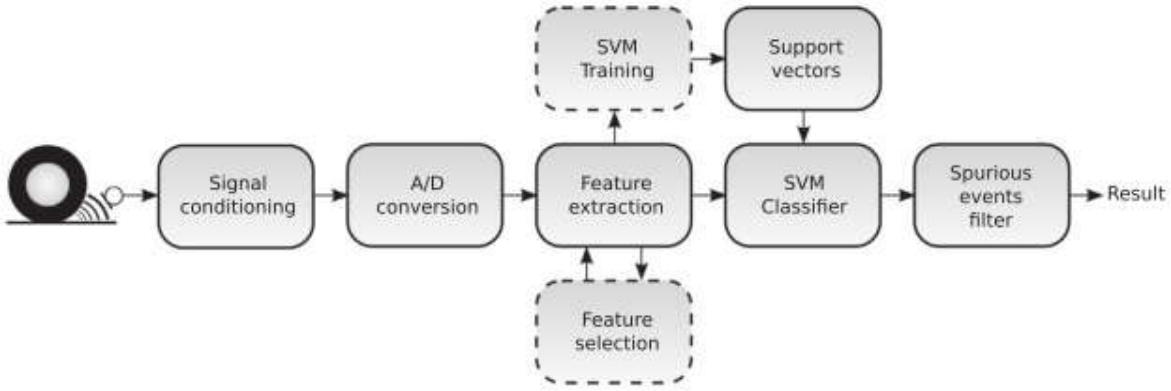


Figure 1-4 friction estimation algorithm using acoustic sensors [31]

Some other studies have used a microphone, installed at a fixed road location, to record the noise generated by the vehicles passing by and use the recorded data to estimate the pavement status [32-35].

### 1.6.3 Tire Tread Sensors:

Tire tread sensors are used to monitor the interaction between tire and the road, and to estimate the deflection of tread elements inside the contact patch. The sensor types are mostly accelerometer and piezo electric and magnetic sensors. Figure 1-5(a) demonstrates the piezoelectric sensor inside the tire (in the tread area), which estimates lateral deflection profile of the carcass and uses it to estimate the friction [36]. Magnets vulcanized into the tread of a Kevlar-belted tire are also used in some studies to measure the deflection of the tread in x, y and z directions as a function of its position inside the contact patch [21, 22], [37-39]. Using the fact that the tread deformation is caused by the total force acting on the tire, the friction is estimated. In other studies, tri-axial accelerometers attached to the innerliner of the tire, shown in Figure 1-5(b), is used to estimate the friction [40].

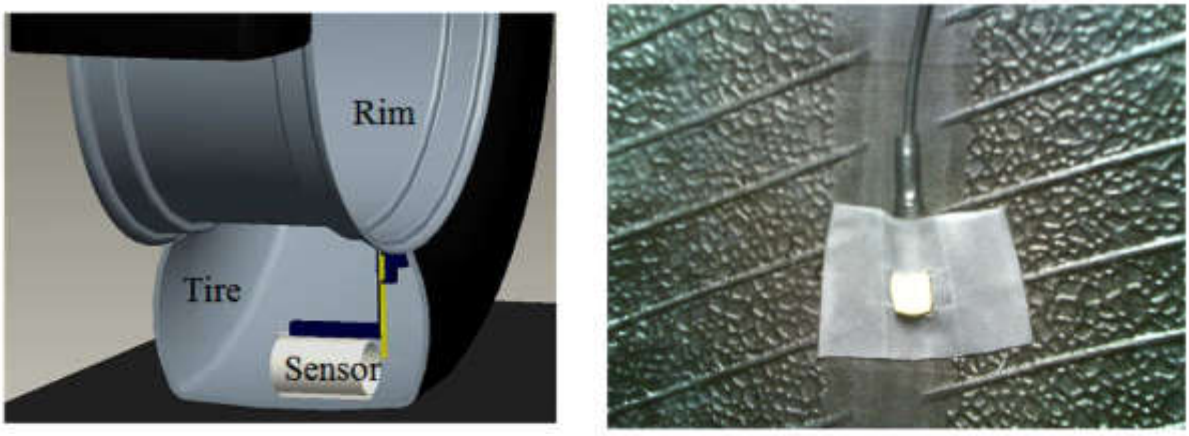


(a) (b)

Figure 1-5 (a) wireless piezoelectric sensor [36] (b) tri-axial accelerometer [40]

Matilainen et al. [41, 42] used the signals from the tri-axial accelerometer inside the tire to estimate contact patch length. The algorithm detects two acceleration peaks in the longitudinal acceleration signal and uses it along with wheel angular speed to estimate contact patch. Khaleghian et al. [43] and Singh et al. [40] utilized a tri axial accelerometer attached to the innerliner of the tire; using a neural network algorithm, they estimated the tire normal load. Niskanen et al. [44-46] used three tri axial accelerometers inside the tire to find friction indicators on smooth ice and concrete surfaces. The radial acceleration signal from the accelerometer is analyzed at the leading edge of the contact patch for friction indicators. They have stated that the vibration in the leading edge due to slip on low friction surfaces can be used to determine the road surface type.

In addition to the studies and approaches that were introduced in this section, several patents have been submitted, have used different experiment based methods to estimate the friction or other related parameters; some of these patents are summarized in Table 1-1.

Table 1-1 summary of the patents which have used experiment based methods

| Inventor Name | Estimated parameters | Summary of invention |
|---|---|---|
| Klein [47] | Friction coefficient | He used a steering system which was controlled by a control module. They estimated the steering gain and steering load hysteresis along with a reference, they determined the friction. |
| Patel et al. [48] | Contact patch length, Tire normal load | They used tire pressure sensor and tire deformation measuring sensor and developed an algorithm to estimate the contact patch length based on the peaks of deformation signal. Then using the data of footprint length, wheel speed and the tire pressure, they trained a neural network algorithm to estimate the tire normal load. |
| Singh [49] , [50] | Tire normal load, Side slipangle | Two strain sensors are attached to the inner and outer sidewalls of a tire (sidewall strain sensors) , using the average power of these signals in different tire pressures to estimate the normal load, also they developed an algorithm to estimate the side slipangle based on properties of strain signals. (then vehicle dynamic based approach was used to estimate the tire longitudinal and lateral force) |
| Singh et al. [51] | Tire normal load, side slipangle | They used a set of strain sensors affixed to opposite sidewalls of the tire. Estimating the slope difference in opposite sidewalls strain signals, they estimated the side slip angle. They also estimated the tire normal load based on the average power of strain signal. |
| Singh et al. [52] | Tire sidewall force | They used a piezo film in one or both sidewalls of the tire. The sensor generates a signal within the contact patch area (can be used to estimate the length of the contact patch), which power of the signal indicates the sidewall deformation. The power to load map for different tire pressure is used to estimate the sidewall force. |
| Miyazaki [53] | Tire forces, Friction coefficient | Several strain sensors are attached to the vicinity of the wheel, on the axle, which provide the strain signals. The produced signals are used to estimate the tire forces and tire-road friction coefficient (from the correlation between strain signals and desired parameters). |
| Giustino et al. [54] | Tire status | They used the tire pressure and magnetic sidewall torsion signal to monitor the status of the tire. If the magnetic signal deviated too much from the signal of undamaged tire or an abrupt change in tire pressure was observed, the system send warning to the driver. |

| Inventor Name | Estimated parameters | Summary of invention |
|---|---|---|
| Hattori [55] | The strain state of the tire | A series of conductors composed of plurality of conductor pieces (embedded in lines at specific interval in circumferential direction of the tire) are used to provide the strain states of the tire. A monitoring device releases signal (pulse electromagnetic wave), also receive the reflected signals from the foils. The time difference between radiation and reception in different conditions is used to evaluate the strain stress of the tire. |
| Hillenmayer et al. [56] | Tire static load,<br>Nature of the road surface | A pressure sensor and a deformation sensor are used in the tire; using frequency-dependent analysis on the sensor signal they estimate the static loading and the nature of the road surfaces. |
| Chen [57] | Crack detection system | A set of optical measuring units, consist of a sensor which has photoelectronic elements in it, an electronic processing unit and a post processing unit is used to detect the tires crack. Once the light passes through the crack, the sensor sends a signal and driver will be notified. |
| Neugebauer et al. [58] | Tire overall deformation | Two transducers are used inside the tire, one end of both are connected to the same particular point and their other ends are connected to two reference points to stablish a triangle in tire's cross-sectional radial plane. The system is used to measure the overall deformation of the tire. |
| Becherer [59] | Tire-road adhesion and friction | A magnetic sensor along with a magnetic field (arranged in the belt by partial magnetization of the belt) are used to determine the tire-road adhesion. The sensor is connected to an evaluation device, which detect the change in magnetic field and use it to estimate desired parameters. |
| Miyoshi et al. [60] | Tire longitudinal force | Two magnetic sensors are used to measure the rotation angle of the wheel and wheel axle. Then they used a computing device to calculate the tire warp angle, which is derived by the difference between tire rotational angle during load and no-load condition. Then the estimated the tire longitudinal force as a function of tire warp angle. |
| Miyoshi et al. [61] | Tire loads | A tire strain sensor and a sensor locator are used to estimate the tire load. Comparing the strain data with the previously stored data on relationship between the strain signal, the sensor position and the tire forces, they estimated the tire forces. |

| Inventor Name | Estimated parameters | Summary of invention |
|---|---|---|
| Carcaterra et al. [62] | Tie adhesion | They used a fiber optic (provided with FBG sensor) fixed to the inner layer of the tire, using a data processing system (spectrum analyzer) which implements the residual grip identification algorithm, thy measured the tire adhesion. |
| Sistonen [63] | The friction on a surface | He developed a new device consist of a wheel, an arm which is attached to wheel axle and a spring, which is attached between measuring wheel and its axle to estimate the friction. The degree of rotation of the measuring wheel at the point, where the wheel starts to slid, is used to estimate the friction. |
| Bell et al. [64] | Friction coefficient | They used tread force sensor, one end of the sensor is fixed on the tread and the other end is on the tire structure, which slipping of small discrete tread element can be detected. Compiling the sensor data of the tire deformation-induced tread gripping force, the friction coefficient is estimated. |
| Wilson [65] | Contact patch length | An accelerometer attached to the inner surface of the tire, in tread area is used to estimate the contact patch length. The starting and end point of the contact patch are observed as two peaks in acceleration signal which is used to estimate the contact patch length, total vehicle mass and tire load. |
| Abe [66] | Dynamic friction coefficient | They developed a new device to measure the dynamic friction coefficient which includes a disk with measuring rubber member, a driving disk adapted to rotate co axially with the disk and dynamometer interconnects the disk and the driving disk. A tachometer is also used to measure the speed of the rubber. Using X-Y recorder, which record the output signals of friction measuring portion and the tachometer, the friction coefficient is estimated. |
| Mancosu et al. [67] | Contact patch length,<br>tire normal load,<br>camber angle<br>cornering angle | They used three accelerometers, fixed in with the same distance in cross-sectional plane of the tire. Analyzing different components of acceleration signal (peak detection, distance between the peaks, and position of the peaks and…) they estimated the contact patch length, the tire load and the camber angle. The camber angle is also derived using other estimated parameters. |

Although the tire-road friction can be estimated using some of the experiment based approaches, in most cases their accuracy is reduced when the testing condition deviates from the condition under which the algorithm was trained. In order to make the estimation algorithms more robust and take the dynamic of the vehicle into account, model-based approaches are introduced.

## 1.7 Model-based:

Model-based approaches contain all the studies that use a mathematical/dynamical model to estimate the friction. No need of any expensive special sensor which are standard on today's vehicles and accuracy and repeatability of the results in most of the cases, make this category more popular as compared with experiment-based approaches. The model-based studies can be divided into three main groups: wheel and vehicle dynamic based, tire model based, and slip-slope based approaches.

### 1.7.1 Wheel and vehicle dynamics based:

Studies, which are based on this approach, use the dynamical model of the system, in which some of the states can be measured (like angular velocity of the wheel) and some other states cannot be measured (like friction force, longitudinal speed, etc.). Based on dynamical model of the system and the measured states, the rest of the states can be estimated using different estimation algorithms such as recursive least square (RLS), Kalman filter, etc. The general flowchart of algorithm which is used in most of vehicle dynamic based studies is shown in Figure 1-6.

Some of the most common dynamical models in the friction estimation studies are wheel tire model, roll dynamic model, bicycle model, quarter-car model, and four-wheel vehicle dynamic model, which are explained in more details next.

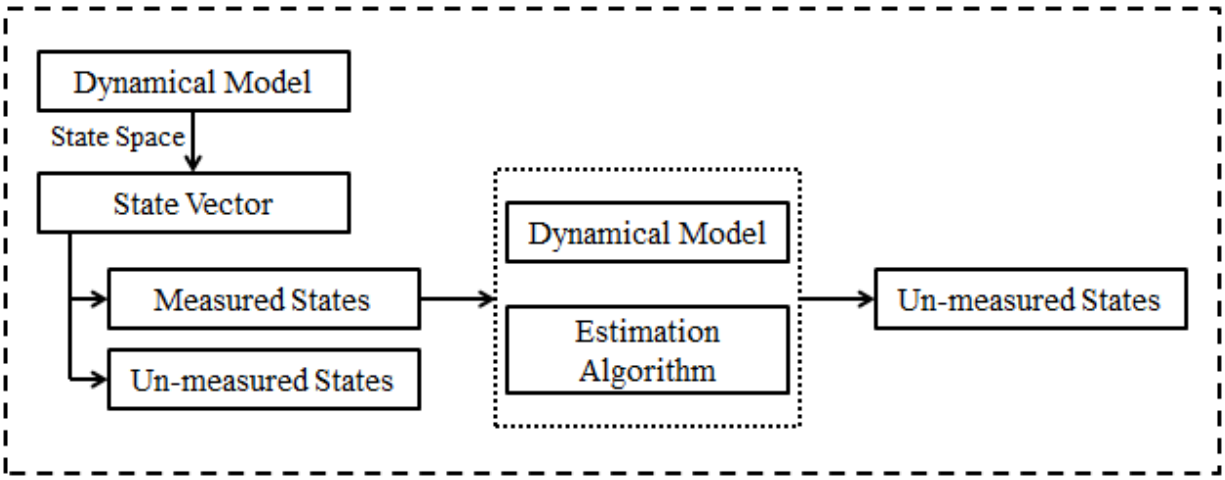


Figure 1-6 the general flowchart for vehicle dynamic based approaches

**Wheel Dynamic Model:**

Free-body diagram of a single wheel is depicted in Figure 1-7 in which, $F_{rr}$ is the rolling resistance force, and $T$ is the transmitted wheel torque. The equations of motion for this problem are as follow:

$$m_w \dot{v}_x = F_x - F_{rr} \tag{2}$$

$$J_w \dot{\omega}_w = (T_w - T_b) - F_x r_w - F_{rr} r_w \tag{3}$$

Where, $m_w$ is the total mass of the wheel, $J_w$ is the moment of inertia of the wheel and $T_w, T_b$ are the drive and brake torques, respectively. The value of wheel rolling resistance force can be calculated as:

$$F_{rr} = f_r W \tag{4}$$

where, $W$ is the weight on the wheel and $f_r$ is the rolling resistance coefficient that can be expressed as a function of tire pressure and wheel velocity. Several equations have been developed over years to estimate the rolling resistance. One suggest following equation for rolling on concrete surface [68]:

$$f_r = f_o + 3.24 f_s \left( \frac{V}{100} \right)^{2.5} \tag{5}$$

where, $V$ is the speed in $mph$ , $f_r$ and $f_o$ are basic coefficient and speed effect coefficient respectively that depend on inflation pressure.

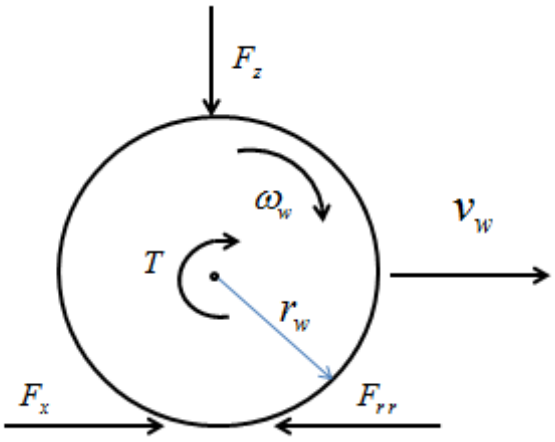


Figure 1-7 free body diagram of a single wheel

Equation (3) is widely used in the literature in order to estimate the tire longitudinal friction force [18, 71, 72]. However, the accuracy of estimated longitudinal force highly depends on the accuracy of the effective rolling radius of the tire ( $r_w$ ). The effective rolling radius is presented as [20]:

$$r_w = \frac{\sin\left[\arccos\left(\frac{r_{static}}{r_0}\right)\right]}{\arccos\left(\frac{r_{static}}{r_0}\right)} \qquad (6)$$

$$r_{static} = r_0 - \frac{F_z}{k_t}$$

Where, $r_0$ is the initial radius of the tire and $k_t$ is the vertical stiffness of the tire. Wheel dynamic model is mostly used with a tire model in order to estimate the longitudinal force and longitudinal friction [70, 71]. Hsiao et al. [73] substituted the measured wheel torque and wheel angular velocity into equation (3), obtained from moment balance equation of each wheel, to estimate the tire longitudinal force. Rajamani et al. [74] used the measured data of angular wheel speed and

proposed a sliding mode observer to estimate the tire longitudinal force based on single wheel dynamic model. Cho et al. [75] used the same approach to estimate the longitudinal tire force and showed that the estimated force is accurate for the low slip vehicle maneuvers. Rabhi et al. [76, 77] used a single wheel model with cascaded first and second sliding observers to estimate the contact force. They used the measured data of longitudinal speed of the vehicle, angular position of the wheel and wheel torque along with robust differentiator and sliding mode observer to estimate the velocity and acceleration of the wheel, longitudinal and vertical tire forces and friction coefficient.

#### 1.7.1.1 1DOF Roll Dynamic model:

The most common vehicle models, which are used to estimate the roll dynamics of the vehicle, are 3DOF model, which represents lateral, yaw and roll motions of the vehicle, and 1DOF model, representing the roll dynamics.

The 1DOF roll dynamic model has practical advantages in comparison to 3DOF model, which does not need the cornering stiffness (which is not easy to be estimated), besides it is not sensitive to the nonlinear tire dynamics. For these reasons, 1DOF model is widely used in the vehicle state estimation studies. Figure 1-8 demonstrates the schematic of 1DOF vehicle roll model [69].

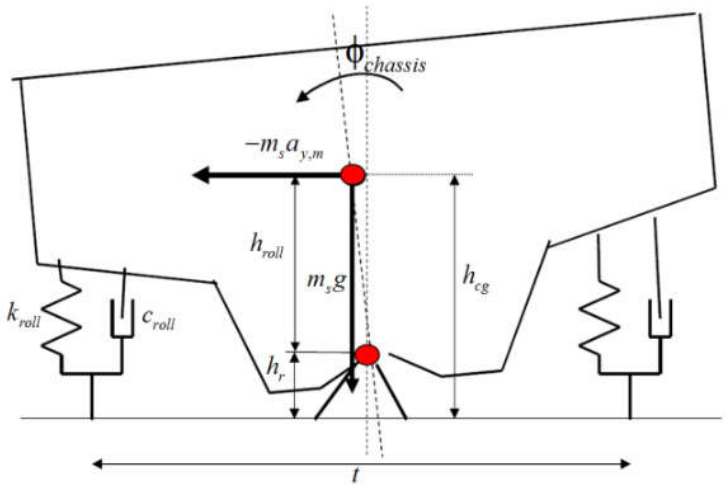


Figure 1-8 the schematic of 1DOF roll vehicle model [69]

Where $k_{roll}, c_{roll}$ are roll stiffness and roll damping coefficients for the combination of tire-suspension, respectively (which are assumed to be constant), and $h_{roll}$ is the distance from the roll center to the vehicle CG. Assuming the roll axis is fixed and there is no vertical motion, the equation of motion is formulated as:

$$\left(I_x + m_s h^2{}_{roll}\right)\ddot{\phi}_{chassis} + c_{roll}\dot{\phi}_{chassis} + k_{roll}\phi_{chassis} = -m_s h_{roll} a_{y,m} \qquad (7)$$

Where $I_x + m_s h^2{}_{roll}$ is the moment of inertia around the roll axis, $I_x$ is the moment of inertia around x axis and $m_s$ is the vehicle sprung mass. The vehicle roll dynamic model is mostly used to estimate the vehicle roll angle, which is a key factor to obtain the normal load at the wheels. Some of the studies, which have used roll dynamic model, are summarized in Table 1-2.

Table 1-2 some of the studies which have used roll dynamic model

| Authors | Measured States | Estimated States | Method |
|---|---|---|---|
| Hac et al. [78] | Lateral acceleration, yaw rate | Roll angle | Closed-loop adaptive observer was used to estimate the roll angle and roll rate with respect to the road |
| Tsourapas et al. [79] | Load transfer ratio | Vehicle roll dynamic | Two roll over indexes are introduced and analyzed; these indexes are: actual lateral transfer ratio (LTR) and predictive lateral transfer ratio and predictive lateral transfer ratio (PLTR) |
| Grip et al. [80] | Roll rate | Roll angle | Combination of vehicle dynamics control system and a roll over mitigation system is used to estimate the roll angle |
| Chen et al. [81]<br>Ryu et al. [82] | Lateral acceleration, yaw rate | Roll angle | They used a roll vehicle model (either 3DOF model or 1DOF model) along with Kalman filter to estimate the roll angle |
| Cho et al. [83] | Longitudinal speed, yaw and roll rate, lateral acceleration | Roll angle | Vehicle state index based switching is used on the roll dynamic and kinematic model to estimate the roll angle |

#### 1.7.1.2 Quarter Car Model:

The quarter car model is a 2DOF model which is mostly used to model the vertical dynamic (especially suspension) of the car. As it is shown in Figure 1-9, quarter car model is represented with two lumped masses, $m_{qs}, m_{qu}$ (sprung mass and un-sprung mass), which are $\frac{1}{4}$ vehicle body mass and wheel mass respectively. The suspension system of the vehicle is presented as a set of spring damper system ($k_s, c_s$) while the tire is presented as a single spring ($k_u$) (however in some other studies, tire is considered as set of spring-damper too).

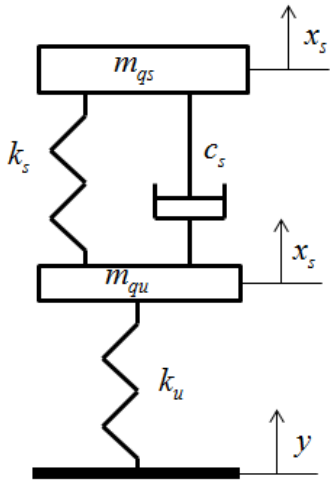


Figure 1-9 schematic of quarter car vehicle model

The equations of the motion for the quarter-car vehicle model shown in Figure 8 are presented as:

$$\begin{aligned} m_s\ddot{x}_s + c_s(\dot{x}_s - \dot{x}_u) + k_s(x_s - x_u) &= 0 \\ m_u\ddot{x}_u + c_s(\dot{x}_u - \dot{x}_s) + (k_u + k_s)x_u - k_s x_s &= 0 \end{aligned} \tag{8}$$

Quarter car model is mainly used in friction estimation studies to obtain the tire normal force and road profile. Several studies have measured the vertical acceleration of the un-sprung mass and the suspension deflection and have used them to estimate the normal force using the following equation [84-86]:

$$F_z = c_s(\dot{x}_s - \dot{x}_u) + k_s(x_s - x_u) - m_u\ddot{x}_u \tag{9}$$

Doumiati et al. [87, 88] used the quarter car model to estimate tire normal load and the road profile. First, they used accelerometer measurements to calculate the vehicle body vertical position, and then used it as a measured state for Kalman filter to estimate the normal wheel load and road profile.

Next, the planar dynamic models of the vehicle are introduced; four-wheel vehicle model and its simplified version, bicycle model are discussed in more details which are widely used in vehicle state estimation studies.

#### 1.7.1.3 Four-Wheel Vehicle Model:

Four-wheel vehicle model (also called two-track model) just considers the longitudinal, lateral and yaw motions of the vehicle, while roll, pitch, and vertical motion are ignored. The schematic of this model is shown in Figure 1-10 [20].

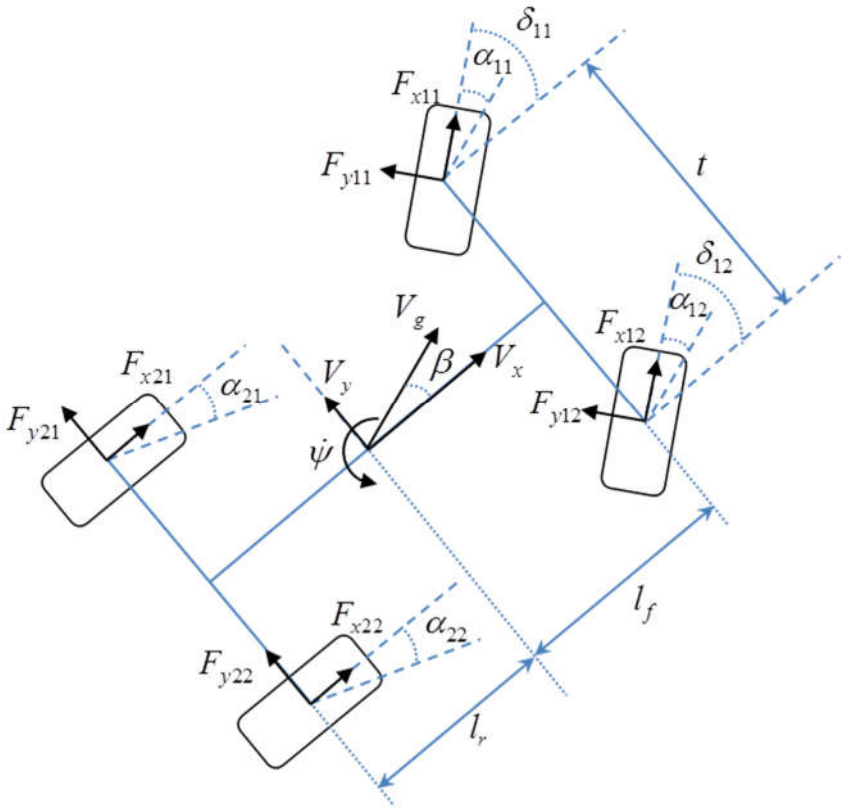


Figure 1-10 The schematic of four wheel vehicle model

Where $t$ is the track length, $l_f, l_r$ are the distance of center of gravity of the vehicle (CG) from the front and rear axle respectively, $V_g$ is the velocity of CG and $V_x, V_y$ are its component in x and y direction respectively. Also $\dot{\psi}$ is the yaw rate, $\delta$ is the steering angle and it is assumed that both

front wheels have the same steering angle ( $\delta_{11} = \delta_{12}$ ). The equations of motion for this model are as follows [20]:

$$\ddot{\psi} = \frac{1}{I_z}\begin{bmatrix} l_f\left[F_{y11}\cos\delta + F_{y12}\cos\delta + F_{x11}\sin\delta + F_{x12}\sin\delta\right] \\ -l_r\left[F_{y21} + F_{y22}\right] + \frac{t}{2}[F_{y11}\sin\delta - F_{y12}\sin\delta \\ +F_{x12}\cos\delta - F_{x11}\cos\delta + F_{x22} - F_{x21}] \end{bmatrix} \tag{10}$$

$$\dot{\beta} = -\dot{\psi} + \frac{1}{m_v V_g}\begin{bmatrix} -(F_{x11} + F_{x12})\sin(\beta - \alpha) \\ +F_{y11}\cos(\beta - \alpha) + F_{y12}\cos(\beta - \alpha) \\ +F_{y11}\cos(\beta - \alpha) + (F_{y21} + F_{y22})\cos(\beta - \alpha) \\ -(F_{x21} + F_{x22})\sin\beta \end{bmatrix} \tag{11}$$

$$a_y = \frac{1}{m_v}\begin{bmatrix} F_{y11}\cos\delta + F_{y12}\cos\delta + F_{y21} + F_{y22} \\ +F_{x11}\sin\delta + F_{x12}\sin\delta \end{bmatrix} \tag{12}$$

$$a_x = \frac{1}{m_v}\begin{bmatrix} -F_{y11}\sin\delta - F_{y12}\sin\delta + F_{x21} + F_{x22}) \\ +F_{x11}\cos\delta + F_{x12}\cos\delta \end{bmatrix} \tag{13}$$

$$\dot{V}_x = V_y\dot{\psi} + a_x \tag{14}$$

$$\dot{V}_y = -V_x\dot{\psi} + a_y \tag{15}$$

$$\dot{V}_g = \frac{1}{m_v}\begin{bmatrix} \left(F_{x11} + F_{x12}\right)\cos(\beta - \delta) + F_{y11}\sin(\beta - \delta) \\ +F_{y12}\sin(\beta - \delta) + \left(F_{x21} + F_{x22}\right)\cos\beta \\ +\left(F_{x21} + F_{x22}\right)\cos\beta \\ +\left(F_{y21} + F_{y22}\right)\sin\beta \end{bmatrix} \tag{16}$$

Where, $I_z$ is the moment of inertia of the car around z axis, $m_v$ is the vehicle mass and $\beta$ is the vehicle side slip angle. Table 1-3 summarizes some of the studies which have used the four-wheel vehicle dynamic model to estimate the friction force, friction coefficient or other parameter related to friction estimation problem.

Table 1-3 some selective studies which have used four-wheel vehicle model

| Authors | Measured States | Estimated States | Method |
|---|---|---|---|
| Samadi et al. [89] | Longitudinal acceleration, lateral acceleration for the front and rear axles, angular velocity of the wheels | Longitudinal tire force for all wheels and lateral force for front and rear axles | They used extended Kalman filter to estimate the tire forces, they used Pacejka as the tire model and nonlinear model for hydraulic braking system |
| Baffet et al. [90] | Yaw rate, velocity of CG, Longitudinal & lateral acceleration, | Tire forces, vehicle velocity, yaw rate | They used extended Kalman filter (with random walk model for the forces) to estimate the tire forces, then they estimated the side-slip angle based on dynamic of the problem. Cornering stiffness was estimated based on the data of tire forces and side slip angle through another Kalman filter algorithm. |
| Shim et al. [91-92] | Longitudinal & lateral acceleration, Steering angle, Wheel angular velocity | Tire forces | They used four-wheel dynamic model and estimate the tire forces base on the analytical tire model (relation between the measured and estimated states) which they proposed. |
| Doumiati et al. [93-97] | Longitudinal & lateral acceleration, Steering angle, wheel angular velocity, yaw and pitch rate, suspension displacement | Tire forces, vehicle side slip angle | They used vehicle roll model to estimate the tire normal force then used a four-wheel vehicle model dynamics of the problem; using two observer (extended and unscented Kalman filter) they estimated the tire force and vehicle side slip angle |
| Ghandour et al. [98, 99] | Longitudinal & lateral acceleration, Steering angle, Wheel angular velocity, yaw and pitch rate, suspension displacement | Tire lateral force and side slip angle | Using the roll vehicle model, they estimated the tire normal load, then they used extended and unscented Kalman filter to estimate the lateral force and side slip angle |

| Authors | Measured States | Estimated States | Method |
|---|---|---|---|
| Ghandour et al. [100] | Longitudinal & lateral acceleration, Steering angle, Wheel angular velocity, yaw and pitch rate, suspension displacement | Lateral load transfer, lateral skid indicator | They used the vehicle roll model for the normal load then they proposed a maximum friction coefficient estimation based algorithm to evaluate a lateral risk skid indicator |
| Dakhlallah et al. [101] Sebsadji et al. [102] | Longitudinal & lateral acceleration, Steering angle, Wheel angular velocity, yaw rate | Tire forces and road grade | They used an extended Kalman filter and Luenberger observer based method on the nonlinear vehicle model to estimate the forces and road grade. |
| Qi et al. [103] | Longitudinal & lateral acceleration, steering angle, wheel angular velocity, yaw rate | Vehicle side slip angle, lateral tire force and tire road friction coefficient | They used unscented Kalman filter based estimation algorithm to estimate the vehicle's desired states and tire road friction coefficient |
| Ray et al. [104, 105] | Yaw and roll rate, wheel angular velocity, longitudinal and lateral acceleration | Slip ratio, slip angle, wheel velocity, normal force at each wheel, longitudinal and lateral force | They used a nine degree of freedom model, which is a four-wheel model with vehicle roll dynamic along with extended Kalman filter to estimate the desired states |
| Jin et al. [106] | Longitudinal & lateral acceleration, steering angle, wheel angular velocity, yaw & roll rate | Tire forces for all wheels, roll angle, yaw & roll rate, velocity of CG | They proposed two extended and unscented Kalman filter based observers which used four-wheel model with the roll vehicle model to estimate the tire forces and other vehicle states |
| Rajamani et al.[107] | Longitudinal & lateral acceleration, steering angle, wheel angular velocity, yaw & roll rate | The tire forces, longitudinal and lateral vehicle velocities, yaw and roll angle | They used extended Kalman filter approach with 8 DOF model (four-wheel model with roll vehicle dynamic model) to estimate the tire forces and other vehicle's states |

The simplified version of four-wheel vehicle model is bicycle model (also called single-track model) which is introduced in the next section.

#### 1.7.1.4 Bicycle model:

The schematic of the bicycle model is shown in Figure 1-11, which was introduced by Segel in 1956 [20]. The bicycle mode is widely used to describe the handling dynamics of the vehicle, in which vertical and roll motions are not taken into account.

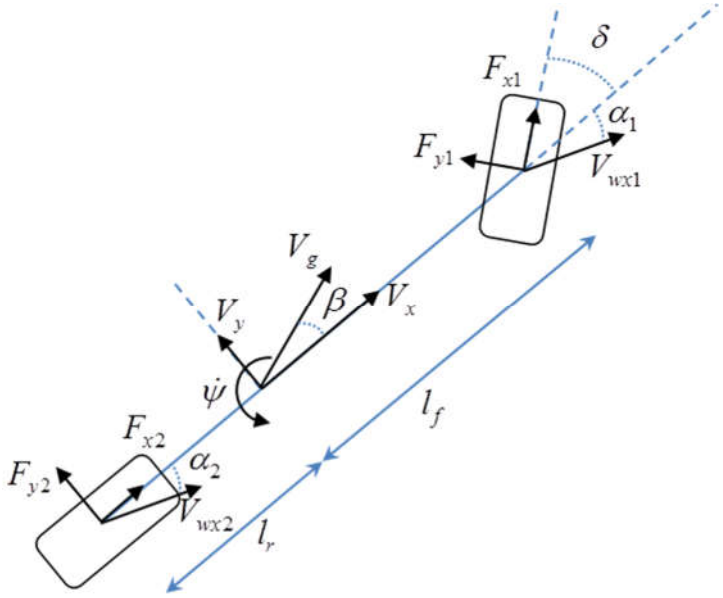


Figure 1-11 The schematic of the bicycle model

The simplified equations of motion for the bicycle model are as follow [20]:

$$\ddot{\psi} = \frac{1}{I_z}\left[l_f\left[F_{x1}\sin\delta + F_{y1}\cos\delta\right] - l_r F_{y2}\right] \tag{17}$$

$$\dot{\beta} = \frac{1}{m_v V_g}\begin{bmatrix} -F_{x1}\sin(\beta-\delta) + F_{y1}\sin(\beta-\delta) \\ +F_{y2}\cos\beta - F_{x2}\sin\beta \end{bmatrix} - \dot{\psi} \tag{18}$$

$$\dot{V}_g = \frac{1}{m_v}\begin{bmatrix} F_{x1}\cos(\delta-\beta) - F_{y1}\sin(\delta-\beta) \\ +F_{x2}\cos\beta + F_{y2}\sin\beta \end{bmatrix} \tag{19}$$

Many studies have used this vehicle model along with some estimation algorithms to estimate the lateral vehicle states, friction force and/or coefficient. Table 1-4 summarizes some of the research which have used bicycle model in their algorithms.

Table 1-4 some studies which have used bicycle model

| Authors | Measured States | Estimated States | Method |
|---|---|---|---|
| Baffet et al. [108, 109]<br>Wei et al. [110] | Yaw rate, longitudinal & lateral acceleration,<br>steering angle | Tire forces, vehicle side slip angel | They used and sliding mode observer to estimate tire road forces, then using and extended Kalman filter they estimated the cornering stiffness and side-slip angle |
| Baffet et al. [90] | Yaw rate,<br>longitudinal & lateral acceleration, vehicle velocity | Tire forces, side slip angle, cornering stiffness | First, they used extended Kalman filter to estimate the tire longitudinal and lateral forces, then another extended Kalman filter algorithm was used to estimate the side slip angle and cornering stiffness |
| Baffet et al. [111] | Longitudinal & lateral acceleration, steering angle,<br>wheel angular velocity, yaw rate | Lateral tire force, vehicle side slip angle and yaw rate and vehicle speed | They used three different extended Kalman filter based algorithm along with Burckhardt and linear tire force model to estimate the tire force, yaw rate, vehicle speed and side slip angle. |
| Ahn et al [112] | Longitudinal & lateral acceleration, steering angle,<br>wheel angular velocity, yaw rate | Lateral force, aligning moment, side slip angle, friction coefficient | They used bicycle model with state estimator to estimate the lateral force and aligning moment, then using a sliding mode observer with brush tire model, they estimated the side slip angle and friction coefficient |
| Zhang et al. [113] | Yaw rate | Side slip angle and yaw rate | They used a nonlinear observer to estimate the side slip angle, its stability condition were obtained from analysis of energy to peak performance of the estimation error system |

| Authors | Measured States | Estimated States | Method |
|---|---|---|---|
| Tianjun et al. [114]<br>Zhao et al. [115] | Longitudinal & lateral acceleration, steering angle,<br>wheel angular velocity | Wheel side slip angle and yaw rate | They used unscented Kalman filter to estimate the side slip angle and the yaw rate |
| Liang et al. [116], [117] | Yaw rate,<br>longitudinal & lateral acceleration, Steering angle,<br>Wheel angular velocity | Vehicle longitudinal and lateral velocity | They used an adaptive unscented Kalman filter to estimate the vehicle longitudinal and lateral velocity |
| Hsu et al. [118] | Yaw rate,<br>longitudinal & lateral acceleration, Steering angle | Tire slip angle | They used a model base estimation approach; utilizing pneumatic trail information they identified the vehicle's lateral limits |
| Ray et al. [119] | Yaw rate,<br>longitudinal & lateral acceleration, the wheel angular velocity | Vehicle's longitudinal and lateral speed, vertical displacement of front, rear and CG, pitch angle, the longitudinal and lateral force for front and rear wheels | They used a nine degree of freedom model, which is a bicycle model with a quarter-car model to simulate each of the front and rear tire and suspension. Using extended Kalman filter, they estimated the tire forces and other states. |
| Gao et al. [120] | Lateral acceleration, yaw rate | Side slip angle | They used a high gain observer along with a nonlinear tire model to estimate the vehicle side slip angle. They compared the results of high gain observer with the estimation results of extended Kalman filter and Leunberger observer |

The most popular vehicle models, which are widely used in friction estimation studies, are introduced in this section; Table 1-5 reviews these vehicle dynamic models, their common

measured states and the states which are usually estimated with these models as a summary of dynamic wheel/vehicle based approaches.

Table 1-5 summary of wheel/vehicle dynamic models which are used for friction estimation

| Model Name | Common Measured States | Common Estimated States | Features |
|---|---|---|---|
| Wheel Dynamic Model | Longitudinal acceleration, wheel angular velocity, drive & braking torque, rolling resistance force | Longitudinal tire force, longitudinal speed, | - Used to study the longitudinal dynamics of the vehicle<br>- The accuracy of the estimation using this model highly depends on the accuracy of the tire effective radius which is used for estimation |
| 1-DOF Roll Model | CG's lateral acceleration | Roll angle, roll rate | - Used to estimate roll dynamics of the vehicle<br>- Roll stiffness and damping coefficient are assumed to be constant<br>- The roll axis assumed to be fixed<br>- Does not need the information of cornering stiffness<br>- It's not sensitive to nonlinear tire dynamics |
| Quarter Car Model | Vertical acceleration of sprung mass and un-sprung mass | Tire vertical force, vertical position and velocity of sprung mass and un-sprung mass | - Mostly used to model vertical dynamics of the vehicle and suspension modeling<br>- Pitch and roll motion are not taken into account<br>- The wheels are assumed to roll without slip and contact loss |
| Four-Wheel Vehicle Model | Longitudinal and lateral acceleration, yaw acceleration, steer angle | Tire's longitudinal and lateral force, wheel hub velocity of each wheel | - Used to study the longitudinal and transversal vehicle dynamics<br>- Roll and pitch motion are ignored<br>- Doesn't have a suspension |

| | | | |
|---|---|---|---|
| Bicycle Model | Lateral acceleration, yaw acceleration, steer angle | Front and rear lateral tire force | - Used to describe lateral dynamics of the vehicle<br>- Rear steering angle assumed to be zero<br>- Vertical and roll motion are ignored |

The tire model based algorithms are introduced next.

### 1.7.2 Tire Model based:

Tire models generally express the relationship between tire forces and moments with slip ratio/slip angle, which have been used in various studies to estimate the friction forces and friction coefficient. It is assumed that the tire forces and moment, also slip ratio and/or slip angle are available (or can be estimated) then by comparing the force/moment – slip data with different tire models, the model parameters and friction coefficient are estimated.

Different mathematical tire models have been developed based on model of the tire and the time behavior that can be captured (steady-state or transient) (Figure 1-12) [69]; some of them which are more common for the friction estimation purpose are introduced in this article.

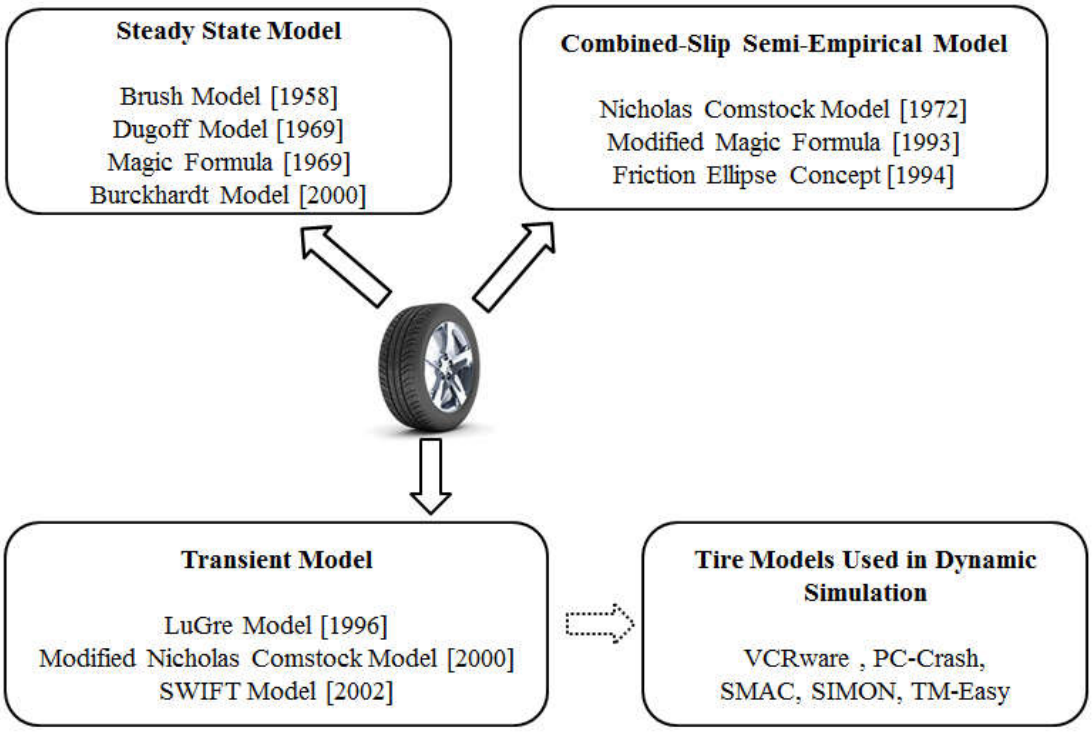


Figure 1-12 Different tire models [69]

### 1.7.2.1 Pacejka Tire Model:

Pacejka tire model (which is also called magic formula) is a semi-empirical tire model that was introduced for the first time by Pacejka in 1964 [121, 122]. The model uses special functions to represent the longitudinal and lateral forces and the aligning moment. The formulation of this tire model for longitudinal and lateral force and aligning moment are as follows:

$$\begin{aligned} F_x\left(s+S_{hx}\right) &= D_x \sin[C_x \arctan(B_x s - E_x(B_x s - \arctan(B_x s)))] + S_{vx} \\ F_y\left(\alpha+S_{hy}\right) &= D_y \sin[C_y \arctan(B_y \alpha - E_y(B_y \alpha - \arctan(B_y \alpha)))] + S_{vy} \\ M_z\left(\alpha+S_{hz}\right) &= D_z \sin[C_z \arctan(B_z \alpha - E_z(B_z \alpha - \arctan(B_z \alpha)))] + S_{vz} \end{aligned} \tag{20}$$

Where $s$ is the slip ratio, $\alpha$ is the side slip angle and $F_x, F_y, M_z$ are the longitudinal force, lateral force and aligning moment, respectively. The meaning of other parameters ($B, C, D, S_h, S_v$) are shown in Figure 1-13.

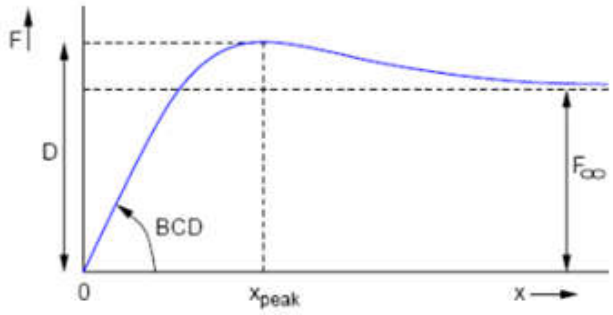


D : Peak Value

C : The Limit value when $x \to \infty$

$$C = 2 - \frac{2}{\pi}\arctan\left(\frac{F_\infty}{D}\right) \qquad C \geq 1$$

B × C × D : The Slope Near the Origin

B , E & C : The Location of The Peak

$$E = \frac{Bx_{peak} - \tan\left(\frac{\pi}{2C}\right)}{Bx_{peak} - \arctan\left(Bx_{peak}\right)} \qquad E \leq 1$$

Figure 1-13 Magic Formula's parameters

In the newer version of the magic formula, the camber angle, cornering stiffness, and load variation also transient properties of the tire are also taken into account [123]. Magic formula has been widely used in literature for vehicle states and tire friction estimation [121, 123, 124]. Oosten et al. [125] clarified the determination of Magic Formula parameters, from the experimental data, and discussed all the difficulties involved. Kim et al [126] used the traditional concept of friction to formulate the friction; they assumed that the coefficients of Magic Formula are known. Using an instrumented vehicle they estimated the forces on each wheel with the help of Magic Formula. Then they estimated the longitudinal and lateral friction coefficients. Yi et al. [127] used an observer-based algorithm, in which the Magic Formula with known parameters was used for the longitudinal force, to estimate the tire road friction coefficient. First, they used a sliding mode observer (angular velocity of the wheel was measured) to estimate the vehicle states, then using a recursive least square algorithm, they estimated the tire road friction coefficient. Jayachandran et al. [128] developed a fuzzy logic based algorithm to estimate the value of longitudinal and lateral forces, also aligning moment based on slip ratio and slip angle. They used Magic Formula with known coefficients to calculate the tire forces and moment based on different slip values; then they

defined a fuzzy membership function between the inputs (slip ratio, slip angle) and outputs (tire forces, aligning moment) of fuzzy-logic algorithm based on the calculated values.

#### 1.7.2.2 Dugoff Tire Model:

Dugoff tire model is a physical model, which was introduced by Dugoff et al. in 1969 [129]. In this model, a uniform vertical pressure distribution is assumed on the tire contact patch. In its simplest form, Dugoff model expresses the relation between longitudinal and lateral force and the slip as a function of two parameters; the tire stiffness ($C_x, C_y$), which explains the slope of force-slip curve in low slip region and the tire-road friction coefficient ($\mu$) that describes its curvature and peak value. The Dugoff model is formulated as follows:

$$
\begin{aligned}
F_x &= C_x \frac{s}{1+s} f(\lambda) \\
F_y &= C_y \frac{\tan(\alpha)}{1+s} f(\lambda) \\
\lambda &= \frac{\mu F_z (1+s)}{2\sqrt{(C_x s)^2 + (C_y \tan\alpha)^2}} \\
f(\lambda) &= \begin{cases} (2-\lambda)\lambda & \lambda < 1 \\ 1 & \lambda \geq 1 \end{cases}
\end{aligned}
\qquad (21)
$$

Where $C_x, C_y$ are the slopes of the longitudinal force – slip ratio and lateral force – slip angel in the low slip values (linear part of the curve respectively). In the following context, some of the studies that have used the Dugoff tire model in order to estimate the friction or related parameters are introduced. Ghandour et al. [130] developed an algorithm, using Dugoff to simulate the lateral force, to estimate the lateral friction coefficient. First, they developed an estimation algorithm to obtain the lateral force and slip angle. Then, they estimated the friction coefficient utilizing nonlinear method of optimization to minimize the error between estimated lateral force and lateral force provided by Dugoff model. In another study, a new algebraic filtering technique was used

by Villagra et al. [131] to estimate the longitudinal and lateral force and slip ratio, then they used a weighted Dugoff model to estimate the friction coefficient, for instance for the longitudinal direction simplifying the Dugoff equation gives:

$$\mu_{x-\max}^2 F_z^2 - 2\mu_{x-\max}\left|C_x\tau\right|F_z + \left|C_x\tau\right|F_z = 0 \tag{22}$$

Where in this equation $\tau = \frac{s}{1+s}$. The solution for this equation is expressed as:

$$\mu_{x-\max} = \frac{\left(\left|C_x\tau\right| \pm \sqrt{C_x\tau(C_x\tau - F_x)}\right)}{F_z} \tag{23}$$

Comparing the behavior of Dugoff model with Pacejka's model, the maximum friction coefficient is obtained as follows:

$$\begin{aligned} &\mu_{x-\max}^D(t_k) = \frac{\alpha_1}{F_z(t)}\left(\left|C_x\tau(t_k)\right| - \sqrt{C_x\tau(t_k)(C_x\tau(t_k) - F_x(t_k))}\right) \quad \lambda(t_k) < 1 \\ &\mu_{x-\max}^D(t_k) = \mu_{x-\max}^D(t_k - 1) \quad \lambda(t_k) \geq 1 \end{aligned} \tag{24}$$

Where $\alpha_1$ is a weighting factor. Nilanjan et al. [132] proposed a sliding mode observer along with modified Dugoff model to estimate the longitudinal velocity and friction coefficient; the only measured state was wheel angular velocity. Doumiati et al. [133] proposed a real time algorithm to estimate the tire-road lateral forces and side slip angle using two estimation algorithms of extended and unscented Kalman filter, in which the lateral force was modeled using Dugoff model. Four-wheel vehicle model was used as the dynamical model of the system, and the measured states were longitudinal and lateral acceleration, yaw and roll rate, left and right suspension deflection and the angular velocity of each wheel.

#### 1.7.2.3 Brush Tire Model:

In this model, it is assumed that the surface area which is in contact with the road can be modeled as infinitesimal bristles. As it is shown in Figure 1-14, the contact patch area is partitioned into two regions [134]; adhesion and sliding. In the first region, the bristles transfer the force by

mechanical adhesion and in the second region the slide of the bristles on the road results in friction force; the vertical pressure distribution is assumed to be parabolic.

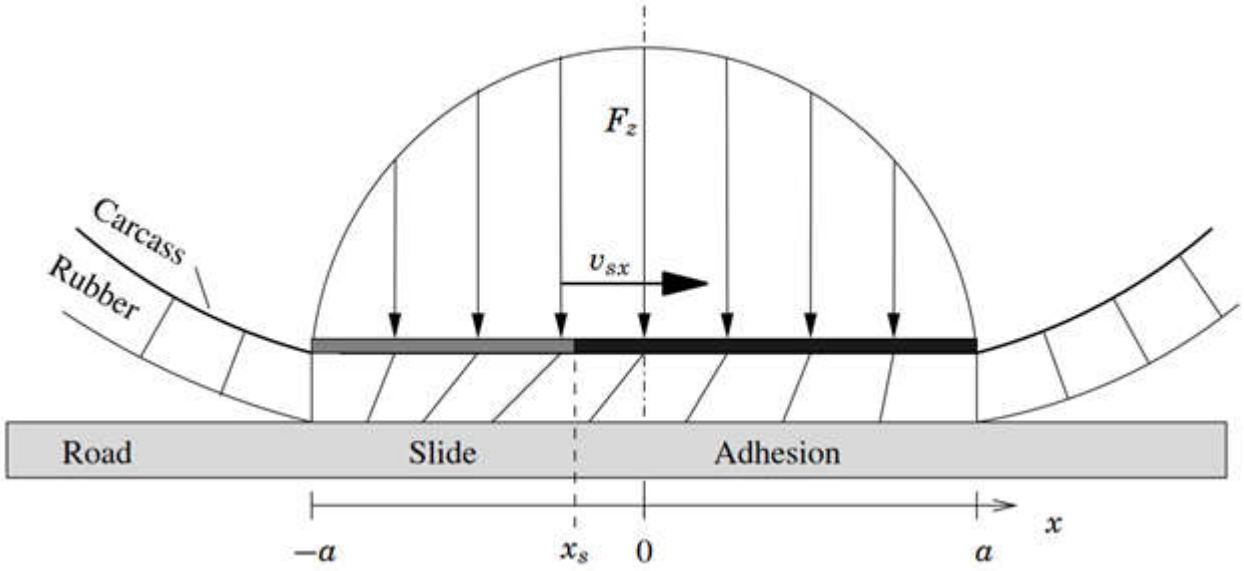


Figure 1-14 the schematic of adhesion and sliding regions in the contact patch [134]

The brush tire model can be divided into 3 cases; pure side-slip, pure longitudinal slip, and combined slip problem.

#### 1.7.2.3.1 Pure side-slip:

Figure 1-15 demonstrates the schematic of the contact patch in small and large side slip conditions. For the pure side slip problem, the formulation of brush tire model for low slip angle values is as follows [135]:

$$F_y = C_{F\alpha}\alpha$$
$$M_z = \frac{a}{3}F_y \qquad (25)$$

Where $\alpha$ is half of the contact patch length and $C_{F\alpha}$ is the cornering stiffness. For large side slip values the equations are expressed as [136]:

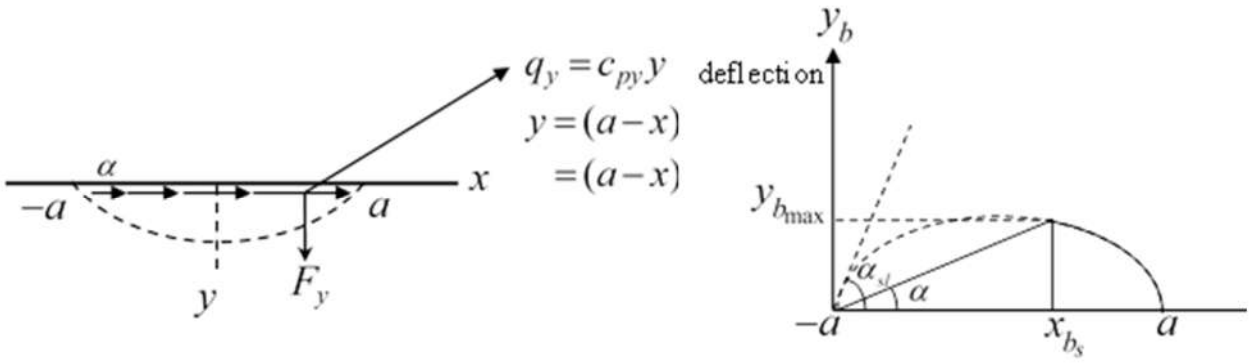


Figure 1-15 schematic of the contact patch

$$F_y = 3\mu F_z \frac{\tan(\alpha)}{\tan(\alpha_{sl})}\left(1 - \left|\frac{\tan(\alpha)}{\tan(\alpha_{sl})}\right| + \frac{1}{3}\frac{\tan^2(\alpha)}{\tan^2(\alpha_{sl})}\right)$$

$$M_z = -\mu F_z a \frac{\tan(\alpha)}{\tan(\alpha_{sl})}\left\{1 - 3\left|\frac{\tan(\alpha)}{\tan(\alpha_{sl})}\right| + 3\frac{\tan^2(\alpha)}{\tan^2(\alpha_{sl})} - \left|\frac{\tan(\alpha)}{\tan(\alpha_{sl})}\right|^3\right\} \qquad (26)$$

$$\mu = \frac{2c_{py}a^2}{3F_z}\tan(\alpha_{sl})$$

Where $c_{py}$ is the lateral stiffness of the tread element per unit length of the contact area, $\alpha$ is the side-slip angle and $\alpha_{sl}$ is shown in Figure 15-b.

#### 1.7.2.3.2 Pure Longitudinal Slip:

With the assumption of pure longitudinal slip, parabolic vertical load distribution, and constant friction level, the longitudinal force is expressed as follows [137]:

$$F_x = \begin{cases} -C_x s + \dfrac{C_x^2 s|s|}{3\mu F_z} - \dfrac{C_x^3 s^3}{27\mu^2 F_z^2} & s < s^o \\ \mu F_z \operatorname{sgn}(s) & otherwise \end{cases} \qquad (27)$$

Where $s^o = 3\dfrac{\mu F_z}{C_x}$ and $s$ is the slip ratio.

#### 1.7.2.3.3 Combined Slip:

For the case that both longitudinal and lateral slip are available, to simplify the problem it is assumed that the normal force distribution is parabolic, and the longitudinal and lateral stiffness of the tread elements, and the longitudinal and lateral friction coefficients are equal [135].

$$\begin{aligned} c_p &= c_{px} = c_{py} \\ \mu &= \mu_x = \mu_y \end{aligned} \tag{28}$$

The theoretical slips are defined as follow:

$$\begin{aligned} \sigma_x &= \frac{s}{1+s} \\ \sigma_y &= \frac{\tan\alpha}{1+s} \\ \sigma &= \sqrt{\sigma_x{}^2 + \sigma_y{}^2} \end{aligned} \tag{29}$$

The magnitude of total force is expressed as follows:

$$\begin{aligned} F &= \begin{cases} \mu F_z \left\{ 3\theta\sigma - 3(\theta\sigma)^2 + (\theta\sigma)^3 \right\} & \sigma \le \sigma_{sl} \\ \mu F_z & \sigma \ge \sigma_{sl} \end{cases} \\ \theta &= \frac{2}{3}\frac{c_p a^2}{\mu F_z} \end{aligned} \tag{30}$$

Where $\sigma_{sl} = \frac{1}{\theta}$ and $a$ is half of the contact patch length as it is shown in figure 14. Several studies have used different forms of brush model in their friction estimation algorithms, some of these studies are summarized in Table 1-6.

Table 1-6 sample studies in which brush model have been used

| Author's name | Method which was used |
|---|---|
| Svendenius [138] | Developed a brush based tire model to derive the tire forces and moment at combined slip, from scaling the forces given by empirical pure slip ( $\sigma_x, \sigma_y, \gamma$ ), at certain pure slips:<br>$(\sigma_{0x}(\sigma_x, \sigma_y, \gamma), \sigma_{0y}(\sigma_x, \sigma_y, \gamma))$<br>$F_x(\sigma_x, \sigma_y, \gamma) = G_{ax} F_{0x}(\sigma_{0xa}) + G_{sx} F_{0x}(\sigma_{0xs})$<br>$F_y(\sigma_x, \sigma_y, \gamma) = G_{ay} F_{0y}(\sigma_{0ya}) + G_{sy} F_{0y}(\sigma_{0ys}) + G_{camy} F_{0cam}(\gamma)$<br>$M_z(\sigma_x, \sigma_y, \gamma) = G_{ay} F_{0y}(\sigma_{0ya}) + G_{mz} M_{0z}(\sigma_{0z}) + G_{camz} F_{0cam}(\gamma)$<br>Where $F_{0x}, F_{0y}$ are from the empirical pure slip model, $F_{0cam}$ is the empirical pure cambering model, the normal load assumed to be parabolic distributed and the scale factors $G_{ij}$ are derived from the analytical expressions of brush model. |
| Andersson et al. [139] | They used an extended brush model in combined with slip mode to estimate the lateral friction. They used self-aligning torque as the estimation basis, instead of lateral force (because it shows more nonlinear behavior at low slip angle) to broaden the operation area of lateral estimator. |
| Nishihara et al. [140] | They used Brush model to describe the essential relation between the tire forces and aligning moment and the grip margin, which is defined as the residual tire forces normalized by the radius of friction circle:<br>$\varepsilon = 1 - \frac{\sqrt{F_x^2 + F_y^2}}{\mu F_z}$<br>It is assumed that the lateral force, aligning moment and the contact patch length are available, the friction coefficient is determined as:<br>$\mu = \frac{\sqrt{F_x^2 + F_y^2}}{(1-\varepsilon) F_z}$<br>$\varepsilon = \frac{1}{729}\left[\frac{2^{1/3}(9\xi + \xi^2)}{W(\xi)} + \xi + \frac{W(\xi)}{2^{1/3}}\right]^3 \qquad \xi = \frac{6M_z}{F_y a}$<br>$W(\xi) = (2\xi^3 + 27\xi^2 + 243\xi + 27\xi\sqrt{\xi^2 + 14\xi + 81})^{\frac{1}{3}}$ |

| Author's name | Method which was used |
|---|---|
| Matilainen et al. [141] | They estimate the friction potential during the lateral driving maneuver without any knowledge of tire stiffness based on brush tire model. Having the tire forces (estimated using bicycle model) the friction potential is calculated as follows: $\mu_{potential}(F_y/F_z,\lambda)=-\frac{F_y/F_z}{(\lambda^3-1)}$ where $\lambda$ is defined as $\frac{M_z}{aF_y}=-\frac{\lambda^3}{\lambda^2+\lambda+1}$ |
| Yamazaki et al [142] | They used brush tire model (with the assumption of parabolic distributed normal load) to estimate the longitudinal friction coefficient for two cases of partially sliding and pure sliding. For the case of partially sliding $\mu$ can be determined from: $9\mu_x^2F_z^2(F_x-C_xs)+3\mu_xF_zC_x^2s^2-C_x^3s^3/3=0$ And for pure sliding mode: $\mu_x=\frac{F_x}{F_z}$ |

#### 1.7.2.4 LuGre Tire Model:

LuGre tire model is a physics based dynamic tire model, which was first introduced by de Wit et al. in 1995. The surfaces are assumed to be in contact through elastic bristles. This is shown in Figure 1-16 [143].

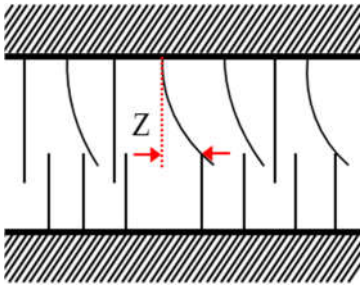


Figure 1-16 LuGre Model-Contact surfaces

The average deflection of the bristles in the lumped LuGre model (which is presented by z) is expressed as [143]

$$\frac{dz}{dt} = v - \frac{|v|}{g(v)} z$$
$$F = \sigma_0 z + \sigma_1 \frac{dz}{dt} + \sigma_2 v \tag{31}$$
$$\sigma_0 g(v) = F_c + (F_s - F_c) e^{-\left(\frac{v}{v_s}\right)^2}$$

Where $v$ is the relative velocity between the two surfaces, $v_s$ is Stribeck velocity, $F_c$ is the Coulomb friction level, $F_s$ is the level of stiction force, $\sigma_0$ is rubber stiffness, $\sigma_1$ is rubber damping coefficient and $\sigma_2$ is the viscous relative damping. In the distributed LuGre Model, an area of contact is assumed between the tire and the road, which formulates the friction force as follows [144]:

$$F(s) = \text{sgn}(v_r) F_n g(s) \left( 1 + \gamma \frac{g(s)}{\sigma_0 L |s|} (e^{-\frac{\sigma_0 L |s|}{g(s)}} - 1) \right) + F_n \sigma_2 r \omega s$$
$$\gamma = 1 - \sigma_1 |v_r| / g(s) \tag{32}$$
$$g(s) = \mu_c + (\mu_s + \mu_c) e^{-|r\omega s / v_s|^{\frac{1}{2}}}$$

Where $F_n$ is the normal load, $L$ is the contact patch length and $v_r = (r\omega - v)$ is the relative velocity. Several studies have used LuGre model to estimate the friction force or friction coefficient. De Wit et al. [145] used a single wheel dynamic model with lumped LuGre friction model and introduced a new parameter which represented the road change. Using the measured data of angular velocity of the wheel, they designed an online observer for the vehicle longitudinal velocity and the road condition parameters [145, 71]. Alvarez et al. [146] also used the same approach to design a tire friction model for emergency braking control. They also used a single wheel dynamic model along with lumped LuGre formulation for the force. Utilizing the measured data of wheel angular speed, the internal state of the LuGre model ($z$), the longitudinal and

relative velocity ( $v_r$ ) are estimated. Chen et al. used a bicycle model and propose the following observer in order to estimate the internal states of LuGre tire Model [137].

$$\dot{\hat{z}} = v_r - \bar{\theta}\sigma_0 f(v_r)\hat{z} + K(\mu_i - \hat{\mu}) \qquad (33)$$

With $\hat{\mu} = \sigma_0\hat{z} - \bar{\theta}\sigma_0\sigma_1 f(v_r)\hat{z} + (\sigma_1 + \sigma_2)v_r$ and $\bar{\theta}$ is a constant, ensure that $\lim_{t\to\infty}\hat{z} = z$ for each tire, $K = 1/\sigma_1$ and $\mu_i = \frac{F_{xi}}{F_{ni}}$ which is calculated form dynamical equation of the motion for each wheel. Knowing the parameters of the LuGre tire model, the friction coefficient is estimated using a recursive least square algorithm. In another study, Alvarez et al. [146] developed an adaptive friction estimation algorithm based on LuGre tire model. They used a quarter car model in which the forces were modeled using LuGre formulation and estimated the vehicle velocity and internal parameters of LuGre model using sliding mode observer. The measured states were the wheel angular velocity and the longitudinal acceleration. Matusko et al. [147] have used lumped LuGre model to explain the dynamics of friction force. They used a single wheel dynamic model along with LuGre tire model to estimate the friction force. A Neural Network (NN) algorithm is also used to compensate the uncertainties in the tire friction model. They used Lyapanov Direct Method to adapt the parameters of the NN algorithm. In some studies, LuGre tire model has been used as the basis to develop new dynamic models. Cleays et al. [72] have developed a LuGre based tire model, which describes the longitudinal and lateral forces and the aligning moment with a set of first order differential equations suitable for use in traction and ABS braking controllers.

In this section, four tire models which have been used more than other tire models were discussed; the overall specifications of these models are summarized in Table 1-7.

Table 1-7 specifications of discussed tire models

| Year | Name | properties | Feature |
|---|---|---|---|
| 1958 | Brush Model | Physical based | 1- It's a general model which is physically derived from variants of brush model<br>2- Describe the forces in: pure accelerating/ braking, pure cornering and combined mode<br>3- The friction assumed to be constant<br>4- Partitions the contact patch to two parts; adhesion and sliding regions<br>5- The effect of carcass deformation is neglected<br>6- The elements are assumed to be linearly elastic |
| 1969 | Dugoff Model | Physical based | 1- It's a velocity independent tire model<br>2- Uses two constants; longitudinal and lateral stiffness ( $C_x, C_y$ )to describe the tire behavior<br>3- Describe the forces in: pure accelerating / braking, pure cornering and combined mode<br>4- Considers a coupled relationship between longitudinal and lateral tire force |
| 1987 | Magic Formula | Semi-Empirical | 1- Can accurately fit to measured data<br>2- Describes the steady state tire behavior<br>3- Has lots of revised version<br>4- It's physically meaningful<br>5- Easy to use |
| 1995 | LuGre Model | Physical based | 1- It's a velocity dependent tire model<br>2- Can capture the Stribeck* effect<br>3- Can describe the hysteresis loop, pre-sliding displacement, …<br>4- Has two versions of lumped mass and distributed mass |

* The friction force decreasing continuously with increasing sliding velocity for low velocities [Stribeck 1920]

The slip-slop based algorithm which is another member of the Model Based approaches are discussed in following section.

### 1.7.3 The slip-slope method:

This method is based on the hypothesis that the low slip – low $\mu$ part of the slip curve (during normal driving condition) can be used to estimate the maximum tire-road friction. This has been claimed in several studies [148-153]. Slip is defined as the relative velocity between the tire and the road [150].

$$\begin{aligned} s &= \frac{\omega_w r_w - v_w}{v_w} \qquad during\ braking \\ s &= \frac{\omega_w r_w - v_w}{\omega_w r_w} \qquad during\ accelerating \end{aligned} \tag{34}$$

Where $r_w$ is the effective rolling radius of the wheel, $\omega_w, v_w$ are the angular and circumferential velocity of the wheel respectively. It is assumed that the values of slip ratio and normalized traction force ($\frac{F_x}{F_N}$) are available (through ABS sensor or other methods). Using different regression models on the linear region of $\mu - slippage$ curve, the maximum value of friction coefficient is estimated. In other studies a linear model has been used to fit the data. Gustafsson [150] suggested the following regression model to be used for $\mu - slippage$ curve:

$$\begin{aligned} &\mu = ks - k\delta \\ &\delta = s\,|_{\mu \approx 0}\ ,\ k = \frac{d\mu}{dx}|_{\mu \approx 0} \end{aligned} \tag{35}$$

Then a Kalman filter supported by change detection algorithm is used to accurately estimate the so-called slip slope. Germann et al. [154] used a second order polynomial to express the $\mu - slip$ relation as follows:

$$\mu = a_0 + a_1 s + a_2 s^2 \quad (36)$$

Where the coefficients of this polynomial are calculated from $\mu - slip$ curve, they showed that this model works well for the slip range of less than 0.3 (30 percent). Muller et al. and Kiencke et al. [155] used the $\mu - slip$ data collected from a braking maneuver and proposed the following regression model:

$$\mu = \mu' \frac{s}{c_1 s^2 + c_2 s + 1} \quad (37)$$

Where $\mu'$ is the slope of $\mu - slip$ curve and $c_1, c_2$ are calculated using a least square algorithm. Several other studies have used similar algorithms to obtain the maximum friction coefficient from the slip-slope curve [151, 156]. Lee et al. [157] used a wheel dynamic model to estimate the longitudinal force and wheel slip; then using recursive least square, they calculated the slope of $\mu - slip$ curve.

## 1.8 Conclusions

Sudden change in the pavement friction, caused by change in weather condition (rain, snow, etc.) plays one of the most important roles in car crashes. Unawareness of the driver about the pavement friction change and malfunction of vehicle's stability controllers lead to fatal car accidents; therefore, friction estimation is of interest to vehicle and tire industries. Several research studies have been conducted to estimate the friction force, friction coefficient and other parameters related to tire-road friction problem.

These studies can be divided into two main categories; experiment-based and model based. In the experiment-based approaches, it is attempted to correlate the measured data to friction related parameters. While in model based approaches, a mathematical model of the problem is developed

first, then based on the developed model and measured states, the friction force or other friction related parameters are estimated. The properties of each of these methods are summarized in Table 1-8. Two factors of accuracy and repeatability are used in this table. Different methods are ranked as low, medium and high, which demonstrates how accurate a method is to estimate the desired parameters or how a study is repeatable.

Table 1-8 Summary of friction estimation approaches

| **Major Category** | **Sub-Category** | **Short description** | **Accuracy** | **Repeatability** |
|---|---|---|---|---|
| Experiment-based | Optical sensors and camera | Using optical sensors and cameras to detect friction related surface properties | Medium | Medium |
| | Acoustic sensors | The tire noise is used to classify the surface type or surface condition and correlate it to the tire-road friction | Medium | Low |
| | Tire tread sensors | Using different sensor inside the tire to monitor the interaction between tire and the road | High | Medium |
| Model-based | Vehicle dynamic based method | Using a dynamical model of the problem and the data of measured states and try to estimate the unmeasured states | High | High |
| | Tire model based method | Using a tire model, which express the relation between slip/slip ratio and tire forces and moments to estimate the friction | High | Medium |
| | Slip-Slope based method | Try to estimate value of friction coefficient in the saturated part of $\mu - slip$ curve based of the slope of the curve in linear region | Medium | Low |

The most important shortcoming of experiment-based approaches is observed to be the repeatability. When the testing conditions have some deviations from which these algorithms were trained, their accuracy decreased dramatically. Also, for the slip slope based approach, although it

is claimed in several studies that there is a direct relation between the slip slope and the maximum friction coefficient, it is observed that changing the testing conditions (tire pressure, tire temperature and etc.) will change the slope of $\mu - slip$ curve in the linear region which affects the accuracy and repeatability of this method.

This literature survey introduces the development of the most popular algorithms which are widely used to estimate tire-road friction and other friction-related parameters.

# 2 Experimental Test Setups

In this chapter, the experimental test setups, which were developed and used in this study, are explained. Three test setups were used:

- Small six-wheeled ground robot
- Portable tire test setup (trailer)
- An instrumented vehicle (Volkswagen Jetta)

To study the application of intelligent tires for improving mobility, a wheeled ground robot was designed and built. The robot was instrumented with appropriate sensors (a tri-axial accelerometer embedded in the tire inner-liner, a single axis accelerometer on the chassis and wheel speed sensor) and a data acquisition system. The wheel longitudinal slip was measured accurately using accurate encoders attached to driven and non-driven wheels.

The second test setup is a portable tire test trailer, which is a quarter car test rig installed in a trailer and towed by a truck. The trailer was equipped with different sensors; a force hub to measure tire forces and moments, a high accuracy encoder to measure the angular velocity of the wheel and a VBOX, which is a GPS based device, was also used to estimate the longitudinal speed of the trailer. Also, an intelligent tire, which has an embedded accelerometer placed on the tire inner-liner, is used in trailer test setup.

The third test setup which was developed for this study was an instrumented Volkswagen Jetta. Different sensors have been added to capture the vehicle dynamics properly; an instrumented steering wheel measures the steering wheel angle and steering wheel angular speed, two intelligent tires (front right and rear left) to monitor the interaction between the tire and road surfaces and two

encoders to measure the angular velocity of these wheels. An Inertial Measurement Unit (IMU) was used to measure roll, pitch, yaw and all three components of acceleration at the center of the mass of the vehicle. VBOX also was used to estimate the longitudinal speed of the Jetta. The test setups are explained in more detail next.

## 2.1 Six-wheel ground robot:

A small wheeled ground robot was designed and built for this study. Different mechanical parts, which are used in the robot, are as follows:

- Chassis
- Motors
- Motor Controllers and batteries
- Wheels and Pneumatic Tires
- Slip Ring
- Sensors
- Data acquisition system

Each of the robot parts, are explained in more details as follows:

### 2.1.1 Chassis

An all-terrain mobile robot platform (ATR) was designed and built for this study. The chassis base is 14.25” wide × 17.25” long, which are surrounded by 2.13” height sidewalls. The chassis gives the options for 4WD and 6WD robot platform and provides enough space for the wheel shafts to be coupled directly to the motors. The chassis and the motors are shown in Figure 2-1.

Figure 2-1 the robot chassis with direct drive motors

### 2.1.2 Motors:

Four $24\,V$ brushed permanent magnet DC motors with planetary gearbox from Shayang Ye Industrial Company (supplied by super droid robots) were used for this study. Based on the information that was provided by Super Droid, the rated speed for the motors is $285$ rpm, the rated torque is $11\,kgf-cm$ and the reduction ratio is 1:12. Each motor has a dual channel/quadrature encoder with 225 pulses per revolution, mounted to the tail shaft of the motor for speed control purposes [158, 159].

### 2.1.3 Motor Controllers and Batteries:

Two RAPCON platforms form ZELTOM, shown in Figure 2-2, were used to control the motors, which offer a seamless interface between physical plants and Matlab/Simulink for implementation of different control algorithms in real-time. Each of RAPCON platforms has two channels to communicate and control two DC motors separately at the time, provides the real time operation with sampling rates up to 15.2 kHz. In order to control the motion of each wheel separately, two of them were used at the same time. Also two 20 cell (24V- DC, 4500 mAhr) rechargeable NiHM

battery pack were used for each of the motor controllers, which provide the required energy for at least one hour under operation with highest speed.

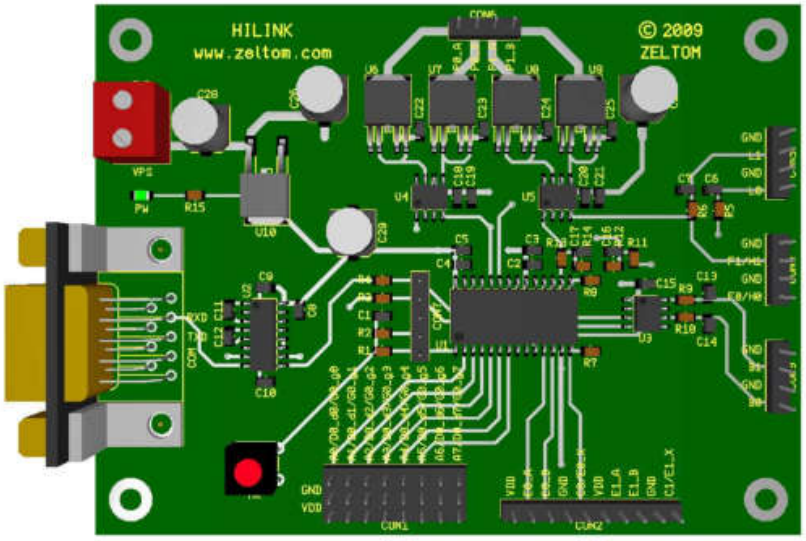


Figure 2-2 RAPCON platform used to control the speed of DC motor

### 2.1.4 Wheels and Pneumatics Tires

Four pneumatic tires were used under the robot in order to simulate real automotive conditions. The tires are 10 inches in diameter and 4 inches wide, which are rated at 30 *psi* with the maximum load capacity of 300 *lb* [160]. Each wheel has a 0.5" thick shaft with 8 *mm* bore at the free end to accept the motor shaft. The pneumatic tire with the wheel shaft is shown in Figure 2-3.

Figure 2-3 the pneumatic tire and the wheel shaft

### 2.1.5 Slip ring

The designed robot had accelerometers inside one of its tire for terrain classification purposes. In order to transmit the electrical signal from the rotating wheel to stationary data acquisition system and vice versa, a SRA-73683 slip ring with 6 input-output circuits from Moog (Blacksburg, VA) was used. The inner bore for this slip ring was 0.5" which made it possible to be mounted on the wheel shaft. The maximum speed for this slip ring is 120 $RPM$ and the maximum voltage is 120 $V$ [161]. A picture of slip ring is provided in Figure 2-4.

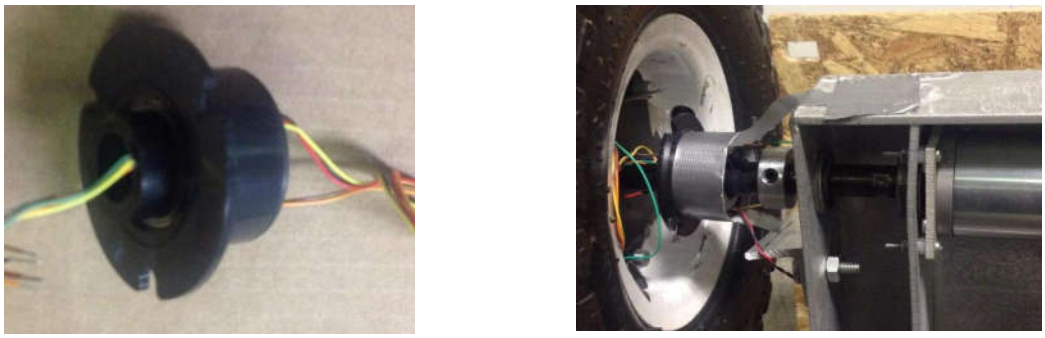

Figure 2-4– Slip ring with six circuit

### 2.1.6 Sensors:

As it was mentioned before, the robot was designed for terrain classification/identification; for this purpose the robot was instrumented with many sensors which are explained briefly next.

#### 2.1.6.1 Tri-Axial Accelerometer Inside the Tire:

A 3023A5 Tri-axial accelerometer from Dytran (Chatsworth, California) is fixed inside the robot's tire using a rubber patch to monitor the vibration of the contact patch in three directions. This technology was developed at the Center for Tire Research (CenTiRe) and was utilized for this project [162.163], [43]. Figure 2-5 provides a picture of the accelerometer inside the tire. Other specifications for the accelerometer were summarized in Table 2-1. Also a hole was made on the tire's rim in order to connect the sensor's wire to the rotary part of the slip ring.

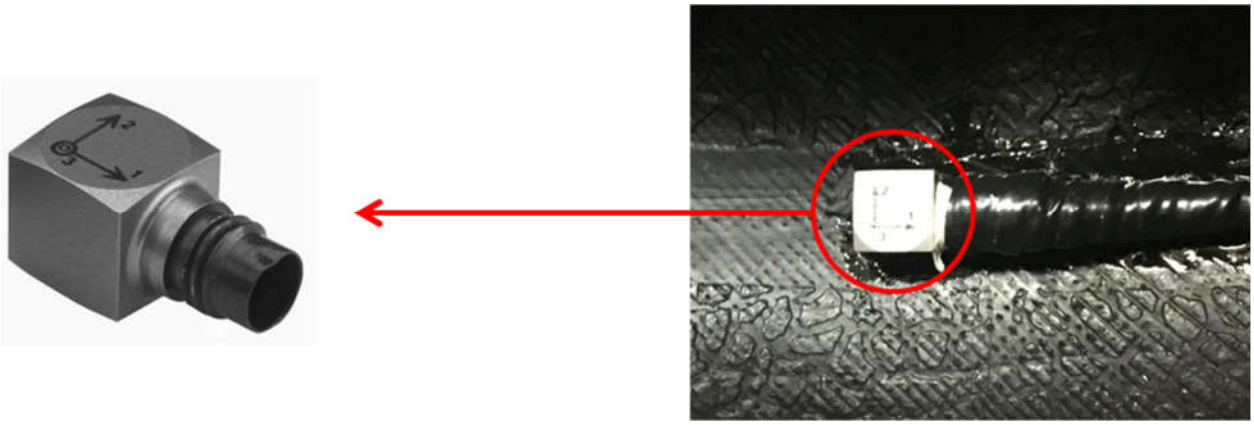

Figure 2-5 Dytran 3023A5 accelerometer attached to the tire

Table 2-1 Dytran 3023A5 accelerometer specifications [164]

| | |
|---|---|
| Sensitivity, ±5% | $10\,mV/g$ |
| Range for ±5*volts* output | $\pm 5000g$ |
| Supply current range | $2 to 20 mA$ |
| Compliance Voltage Range | $18-30 volts$ |

#### 2.1.6.2 Single axis accelerometer on the chassis:

A Dytran 3225F1 single axis accelerometer was attached to the chassis in order to monitor the dynamics of the robot in longitudinal direction and estimate the robot speed. To reduce the vibration induced by the chassis, a rubber damper was used and the sensor was attached on top of the damper. Dytran 3225F1 has exact same characteristics as 3023A5, presented in Table 2-1. To power the accelerometer, Dytran Model 4116 signal conditioner/amplifier was used.

#### 2.1.6.3 External encoder for the wheel angular speed

To measure the angular speed and the slip of the wheel accurately, two model 15S encoders from Encoder Product Company (Sagle, Idaho) were attached to a driven and un-driven wheel of the robot externally. Figure 2-6 depicts the encoder and a simple mechanism that was designed to hold the encoder (Figure 2-6-b). Table 2-2 summarizes the encoder characteristics.

(a)

(b)

Figure 2-6 (a) model 15S encoder , (b) designed mechanism to hold the encoder

Table 2-2 model 15S encoder characteristics[165]

| | |
|---|---|
| Count per Revolution | 10000 |
| Output Format | Incremental |
| Max. Frequency | 1 MHz |
| accuracy | Within 0.017 degree |

The other important part of the robot is data acquisition system which is explained briefly next.

### 2.1.7 Data Acquisition System:

NI USB 6218 data acquisition system was used to collect data from all of the sensors. This is a 16-bit, 250 $kS/s$ USB devices with 32 analog inputs and 8 digital inputs and two 32-bit counters. The accelerometers were connected to the analog input channels and the encoders were attached to the counter/timer pins of this device. This measures a number of time-related quantities, counting events or totalizing, and monitoring position with quadrature encoders. A data collecting routine was developed using LabVIEW to collect the data of all sensors at the same time with the same sample rate, 1000 Hz, for this study. Figure 2-7 shows the schematic of the robot and data collecting system and the LabVIEW user interface designed for this study is shown in Figure 2-8.

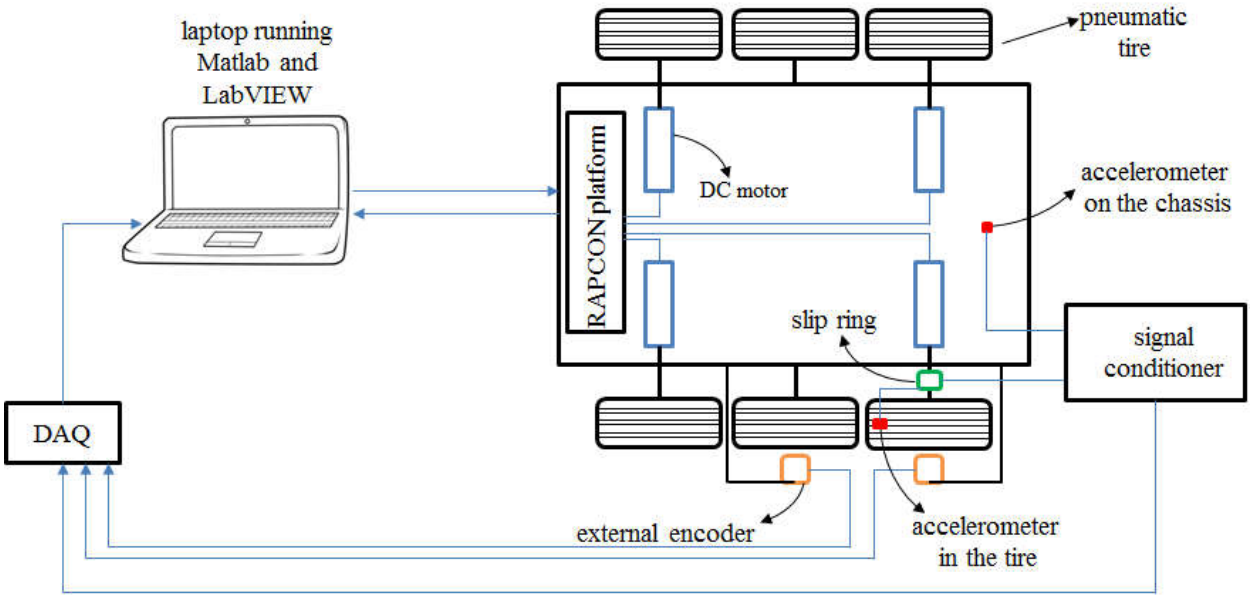


Figure 2-7 schematic of the robot and data collecting system

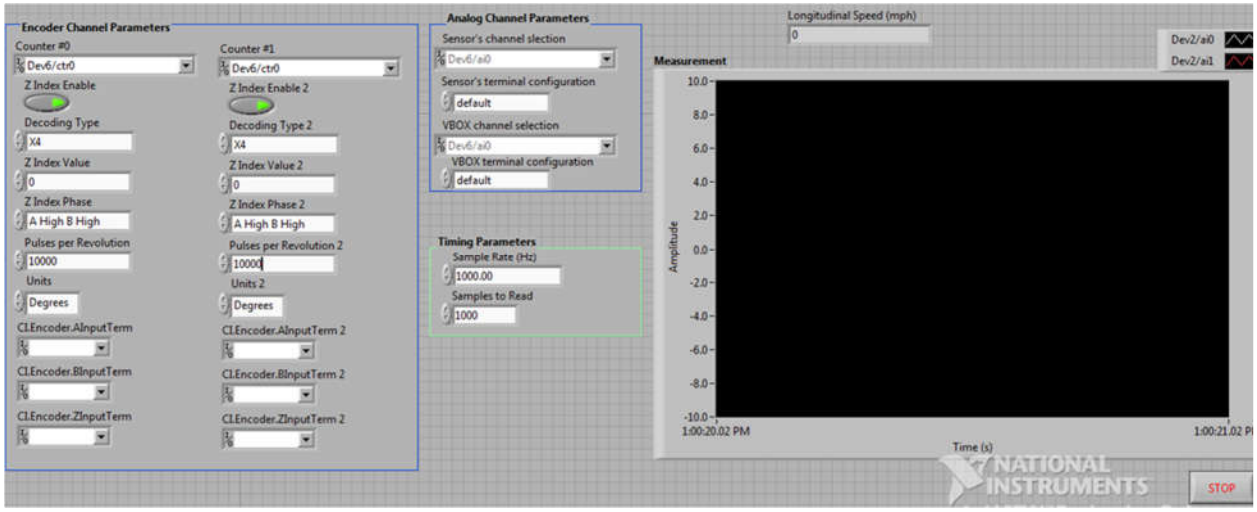


Figure 2-8 LabVIEW interface, designed to collect the data of accelerometers and encoders

### 2.1.8 The speed control algorithm:

RAPCON platform was used to control the motors, works perfectly with Matlab/Simulink real-time toolbox. A simple PID controller was designed in Matlab/Simulink, shown in Figure 2-9, to control the speed of each wheel separately, used the encoder signal of the motors as the feedback. The PID parameters were tuned by trial and error to achieve the best performance in both high and low speed. Figure 2-10 shows the Simulink block diagram used for speed control.

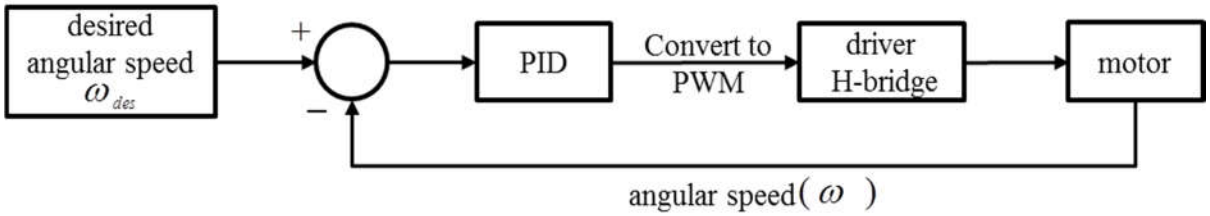


Figure 2-9 the robot's speed control algorithm

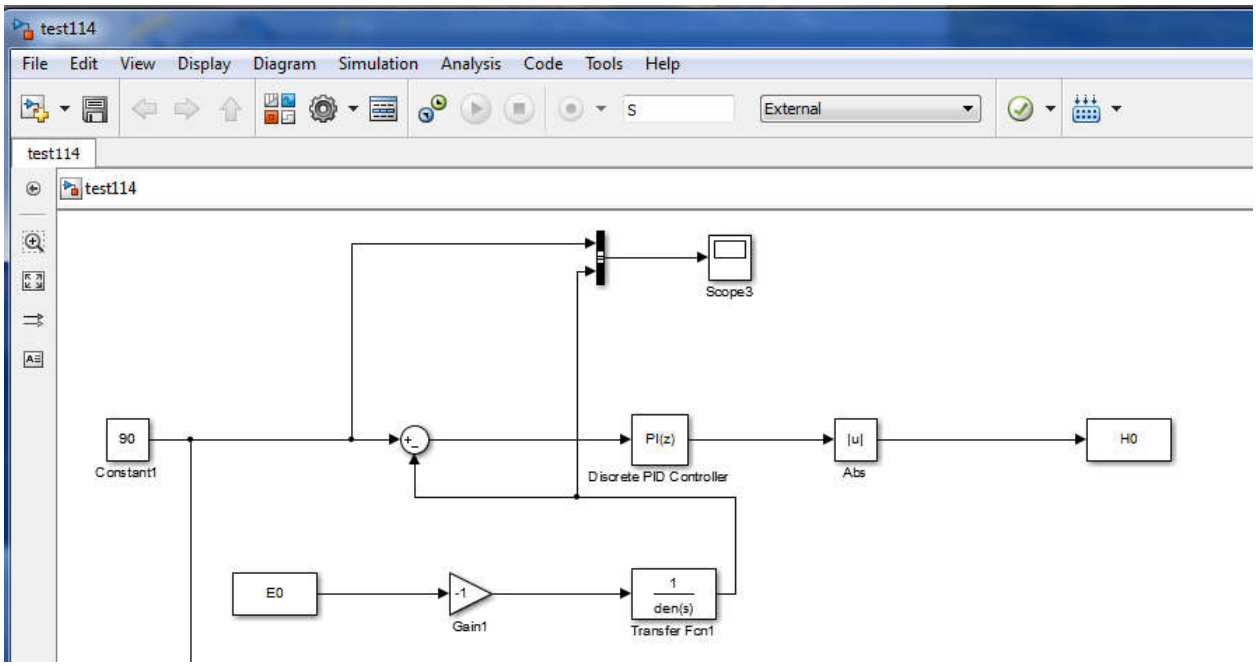


Figure 2-10 Simulink block diagram used to control the speed

Sample data collected using the small ground robot is shown in Figure 2-11.

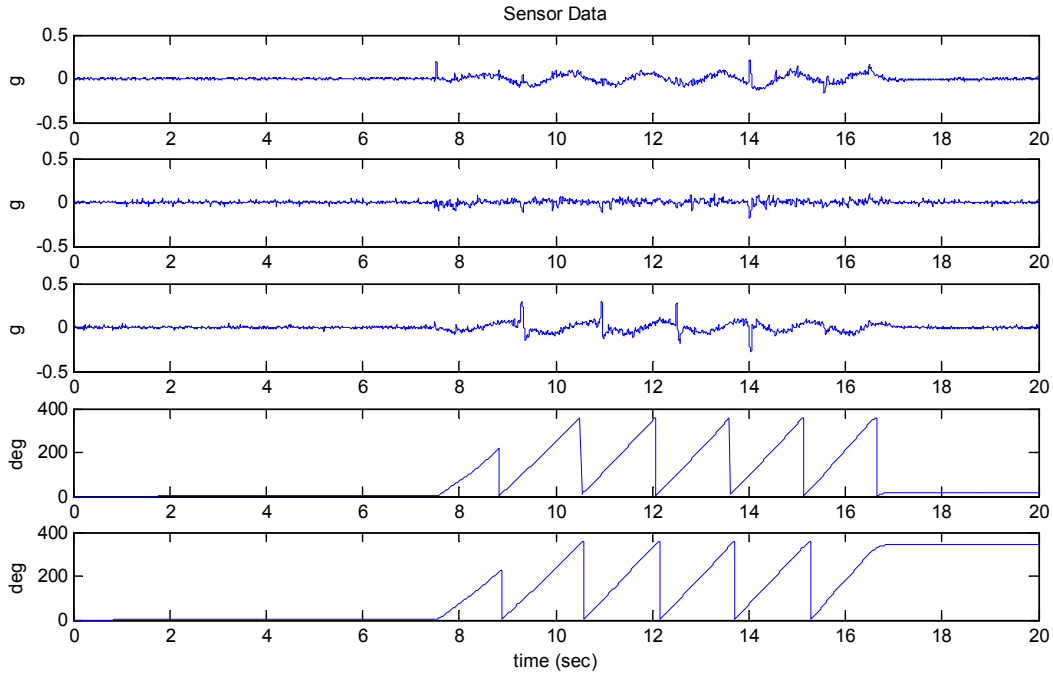


Figure 2-11 sample data collected using small ground robot

## 2.2 Portable Tire Test Setup:

A trailer test setup was used for this study, shown in Figure 2-12, which is a trailer towed by a truck. The trailer has a quarter car test rig equipped with different sensors to capture the dynamics of the setup properly; different parts of the test setup are shown in Figure 2-13.


Figure 2-12 portable trailer tows by a truck

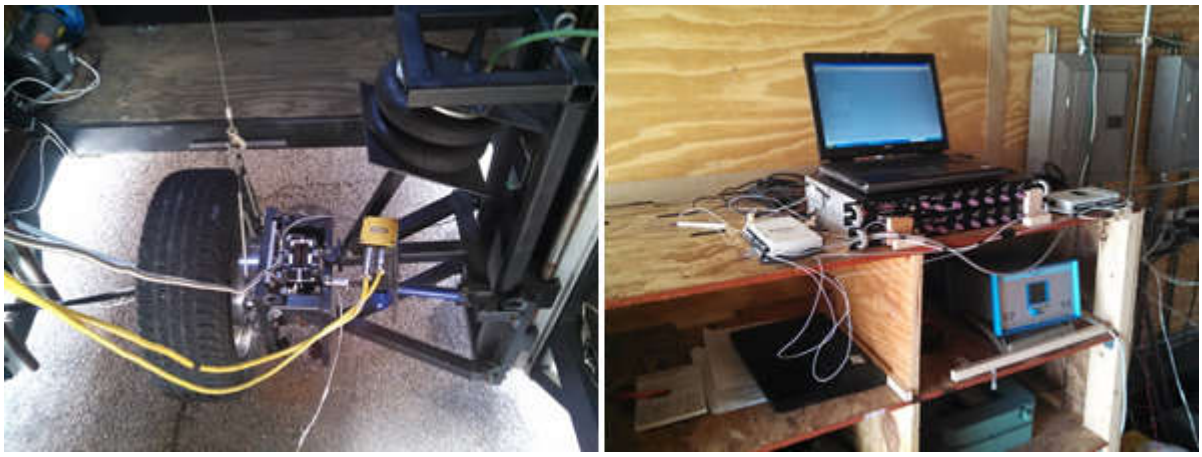

Figure 2-13 quarter car test rig embedded into portable trailer

A Kistler six DOF (Degree Of Freedom) force hub was used to measure the tire forces and moments in all three directions. Table 2-3 shows the specifications of the force hub used in trailer test setup.

Table 2-3 force hub specifications used in trailer test setup [166]

| | |
|---|---|
| $F_x$ and $F_y$ measuring range | -20 to 20 (kN) |
| $F_z$ measuring range | 0 to 30 (kN) |
| $M_x$ measuring range | -7.86 to 7.86 (kN.m) |
| $M_y$ measuring range | -3 to 3 (kN.m) |
| $M_z$ measuring range | -1.24 to 1.24 (kN.m) |
| Max rotational speed | 2000 (rpm) |
| Natural frequency | 2400 (Hz) |

An accurate encoder was attached to the force hub to measure the angular position and speed of the wheel. The encoder specifications are presented in Table 2-4. A bracket shape mechanism is used along with a coupler to attach the encoder to the force hub which is shown in Figure 2-14. Also, VBOX, a GPS based device, is used to measure the longitudinal speed of the trailer.

Table 2-4 specifications of encoder used in trailer test setup (model 755A) [167]

| | |
|---|---|
| Max speed | 7500 rpm |
| resolution | 30000 CPR |
| Input voltage | 4.75 to 28 VDC |
| Input current | 100 mA max |
| Max frequency | 100 kHz |

| Output type | Incremental |
|---|---|
| Rise time | Less than 1 microsecond |

Figure 2-14 the encoder attached to the force hub to measure angular velocity of the wheel

Once the angular and longitudinal speeds of the wheel are measured, the slip ratio is calculated as follows [150]:

$$s = \frac{\omega_w r_w - v_w}{v_w} \quad during\ braking$$
$$s = \frac{\omega_w r_w - v_w}{\omega_w r_w} \quad during\ accelerating \qquad (1)$$

Where $r_w$ is the effective rolling radius of the wheel, $\omega_w, v_w$ are the angular and circumferential velocity of the wheel, respectively. A parker servo motor-motor controller was used to apply the slip angle in the range of $\pm 25$ degrees. A rotary to linear motion convertor was attached to the servo motor; using LabVIEW communicating with the motor controller through USB NI DAQ, desired slip angle is applied. The schematic of slip angle controller mechanism is shown in Figure 2-15.

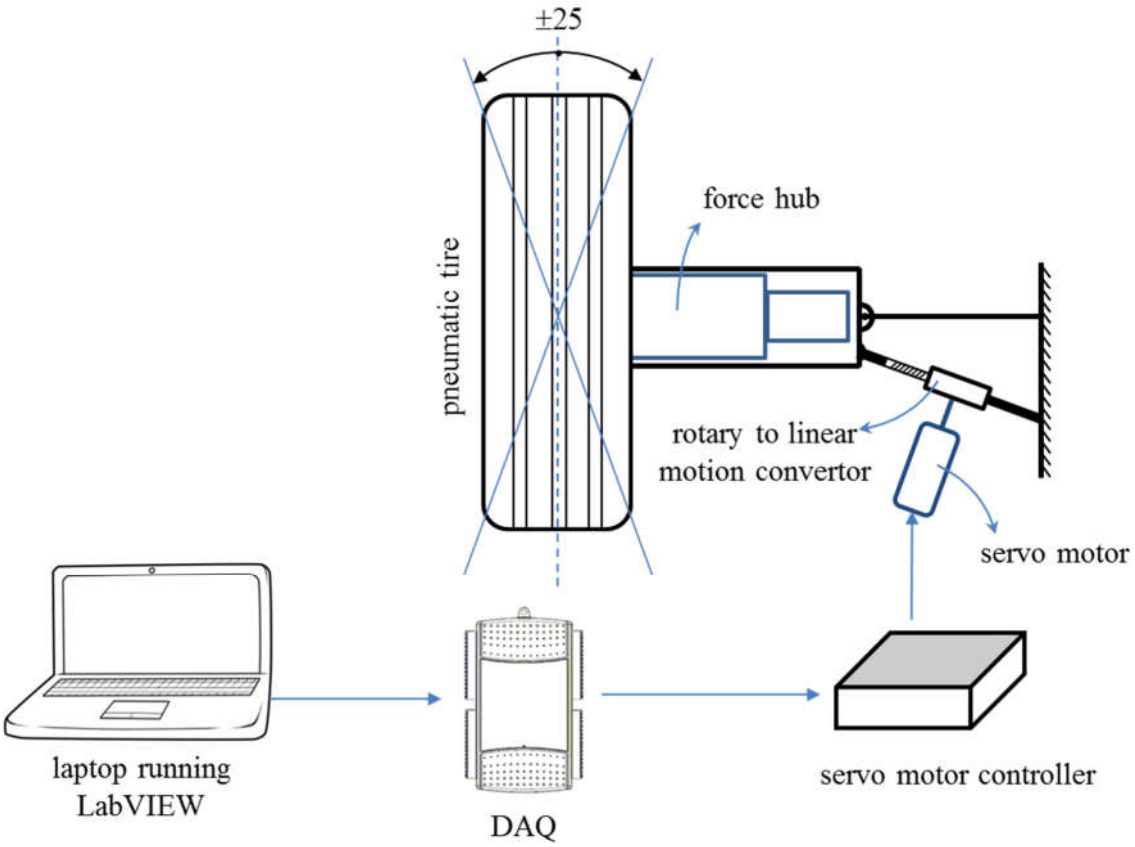


Figure 2-15 schematic of the slip angle controller mechanism

The tire normal load was also controlled using an air spring along with a TESCOM transducer, the specifications of TESCOM transducer is shown in Table 2-5. A PID controller was designed in LabVIEW, using the measured normal load from the force hub as feedback; the tire normal load is controlled. The schematic of normal load algorithm is shown in Figure 2-16. The maximum load capacity for the normal load controller system (considering the weight of the trailer and air spring and transducer loading capacity) is 10000 pounds.

Table 2-5 Specification of TESCOM electropneumatic controller (ER3000) [168]

| | |
|---|---|
| Control algorithm | External feedback |
| Set point signal source | External analog (4-20 mA or 1-5 VCD) |
| Feedback signal source | External analog (4-20 mA or 1-5 VCD) |
| Max vacuum pressure | 20000 psig / 1379 bar |
| Max pressure that can be controlled | 0-100 psig |

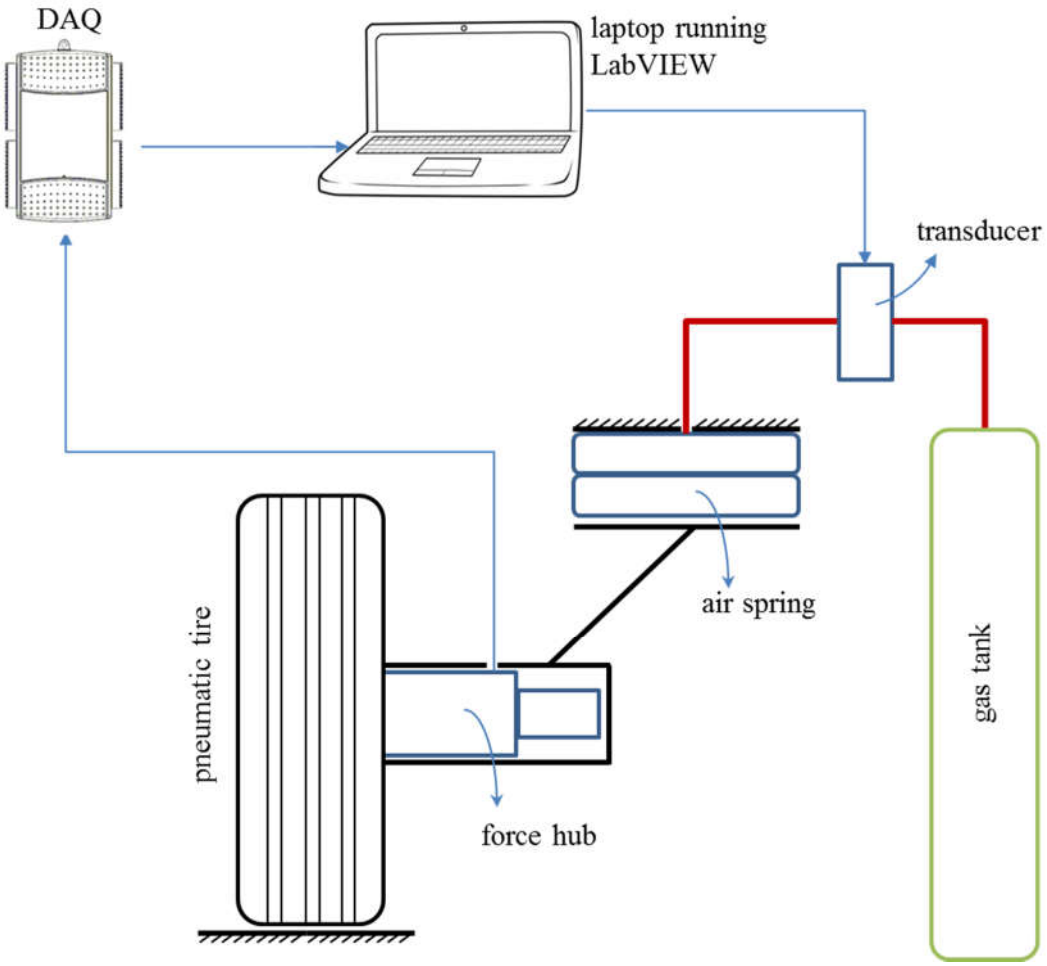


Figure 2-16 the front view of normal load controller algorithm

A water tank – water pump system was also placed in the trailer which provided both wet and dry test conditions. An intelligent tire which is a tire with a tri-axial accelerometer embedded to its inner liner was used in this study, which is shown in Figure 2-17. The radius of the tire is 20" with recommended inflation pressure of 32 psi.

Figure 2-17 tire with a tri-axial accelerometer embedded to its inner liner

A data collecting routine was developed in LabVIEW to collect the data of different sensor at the same time with the same sample rate, the sample rate of 1000 Hz was used for all the sensors in this study, also to control the normal load and slip angle. USB NI- DAQ 6218 was also used as the data acquisition board. The schematic of data collecting system is shown in Figure 2-18.

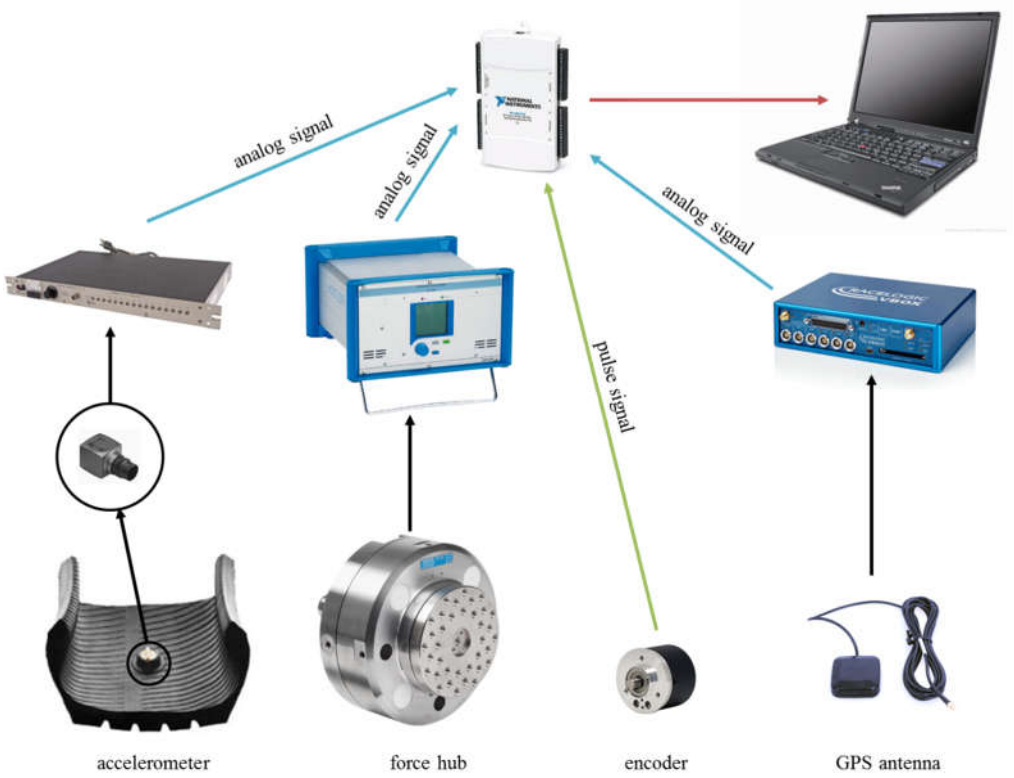


Figure 2-18 schematic of data collecting system used in trailer test setup

## 2.3 Instrumented Volkswagen Jetta:

The third setup developed for this study is an instrumented vehicle, since we had all the vehicle parameters for Volkswagen Jetta 2000 to 2003; a 2003 Jetta was purchased for this purpose. The vehicle was equipped with different sensors, which are explained next.

A DATRON Measurement Steering Wheel (MSW), as shown in Figure 2-19, was used to measure the steering angle, steering velocity and the input steering torque. The MSW specification is presented in Table 2-6.

Figure 2-19 the DATRON MSW used in Jetta

Table 2-6 the specification of DATRON MSW used in Jetta [169]

| | |
|---|---|
| The encoder resolution | Up to 7200 pulses per revolution |
| Powers supply | 10-36 V- DC |
| Mass moment of inertia | 60 $kgcm^2$ |
| Angle resolution | 0.1 Degree |
| Max steering torque measurement range | ± 50 Nm |
| Max steering speed | 1000 degree /sec |

Two tri-axial accelerometers were placed in one of the front and one of the rear tires of the Jetta in order to monitor the interaction between the tires and different surfaces, also to find some correlation between acceleration signals (from the accelerometer embedded to tires inner liner) and different vehicle maneuvers.

To transmit the sensor signals from the rotating tire to the vehicle and measure the angular velocity of the wheels, two water resistance SR10AW/PE512 slip rings with build in encoders from Michigan Scientific were used. The slip ring and the adaptor, designed to mount the slip ring to the wheel are shown in Figure 2-20 and the specification of SR10AW/PE512 slip ring is presented in Table 2-7.

Figure 2-20 SR10AW/PE512 slip ring and the designed mounting adaptor

Table 2-7 the specification of SR10AW/PE512 slip ring / encoder [170]

| | |
|---|---|
| Number of circuits | 10 |
| Current capacity | 500 mA |
| RPM rating | 10000 |
| Maximum peak noise | 0.1 ohm |
| Temperature range | -40°C to 100°C |

To measure the accelerations components and roll peach and yaw of the vehicle, an IB6-XY3-Z5-GX100-GY100-GZ100 IMU/accelerometer from TEXYS was placed at the Center of Gravity (CG) of the Jetta. The specification of the IMU unit is given in Table 2-8.

Table 2-8 the IMU unit placed at the CG of the Jetta [171]

| | |
|---|---|
| Range of XY Acceleration | ± 3g |
| XY sensitivity | ≈ 660 mV/g |
| Range of Z Acceleration | ± 5g |
| Z sensitivity | ≈ 385 mV/g |
| Range of Gyro XYZ | ± 50° |
| Gyroscope sensitivity | ≈ 20 mV/°/s |

| | |
|---|---|
| Gyroscope offset drift | ± 25 mV |
| Gyroscope gain drift | ± 1 % |

To measure the longitudinal speed of the vehicle VBOX, a GPS based device, is used which provides the velocity with the accuracy of 0.1 km/h. To acquire the data of all of the sensors a NI data acquisition board (NI USB-6363) was used, which had thirty-two 16 bits analog inputs, four 32 bits counters and provided the maximum sample rate up to 1 MHz. The schematic of data acquisition system used in Jetta is shown in Figure 2-21.


Figure 2-21 the schematic of Jetta's data acquisition System

A data collecting routine was developed in LabVIEW that acquire the data of all the sensors at the same time with same sample rate (1000 Hz was used in this study). For all of the test setup in this study the sample rate of 1000 Hz was used, this number was selected using trial and error to find

an optimum value that reflects the signal properties and to be practical. So this specific sample rate was selected for all test setup used in this study.

## 2.4 Conclusions:

In this chapter, different testing setups that used for this study were introduced and were explained in details. Three testing setups were used; first, a six wheel ground robot where designed and built for surface classification purposes. The wheeled robot was equipped with different sensors, an intelligent tire which is a tri-axial accelerometer embedded to the tire inner-liner, two accurate encoders attached to the driven and non-driven wheels of the robot and a single axis accelerometer attached to the chassis to capture the robot's vertical vibration.

Second, a portable tire test trailer, which is a quarter car test rig installed in a trailer and towed by a truck. The trailer was equipped with different sensors; a high accuracy encoder to measure the angular velocity of the wheel, a VBOX, which is a GPS based device, was used to estimate the longitudinal speed of the trailer and a force hub to measure tire forces and moments. Also, an intelligent tire was used in trailer test setup.

The third test setup was an instrumented Volkswagen Jetta. Different sensors were used in Jetta; an instrumented steering wheel measures the steering wheel angle and steering wheel angular speed, two intelligent tires (one front and one rear) to monitor the interaction between the tire and road, an IMU to measure roll, pitch, yaw and acceleration components at the center of the mass of the vehicle and encoders to measure Jetta's wheel angular velocity.

# 3 Methodology

Five different algorithms were developed for this study, are explained in the following sections.

- Fuzzy Logic based terrain classification algorithm
- A Neural Network algorithm to estimate the tire normal load
- A two-step Neural Network pressure monitoring algorithm
- A Neural network road condition monitoring algorithm
- A friction estimation algorithm which is a combination of experimental and vehicle dynamic based friction estimation approaches

Each of these algorithms is explained in more details next.

## 3.1 Fuzzy Logic based terrain classification algorithm:

Terrain Identification is one of the most important issues related to the mobility of small ground robots. Once the terrain is identified, the robot can adapt its performance according to the terrain characteristics. Terrain analysis can be classified into two major categories, first terrain classification, aims at associating terrain with well-defined categories, such as asphalt, concrete, gravel and sand. Second, terrain characterization which is determination of the terrain characteristics [172].

Different types of sensors are used in terrain classification problem, contact and non-contact. In the studies with the contact sensors, characteristic like vibration frequency is used to classify the surface. Parka et al. [173] designed a mobile robot and using the data from tire contact sensors, they developed a method to extract the terrain features. Brooks et al. [174, 175] used a robot with an accelerometer on its chassis. They used the vibration of the chassis to classify the surfaces. Weiss et al. [176, 177] attached an accelerometer to the vehicle body to measure it's vibration in

the direction perpendicular to the ground. Then, applied fast Fourier transform (FFT) and power spectral density (PSD) to the data and trained a Support Vector Machine (SVM) algorithm to classify the surfaces. They also compared different approaches in vibration based terrain classification [178]. DuPont et al. [179-181] attached an accelerometer to the body of an unmanned ground vehicle (UGV), using the dominant vibration frequency of the UGV's body they trained a Neural Network (NN) to identify the terrain. Collins et al. [182] presented a vibration-based terrain classification algorithm for UGV by mapping the vibration outputs to the terrain inputs using the AGV vibration transfer function.

Non-contact sensors studies mostly used optical, sonar or acoustic sensors for terrain classification/characterization purpose. Manduchi et al. [183] used two sensor systems; a color stereo camera and single axis ladar that complement each other. Using stereo range measurements, they developed a color-based classification system to classify the detected terrains [184-186]. Larson et al. [187] used a single camera; with a little processing of visual information they developed a new terrain classification technique. Vandapel et al. [188] used a rover with s 3-D ladar for terrain classification. Lee et al. [189] used a CCD camera; they extracted colors and textures from sensor data and classify the surfaces. Liang Lu et al. [190] used a laser stripe-based structured light sensor, which already has infrared camera component that allows sensing at night without external lightening to sense the terrain directly. Their classification does not rely on measure of the color, which can be messed up due to weather condition and illumination. Their method was based on spatial frequency from range data and texture from camera data. Many studies have used a combination of contact and non-contact sensors for terrain classification. Ojeda et al. [191, 192] used a small robot with a gyro, accelerometer attached to its chassis, wheel encoder

which, microphone, infrared sensor and ultra-sonic range sensor and developed an algorithm to classify different terrain to commonly known classes like gravel, sand and asphalt.

Also, many researchers have developed various methodologies to characterize different terrains [193- 195]. Howard et al. [196] used a mobile robot with a vision system; they used an Artificial Neural Network (ANN) for real time terrain characterization. Cuong et al. [197] designed a test rig and used it to measure the vertical damping ratio of tire-soil system using free-vibration logarithmic decay method. Pinnington et al. [198] performed some experiments for both terrain characterization and classification.

In this study, a fuzzy logic algorithm was developed for terrain classification purposes. Using the power of the acceleration signal, the wheel slip ratio and the robot speed as inputs, surfaces were categorized into four different categories; asphalt, concrete, sand and grass.

### 3.1.1 Methodology:

In this study, a Fuzzy logic algorithm was developed and used to classify different terrains. Fuzzy logic is an extension of Boolean logic by Lotfi Zadeh which was developed in 1965 [199, 200], which provides a very valuable flexibility for reasoning. Unlike the Boolean logic that the membership of a variable to a set can be true or false (0 or 1), in Fuzzy logic the truth value of membership may be any real number between zero and one. It is written in mathematical language as: if $X$ is a set, a Fuzzy subset $A$ of $X$ is characterized by membership function as follows:

$$f^a : X \rightarrow [0,1] \qquad (1)$$

Where $f^a$ is the membership function of the Fuzzy subset $A$. For instance, the amount of tip should be paid in a restaurant is considered as the problem. Undoubtedly the amount of tip depends on

the quality of service and quality of food. The inputs of this problem are the quality of food and quality of the service and the output is the amount of tip, shown in Figure 3-1.

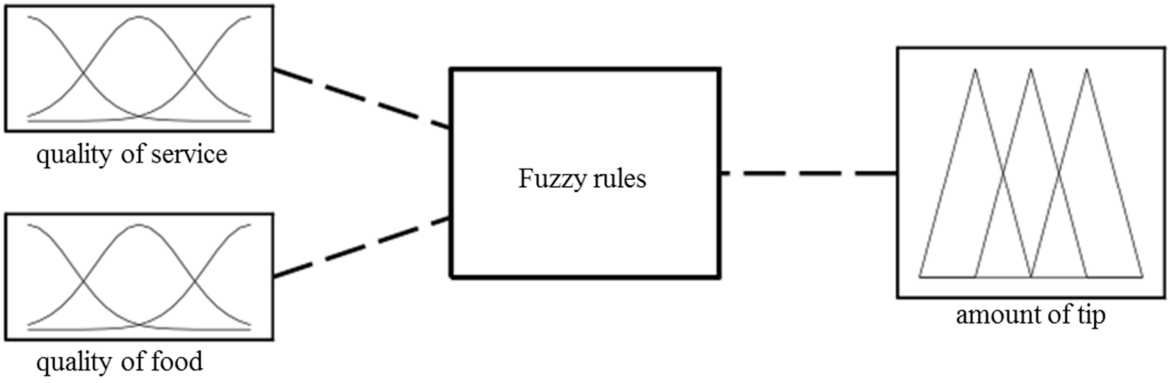


Figure 3-1 the inputs and output for the tip problem

The shape of membership function is chosen arbitrary using the result of statistical analysis or by following the advice of the expert and can be assigned as sigmoid, Gaussian, hyperbolic, exponential, tangent or any other desired forms. Figure 3-2, Figure 3-3 and Figure 3-4 show sample membership functions, selected for the fuzzy set "quality of service", "quality of food" and "tip amount" respectively.

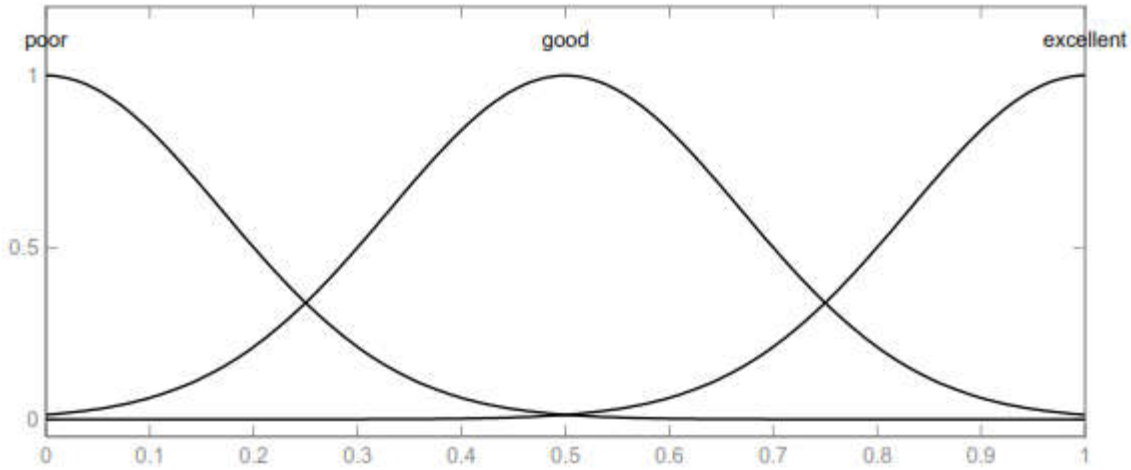


Figure 3-2 the selected membership function for quality of service

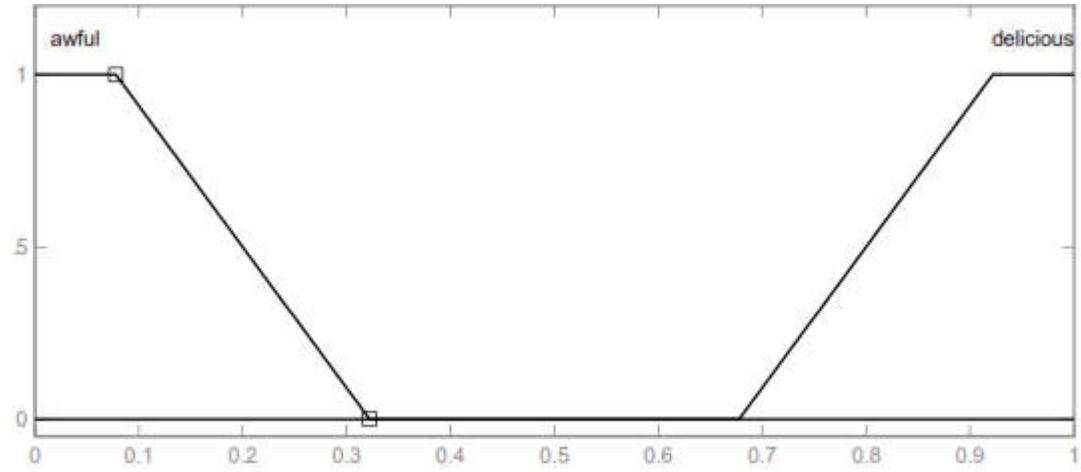

Figure 3-3 the selected membership function for quality of food

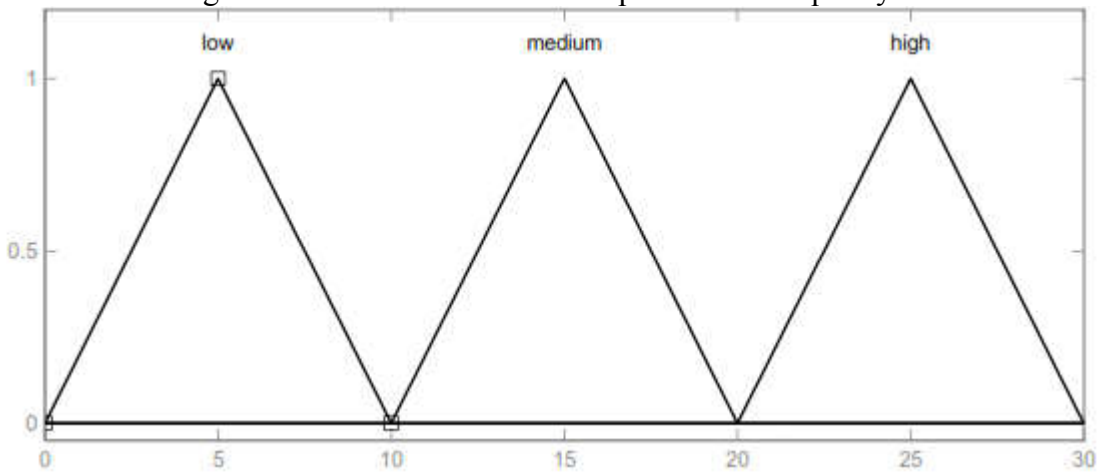

Figure 3-4 the selected membership function for tip amount

The concept of membership function allows to define a fuzzy system in natural language, which makes defining of the rules easier. The definitions of operators on fuzzy sets are not always the same and are chosen like membership functions. Table 3-1 shows two sets of operator definitions use for fuzzy sets, in which the membership function of a fuzzy set $A$ is shown as $\mu_A(x)$

Table 3-1 the operator definitions use for fuzzy sets

| **Name** | **Intersection (AND)** $\mu_{A\cap B}(x)$ | **Union (OR)** $\mu_{A\cup B}(x)$ | **Complement (NOT)** $\mu_{\overline{A}(x)}$ |
|---|---|---|---|
| Zadeh (min/max) | $\min\left(\mu_A(x),\mu_B(x)\right)$ | $\max\left(\mu_A(x),\mu_B(x)\right)$ | $1-\mu_A(x)$ |
| Probabilistic (prod/probor) | $\mu_A(x)\times\mu_B(x)$ | $\mu_A(x)+\mu_B(x)$ $-\mu_A(x)\times\mu_B(x)$ | $1-\mu_A(x)$ |

The fuzzy reasoning also known as approximate reasoning is depends on fuzzy rules, which are expressed in natural language. For example, for the tip problem which was mentioned before one of the rules can be defined as follows:

*if (the quality of service was low), then (tip is low)*

The degree of membership of the variable "quality of food" to the fuzzy set "low" depend on how worst the food was which specify the degree of membership of the variable "tip" to the fuzzy set "low". To determine the degree of truth of the proposition fuzzy "tip is low" the fuzzy implication should be defined, wide choices of fuzzy implications also exist. Table 3-2 shows two of the implications which are commonly used.

Table 3-2 definition of two of the most common fuzzy implication

| **Name** | **Truth value** |
|---|---|
| Mamdani | $\min\left(f_a(x),f_b(x)\right)$ |
| Larsen | $f_a(x)\times f_b(x)$ |

The result of the implication of fuzzy rules depend on the definition of the implication which was used, the membership function which was selected and the degree of validity of a fuzzy set in membership function. In order to get the final output, it should be clarified how each of the fuzzy rules impact the final output. This process is called defuzzification. Different methods are exist for

defuzzification, two of the most common methods are the method of the mean of maxima (MeOM) and the centroid method, which are explained in Table 3-3.

Table 3-3 the definition of the most common defuzzification method

| Method | Decision |
|---|---|
| MOM | $Decision = \frac{\int_s y dy}{\int_s dy}$ Where $S = \{y_m \in R, \mu(y_m) = SUP_{y \in R}(\mu(y))\}$ and R is the fuzzy set resulting from the aggregation of implication results. |
| centroid | $Decision = \frac{\int_s y\mu(u)dy}{\int_s \mu(u)dy}$ which $\mu(u)$ is the result of the rules were added together |

The centroid method is more commonly used. The specification of the Fuzzy logic system, used in this study is presented in Table 3-4.

Table 3-4 specification of the fuzzy algorithm, used in this study

| | |
|---|---|
| definition of AND | min |
| definition of OR | max |
| implication method | Mamdani |
| defuzzification method | centroid |

### 3.2 Neural Network Algorithm to Estimate The Tire Normal Load

Routine measurement of normal force at the tire-road contact patch has always been a challenging problem due to technical difficulties of mounting and implementing accurate sensors in tires. Intelligent tire concept has made it possible to measure various characteristics of tire-road interaction as well as estimate other parameters such as contact patch normal load.

Many studies have been done on integrating various types of sensors in tires [201, 202]. The so called “intelligent tire” concept has been used specifically to estimate tire-road friction in a few studies [203], [40] that show the application of intelligent tires in terrain/ride characteristics

identification [204, 205]. On the other hand, estimation of tire forces has also been investigated in other works [206, 207]. Although all of the estimations mentioned above help enhance vehicle/tire performance, estimation of contact patch length and normal load are the missing pieces of the puzzle.

In this study, a simple approach is introduced to estimate the contact patch length and normal load on the tire with constant inflation pressure by training an artificial neural network. A parameter will be introduced that is proportional to the contact patch length. That parameter, along with longitudinal velocity, will be used as inputs to the neural network. Two sets of data will be used to train and validate the neural network respectively.

### 3.2.1 Methodology

While the accelerometer attached to the inner-liner of the tire goes in and out of the contact patch two peaks are appeared in circumferential and radial component of the acceleration signal [40], [163]. The contact patch length is calculated as follows:

$$2a = \Delta t_p . v \qquad (2)$$

Where $a$ is half of the contact patch length, $\Delta t_p$ is the time difference between acceleration peaks and $v$ is longitudinal speed of the wheel. Sample data of accelerometer (radial and circumferential components) is shown in Figure 3-5. Although both radial and circumferential components of acceleration can be used to estimate the normal load, using circumferential component of acceleration leads to more accurate estimation of contact patch length [208] this is shown in Figure 3-6. For each tire revolution, the contact patch is determined using Equation 2; the encoder signal was used to extract the data of each tire revolution. Once the contact patch length is estimated, using the fact that in specific tire pressure the contact patch length is correlated to the tire normal

load, an Artificial Neural Network (ANN) based formulation was developed to estimate the tire normal load in terms of wheel angular velocity, inflation pressure and the contact patch length.

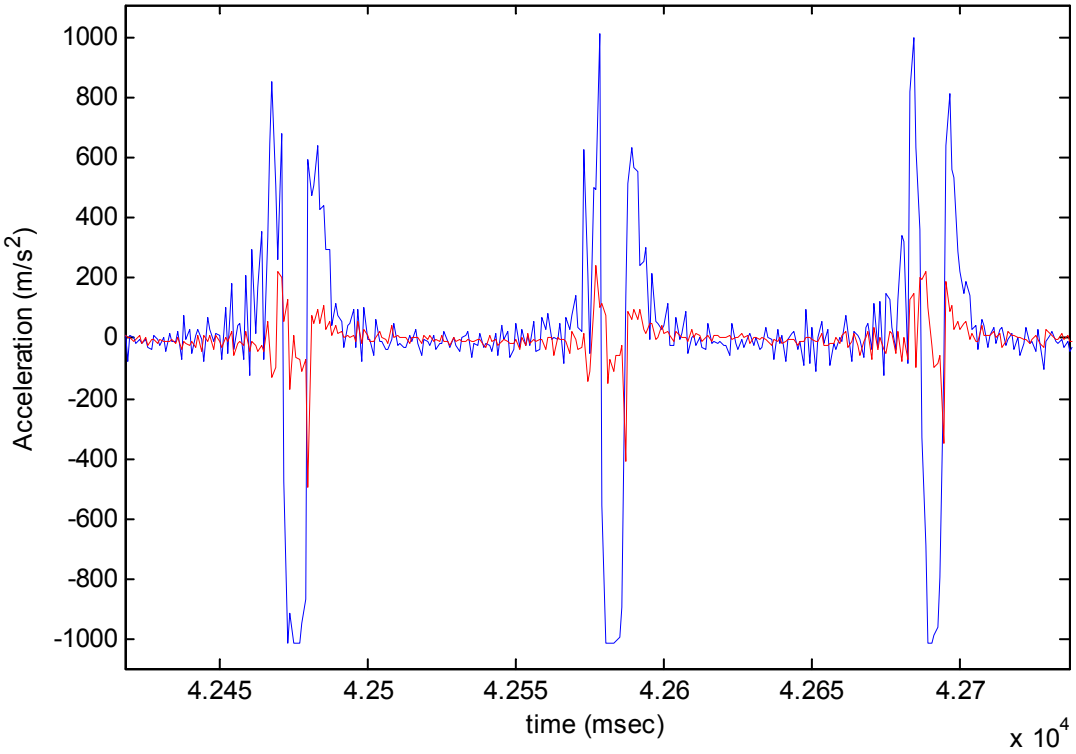


Figure 3-5 Radial(blue) and Circumferential(red) components of acceleration (raw data)

A two-layer feed-forward network with sigmoid hidden neurons and linear output neurons [209, 210], which uses thirty-five neurons in its hidden layer and also is appropriate for a multi-dimensional mapping problem, is used to fit on the data. The normal load estimation algorithm is presented in Figure 3-7.

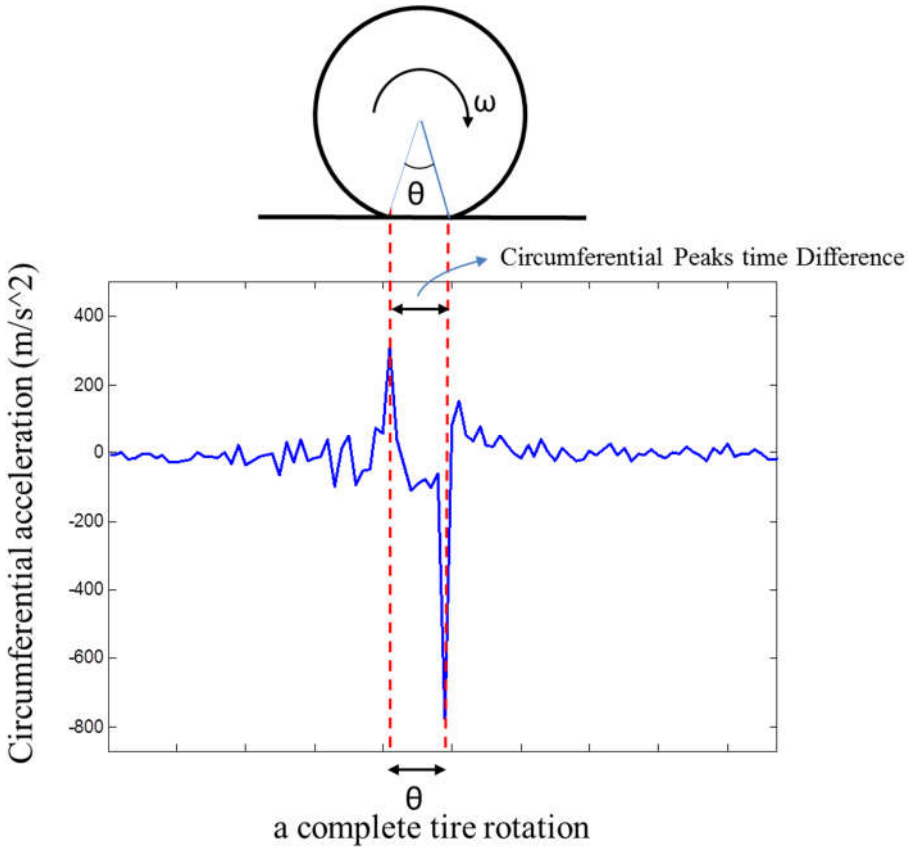


Figure 3-6 Circumferential component of acceleration signal indicates the contact patch length

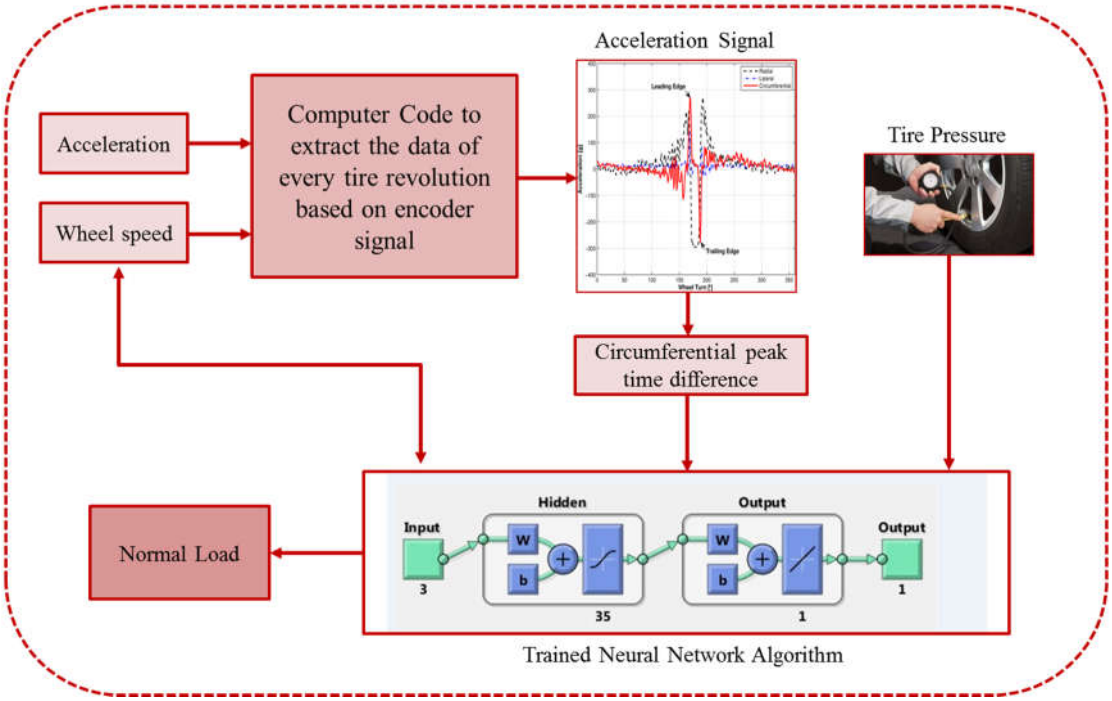


Figure 3-7 tire load estimation algorithm

### 3.3 Intelligent Tire Based Pressure Monitoring Algorithm

The other algorithm which is presented in this study is a tire pressure monitoring algorithm that uses the acceleration signal from the intelligent tire to monitor the pressure condition of the tire. For specific wheel speed and normal load, the deformation of the tire increases once the tire pressure drops below the nominal pressure. This leads to higher power in radial component of acceleration measured at the center of the inner-liner. Figure 3-8 shows the power of Radial acceleration for the longitudinal speed of 25 mph (11.176 m/s) and the normal load of 3000N.

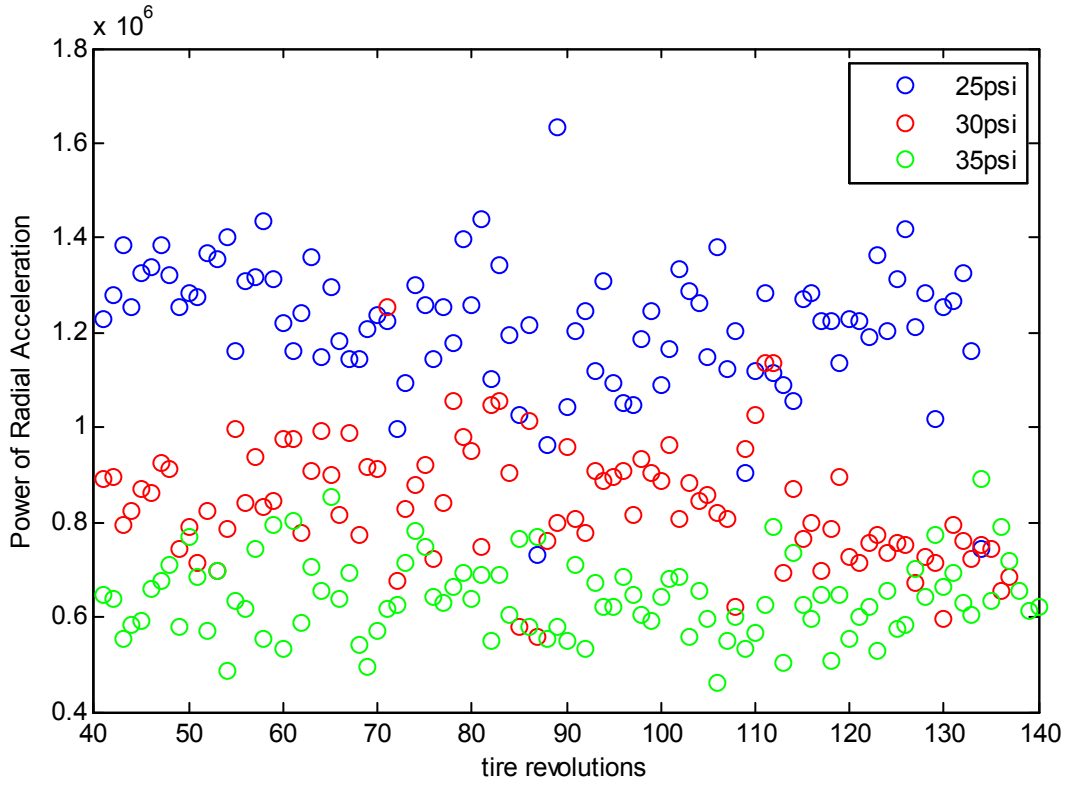


Figure 3-8 Power of acceleration signal in different tire inflation pressure

Reviewing the tire acceleration signal, another parameter was found in radial component of acceleration signal, which doesn't change much with the normal load and is sensitive to the tire inflation pressure and wheel speed, this parameter is shown in Figure 3-9. The radial peak difference doesn't change significantly with changing the normal load; however it changes with

the tire inflation pressure and the wheel velocity; this can be seen in Figures Figure 3-10 and Figure 3-11.

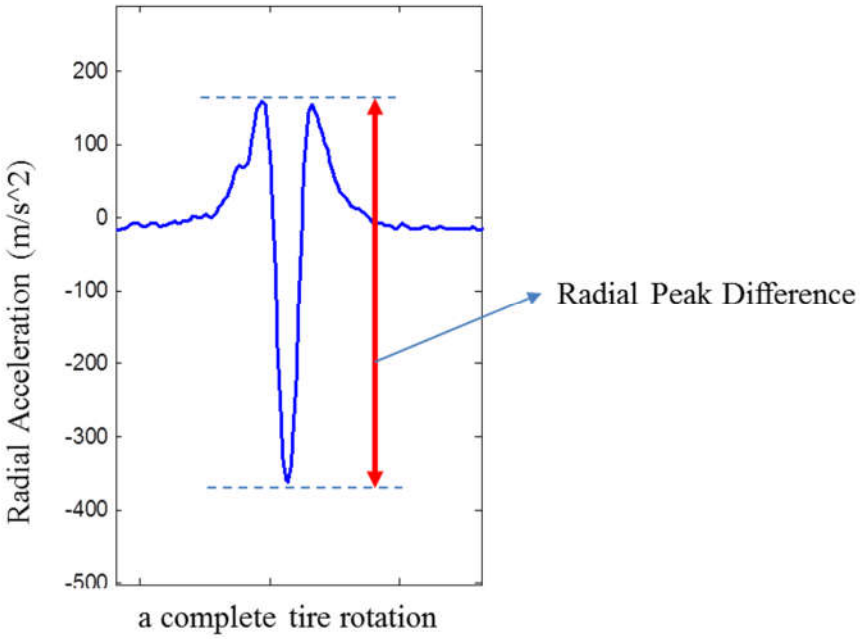


Figure 3-9 the radial peak difference

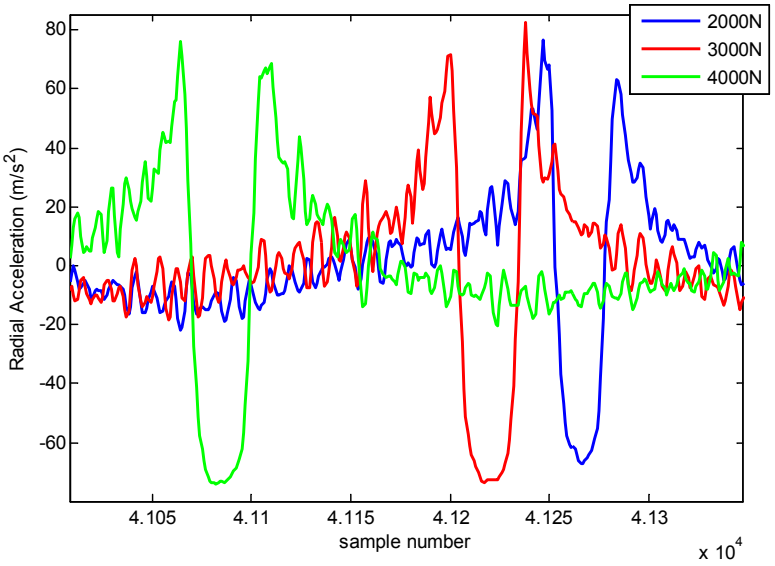


Figure 3-10 Radial acceleration for different normal loads

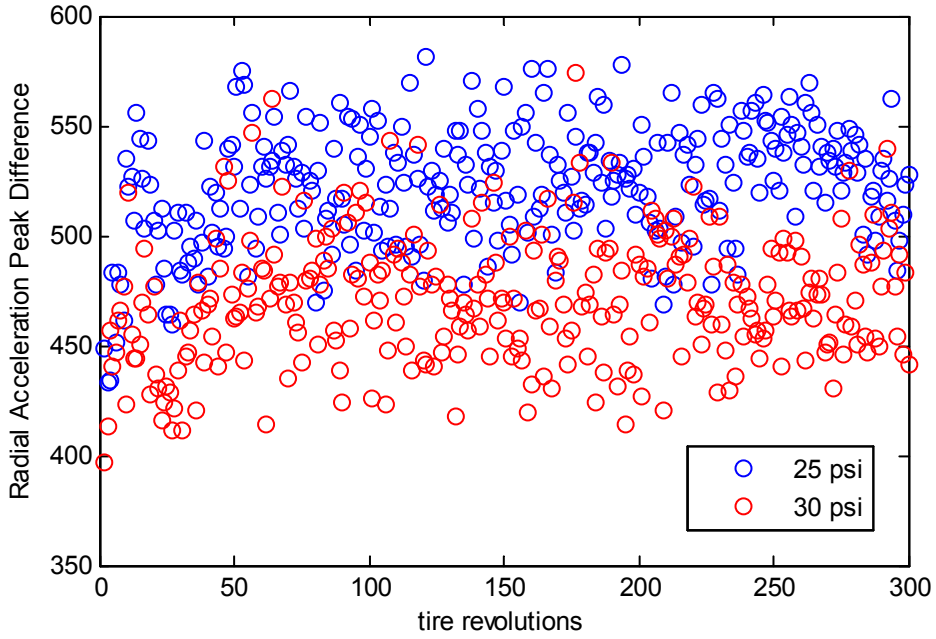


Figure 3-11 Radial acceleration peak difference for longitudinal velocity of 30 mph and different tire inflation pressures

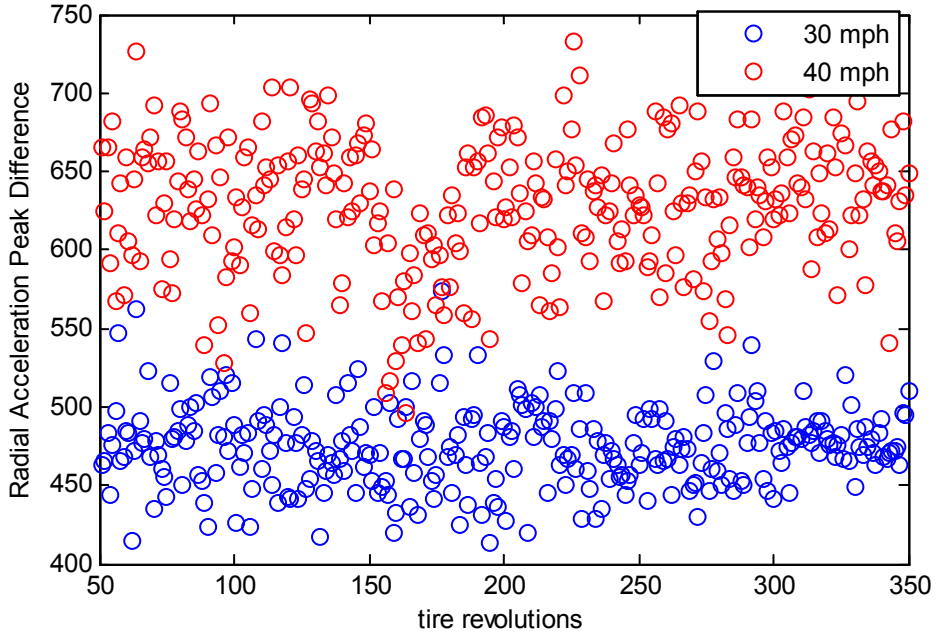


Figure 3-12 Radial acceleration peak difference for tire inflation pressure of 30psi and different longitudinal velocities

As it was discussed in the previous section, the circumferential acceleration peak's time difference (the time difference between circumferential peaks) represents the contact patch length, which is correlated to the tire normal load in specific speed and tire pressure. In another word, the contact patch length is proportional to the normal load and the radial peak difference is proportional to the wheel velocity and tire pressure. Using the data of the intelligent tire with the nominal pressure (in this case 30 psi), a Neural network was developed and trained to estimate the wheel speed based on circumferential peak's time difference (represents the normal load) and the radial peak difference. Since the radial peak difference is proportional to both tire inflation pressure and wheel speed, it is expected that the results of trained Neural Network algorithm (just using the data of nominal inflation pressure) would be off for other inflation pressures below the nominal pressure. Although the estimated wheel speed using this algorithm is different with the measured wheel speed (which is an available signal), the difference is not high enough that could be used as a powerful tool to estimate the tire inflation pressure.

Another Neural Network algorithm was developed and trained to estimate the power of radial acceleration signal using the intelligent tire data with nominal tire pressure. The inputs for this algorithm are the estimated wheel speed from the previous step, circumferential acceleration peaks' time difference (represents the normal load) and the radial peak difference (represents the tire inflation pressure). Again, it is expected that the estimated power of radial acceleration using the trained algorithm would be off for the cases with the tire pressure other than nominal pressure, since jus the data of a tire with the nominal pressure was used to train the algorithm. However, in this case difference (between estimated power and actual power) would be significant that could be used to monitor the tire pressure. The two steps pressure monitoring algorithm is shown in Figure 3-13.

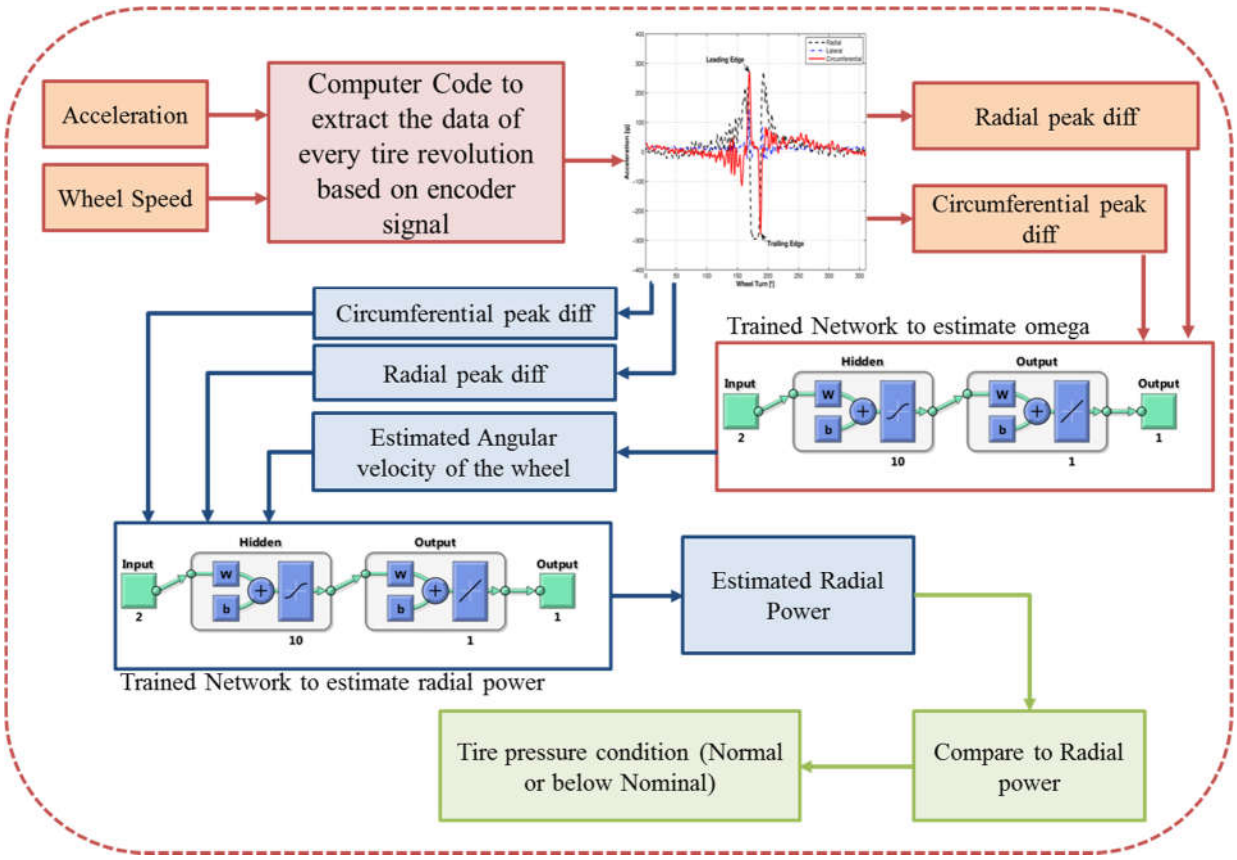


Figure 3-13 The two steps algorithm to monitor the tire inflation pressure

## 3.4 Intelligent Tire Based Road Condition Monitoring Algorithm

The other intelligent tire based estimation algorithm which was developed in this study is a road condition monitoring system. It was shown in the literature that the contact patch length (the circumferential peaks' time difference) and the radial acceleration signal in both time and frequency domains do not change much by changing the road condition from wet to dry [69]. However, it is observed that the power of circumferential component of acceleration changes significantly when the road surface changes from dry to wet, especially for the frequencies between 10-100 Hz. Figure 3-14 shows the Power Spectral Density for two cases with the same wheel speed and tire pressure on wet and dry surfaces.

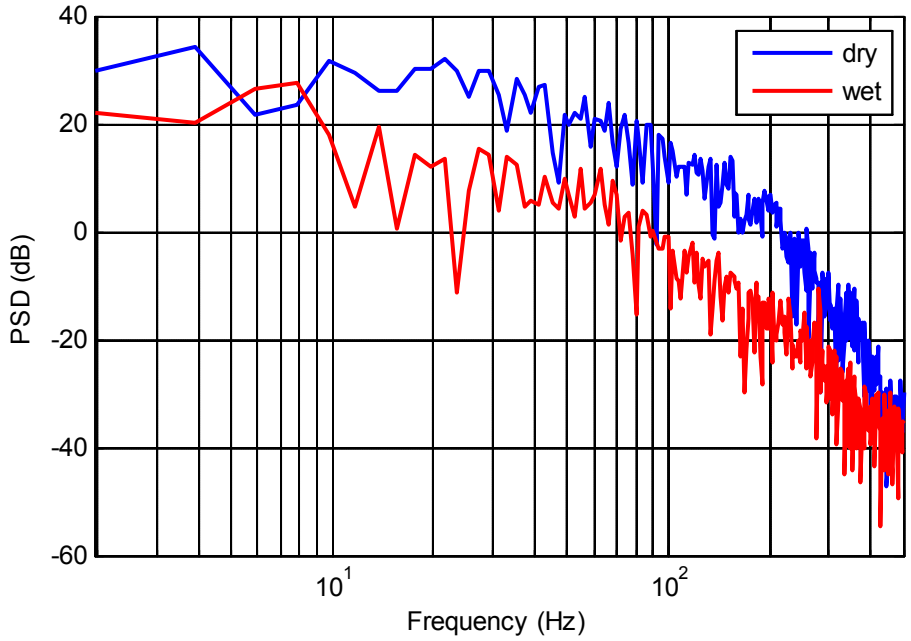

Figure 3-14 Power spectral density of Circumferential acceleration, longitudinal speed = 30mph and tire pressure = 30 psi

A Neural Network is trained to estimate the road conditions. The algorithm works once every five revolutions of the wheel, and takes the average data of those five revolutions as input. The inputs to the algorithm are the power of circumferential acceleration signal (for the frequencies between 10-100 Hz), the average of circumferential peaks' time difference (represents the contact patch length and normal load), the average of radial acceleration peak difference (represents the tire pressure) and the average of angular speed of the wheel. The schematic of the road condition monitoring algorithm is presented in Figure 3-15.

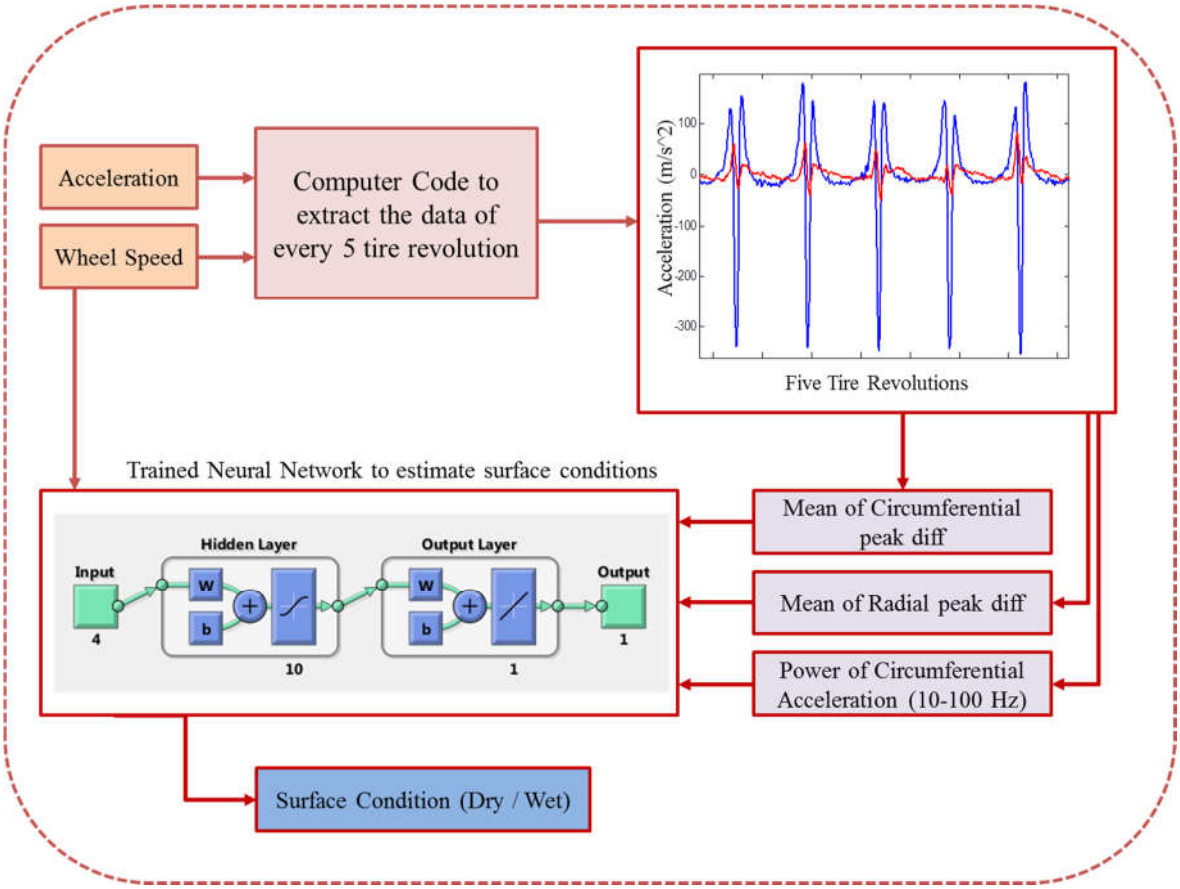


Figure 3-15 the road condition monitoring algorithm

### 3.5 New Friction Estimation Algorithm:

Tire-road friction estimation plays one of the most important roles in designing traction and stability controllers. Accurate estimation of tire-road friction potential will increase the effectiveness of traction, stability and ABS controllers, which can lead to reduction of the number of weather related crashes. The tire-road friction estimation has been a topic of research for several decades.

A three-step intelligent tire based friction estimation algorithm is proposed in this study. In the first step the tire's normal load is estimated using intelligent tire (which was explained in previous section). The tire forces (longitudinal and lateral) are estimated in the second step using Kalman

filter along with the measurements of the vehicle's regular sensors. Once the tire forces and tire load are available, the friction is estimated as follows [20]:

$$\rho = \frac{\sqrt{F_x^{\,2} + F_y^{\,2}}}{F_z} \qquad (3)$$

Where $F_x, F_y, F_z$ are longitudinal, lateral and normal load respectively, $\rho$ is a factor between 0 and 1, its maximum value is friction coefficient $(\mu)$. The friction estimation algorithm is shown in Figure 3-16.

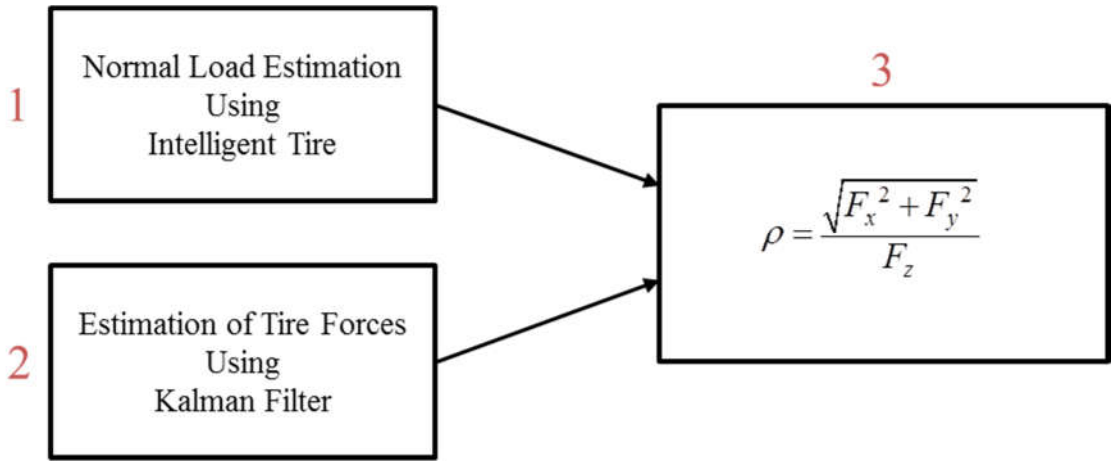


Figure 3-16 three-steps friction estimation algorithm

### 3.5.1 Methodology:

Different algorithms have been used to estimate the tire-road friction; some of them are discussed next.

#### 3.5.1.1 Open loop Friction estimation:

The first method which is discussed in this study is open loop estimation algorithm which is directly based on dynamical equation of the motion. To estimate the longitudinal force, single wheel tire model is used; Figure 3-17 shows the free body diagram of one wheel model in acceleration mode [214].

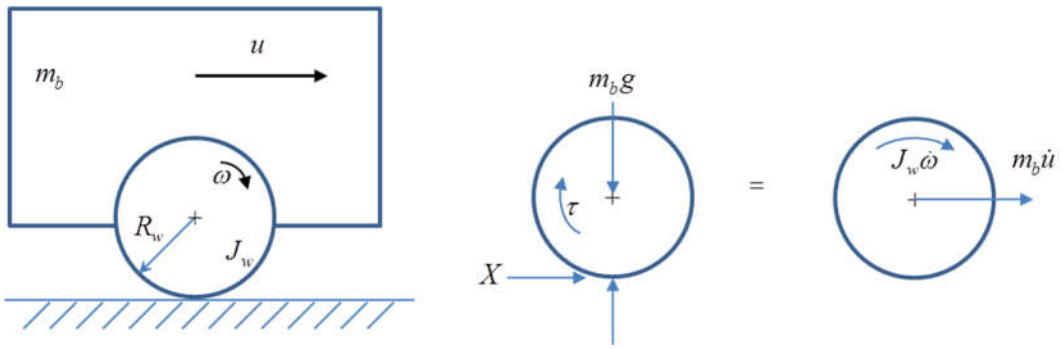


Figure 3-17 Free body diagram of single wheel model in acceleration mode

The angular dynamical equation of the motion for the wheel is given as:

$$J_w\dot{\omega} = (T_{drive} - T_{brake}) - F_x R_w - F_{rr} R_w \qquad (4)$$

Where $J_w$ is the tire's moment of inertia, $R_w$ is the effective radius of the wheel and $F_{rr}$ is the rolling resistance force which can be calculated as follows:

$$F_{rr} = 0.005 + 3.24 \cdot 0.01 \cdot (R_w\omega)^2 \qquad (5)$$

Rearranging equation (2), the longitudinal force can be found as follows:

$$F_x = \frac{(T_w - T_b) - J_w\dot{\omega}}{R_w} - F_{rr} \qquad (6)$$

Here the equation of motion was presented for one of the wheels; however they are valid for all four wheels. The planar model is used to estimate the lateral force; Figure 3-18 shows the free body diagram for this model [214].

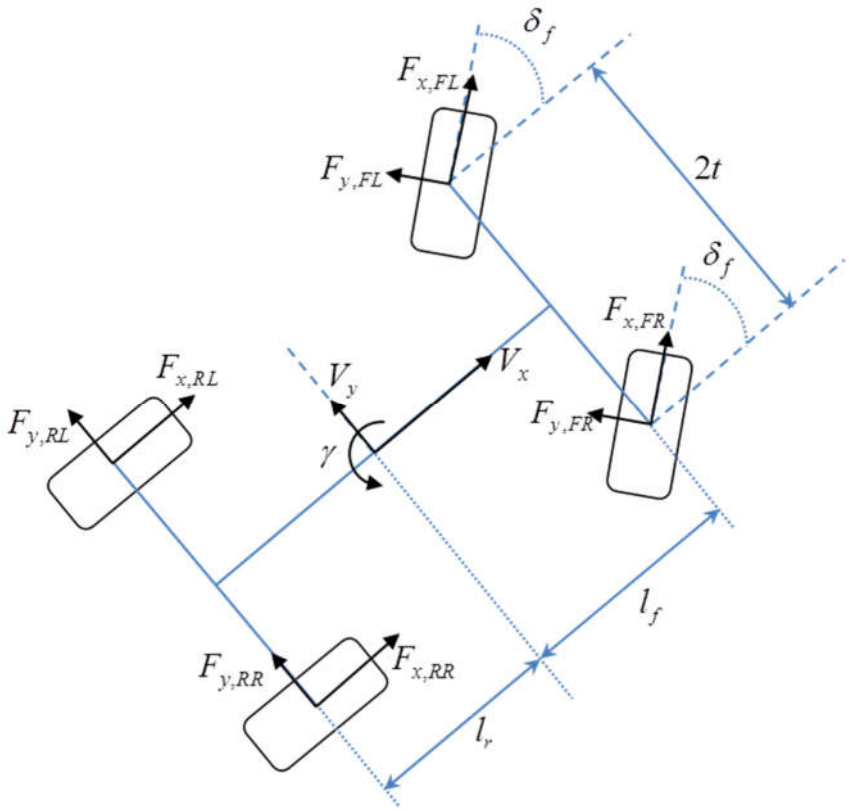


Figure 3-18 the free body diagram for the planar model

The lateral tire forces, shown in Figure 16 are presented as follows:

$$F_{y1} = F_{y,FL} + F_{y,FR}$$
$$F_{y2} = F_{y,RL} + F_{y,RR} \qquad (7)$$

Where the subscripts FL, FR, RL and RR stand for front left, front right, rear left and rear right, respectively. Assuming small steering angle ( $\delta$ ), the estimated lateral tire forces are calculated as follows [211]:

$$F_{y1} = \frac{ml_f a_y + I_z\dot{\psi} - t(F_{x,FL} + F_{x,RL} - F_{x,FR} - F_{x,RR})}{l_f + l_r} - (F_{x,FL} + F_{x,FR})\delta$$
$$F_{y2} = \frac{ml_f a_y - I_z\dot{\psi} + t(F_{x,FL} + F_{x,RL} - F_{x,FR} - F_{x,RR})}{l_f + l_r} \qquad (8)$$

Where $m$ is total mass of the vehicle, $l_f$ , $l_r$ are the distance of the vehicle's CG from the front and rear axle respectively, $t$ is half of the track length, $a_y$ is lateral acceleration at the CG, $I_z$ is the vehicle's moment of inertia around z axis and $\dot{\psi}$ is the yaw rate.

The open loop estimation method is an easy way to estimate the longitudinal and lateral force and it might work for simulation of low slip vehicle maneuvers (the data without noise), however in real world the sensors data are noisy, also to solve for the longitudinal force from equation 4, the time derivative of angular speed is needed which is not available directly in real world measurements. Kalman filter and sliding mode observer are two other estimation algorithms which are explained next as two alternatives for estimating the tire forces.

#### 3.5.1.2 Kalman Filter:

Kalman filter is a recursive estimation method which is used to estimate the tire longitudinal force. A linear system can be modeled as a combination of measurements with a stochastic process [212]. The model is shown in equations 8 and 9.

$$x_k = Ax_{k-1} + Bu_k + w_k \tag{9}$$

$$z_k = H_k x_k + v_k \tag{10}$$

Where $x_k$ is the state vector at time k, $u_k$ is the input control vector, $w_k$ is process noise, $z_k$ is the measurement made at time k, $v_k$ is additive measurement noise and $H_k$ is the observation matrix. The Process noise and measurement noise are assumed to be mutually independent random variables, spectrally white with normal probability distributions

$$p(w) = N(0, Q) \tag{11}$$

$$p(v) = N(0, R) \tag{12}$$

Where, process noise covariance Q and measurement noise covariance R matrices are assumed to be constant. The Kalman filter estimates the state by minimizing the posteriori estimation error covariance using two stages of prediction and correction.

$$prediction \begin{cases} \hat{x}_k^- = A\hat{x}_{k-1} + Bu_k \\ P_k^- = AP_{k-1}A^T + Q \end{cases} \tag{13}$$

$$correction \begin{cases} K_k = P_k^- H^T (HP_k^- H^T + R)^{-1} \\ \hat{x}_k = \hat{x}_k^- + K_k (z_k - H\hat{x}_k^-) \\ P_k = (I - K_k H) P_k^- \end{cases} \tag{14}$$

Where, $K$ is the Kalman gain matrix. In this study, again, a single wheel vehicle model is used as the simplified dynamic model to estimate the longitudinal force and random walk model is assumed for the longitudinal friction force ( $\dot{F}_x = 0$ ). A linearized set of equations is given as:

$$\dot{u} = -\frac{1}{m_b} F_x - \frac{1}{m_b} F_{rr} \tag{15}$$

$$\dot{\omega} = \frac{(T_{drive} - T_{brake}) - F_x R - F_{rr} R}{J} \tag{16}$$

$$\dot{F}_x = 0 \tag{17}$$

Where $m_b$ is one fourth of the total vehicle mass. It is assumed that the angular speed of the wheel is measured; A, B and H matrices in equations 11 and a12 are as follow:

$$A=\begin{bmatrix} 0 & 0 & \frac{-1}{m_b} \\ 0 & 0 & \frac{-R}{J} \\ 0 & 0 & 0 \end{bmatrix}, B=\begin{bmatrix} \frac{-1}{m_b} & 0 & 0 \\ \frac{-R}{J} & \frac{1}{J} & \frac{-1}{J} \\ 0 & 0 & 0 \end{bmatrix}, H=\begin{bmatrix} 0 & 1 & 0 \end{bmatrix} \quad (18)$$

### 3.5.1.3 Sliding Mode Observer:

Sliding mode observer uses a sliding mode structure, the estimated state $\hat{\omega}$ (the estimated angular velocity of the wheel) and angular motion of a single wheel to estimate the tire's longitudinal force. Again; random walk model ( $\dot{F}_x = 0$ ) is used to model the force. The proposed sliding mode observer is expressed as:

$$\begin{aligned} J\dot{\hat{\omega}} &= (T_{drive} - T_{brake}) - \hat{F}_x - F_{rr}R + \lambda \operatorname{sgn}(\omega - \hat{\omega}) \\ \dot{\hat{F}} &= -\eta \operatorname{sgn}(\omega - \hat{\omega}) \end{aligned} \quad (19)$$

Where $\lambda, \eta$ are observer gains and sgn is the signum function which is defined as:

$$\operatorname{sgn}(x) = \begin{cases} 1 \; if \;\; x > 0 \\ 0 \; if \;\; x = 0 \\ -1 if \;\; x < 0 \end{cases} \quad (20)$$

It is proved that if $\lambda$ is positive the observer is stable and $\hat{F}_x \to F_x$ as $t \to \infty$ [213].

Both of Kalman filter and sliding mode observer are expected to show good performance for normal driving conditions, however in extreme driving maneuvering conditions which the slip ratio is high, their performance is not satisfactory. To solve this problem, combined tire-force estimation is introduced.

#### 3.5.1.4 Combined Tire-Force Estimation:

The combined tire-force observer is a Kalman filter based observer, which uses planar dynamic model and longitudinal acceleration, lateral acceleration and yaw rate as the measured states. New states are defined as follow [211]:

$$\begin{aligned}
\xi_1 &= F_{y,f} - \hat{F}_{y,f} \\
\xi_2 &= F_{y,r} - \hat{F}_{y,r} \\
\xi_3 &= F_{x,FL} - \hat{F}_{x,FL} \\
\xi_4 &= F_{x,FR} - \hat{F}_{x,FR} \\
\xi_5 &= F_{x,RL} - \hat{F}_{x,RL} \\
\xi_6 &= F_{x,RR} - \hat{F}_{x,RR}
\end{aligned} \tag{21}$$

Where $F_{y,f}, F_{y,r}, F_{x,i}$ are real values and $\hat{F}_{y,f}, \hat{F}_{y,r}, \hat{F}_{x,i}$ are estimated values from one of the methods of Kalman filter or sliding mode observer which were introduced previously. The dynamic equations along longitudinal, lateral and yaw rate are expressed as follow [211]:

$$\begin{aligned}
ma_x &= F_{x,FL} + F_{x,FR} + F_{x,RL} + F_{x,RR} - F_{y,f}\delta \\
ma_y &= F_{y,f} + F_{y,r} + F_{x,FL}\delta + F_{x,FR}\delta \\
I_z &= l_f F_{y,f} - l_r F_{y,r} + t(-F_{x,FL} + F_{x,FR} - F_{x,RL} + F_{x,RR}) + l_f (F_{x,FL} + F_{x,FR})\delta
\end{aligned} \tag{22}$$

Once the Longitudinal and lateral tire force were estimated, using the value of the normal load obtaining from intelligent tire technology, the friction coefficient is estimated in the third step.

#### 3.5.1.5 Combined experiment vehicle dynamic based friction estimation algorithm:

In this section, the combined experiment-vehicle dynamic base model is explained in more detail, Figure 3-19shows the schematic of new friction estimation algorithm.

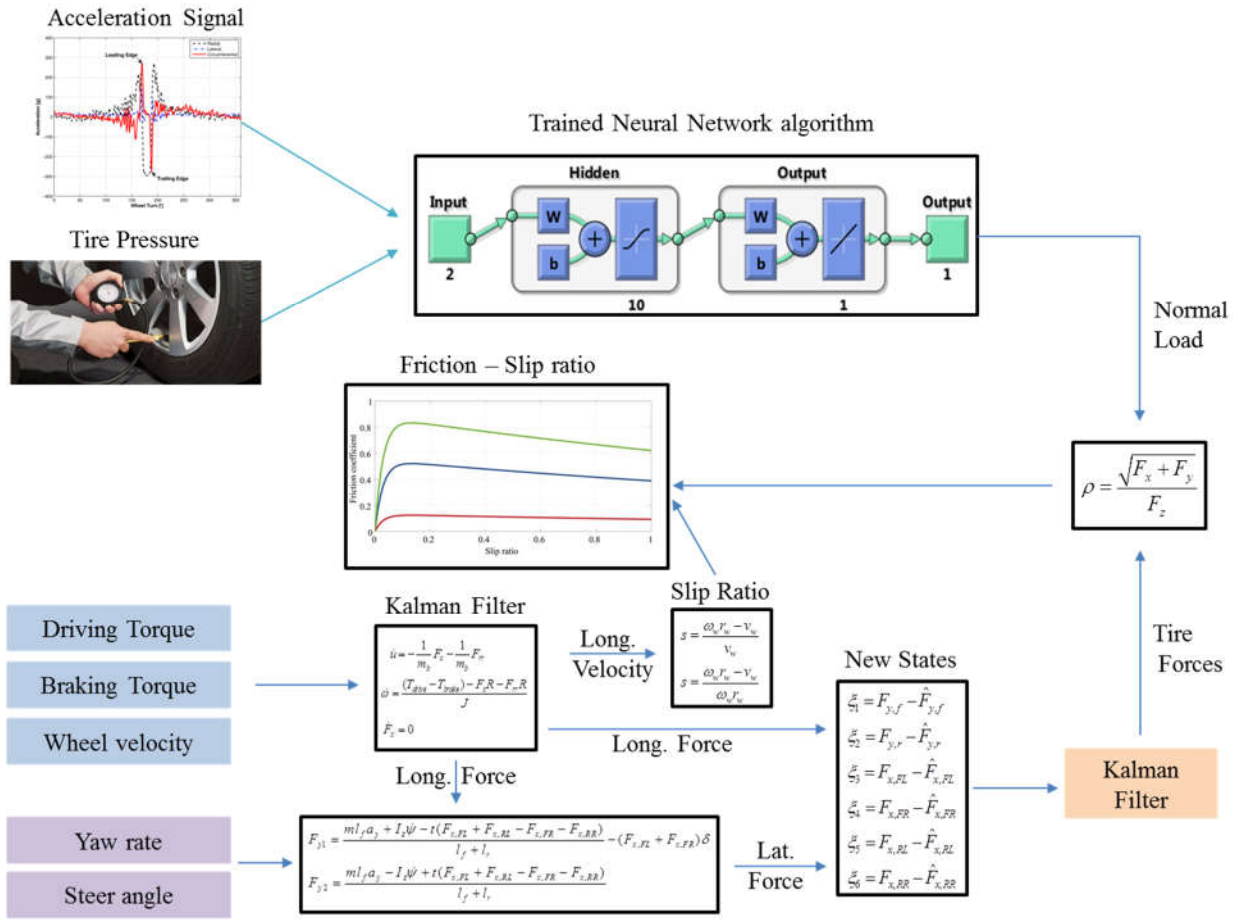


Figure 3-19 Schematic of combined experiment-vehicle dynamic based algorithm

This algorithm can be applied in real-time, in each tire revolution, the tire normal load is estimated using the trained Neural Network algorithm; the inputs of this algorithm are the acceleration signal from the intelligent tire and the tire pressure. The tire longitudinal speed and tire longitudinal force (the first estimation of tire longitudinal force) are estimated using the Kalman filter, which was introduced in section 3.5.1.2. The longitudinal speed is used to estimate the slip ratio using Equation (2.1).

The first estimation of the lateral tire force is made using Equation (8); the inputs are the estimated longitudinal force, steering angle and the yaw rate. As it was shown in previous sections, the estimated tire forces (presented in section 3.5.1.2. & 3.5.1.3.) are not accurate enough in high slip

vehicle maneuvers, so the estimated tire forces (from Kalman filter method) are used as the first guess and new states are defined by Equation (21). Using the combined tire-force estimation method presented in section 3.5.1.4., the tire forces are estimated.

Once the tire forces and tire load are estimated, the friction is estimated using Equation (3). Finally μ-slip curve is plotted using the estimated data of friction and slip ratio.

## 3.6 Conclusions:

Different algorithms developed in this study were discussed in this chapter. Five main algorithms were presented; first, a Fuzzy Logic based terrain classification algorithm for the wheeled ground robot. The algorithm used the wheel velocity, power of acceleration signal from the intelligent tire and the wheel slip as inputs and classified all surfaces into four known categories; asphalt, concrete, grass and soil. The second algorithm which was developed in this study was a Neural Network algorithm to estimate the tire contact length and normal load. The inputs of this algorithm are the tire pressure, angular speed of the wheel, and the acceleration signal from the intelligent tire, and the output is the tire normal load.

The third algorithm was a two-step pressure monitoring algorithm; in its first step, the angular velocity of the wheel is estimated based on radial acceleration peak difference and circumferential acceleration peaks' time difference using a trained neural network. Then the estimated wheel angular velocity from the first step is used along with the circumferential acceleration peaks' time difference, and radial acceleration peak difference to estimate the power of radial acceleration. The estimated power is compared to the actual one and the tire pressure condition is judged to be "normal" or "low pressure".

The forth algorithm, which is also an intelligent tire based algorithm, was a road condition monitoring algorithm. Using the power of circumferential acceleration for the frequencies between 10-100 Hz, circumferential acceleration peaks' time difference, the angular speed of the wheel and radial acceleration peak difference, the road condition is classified into wet and dry surfaces through a trained neural network algorithm. Finally, different model based friction estimation algorithms were introduced. Also, a new combined experiment-vehicle dynamic based friction estimation algorithm was proposed.

# 4 Results and Discussion

In this chapter, some of the results of the algorithms, which were introduced in Chapter Three are presented. First, the results for the proposed Fuzzy Logic based algorithm which uses the robot's wheel velocity, power of acceleration signal from the interaction between tire and surface and the wheel slip as inputs and classifies all different surfaces into four known categories; asphalt, concrete, grass and soil are discussed.

Second, a Neural Network (NN) algorithm was trained to estimate the tire normal load using the acceleration signal measured inside the tire. The inputs of the algorithm are the acceleration signal, the wheel speed and the tire pressure and the output is the tire normal load. Third, a two-step intelligent tire based algorithm was proposed to monitor the tire pressure. The inputs of this algorithm are acceleration signal from the intelligent tire and the wheel speed and the output is the tire pressure condition.

Forth, another intelligent tire based algorithm was proposed to monitor the road conditions. The inputs of this algorithm are also the acceleration signal and the wheel velocity and the output is the road condition. Also, different model based friction estimation algorithms were presented in the previous chapter, the performance of each of these algorithms was evaluated in high-slip and low-slip vehicle maneuvers using Carsim data.

## 4.1 Fuzzy Logic Based Terrain Classification:

The six-wheeled ground robot was used to terrain a fuzzy logic based surface classification algorithm. It was observed that the power of the acceleration signal, acquired from the interaction between the robot's tire and different surfaces is different for the frequencies below 20 Hz. Figure 4-1 shows the power spectral density of the acceleration signal with the same speed on different surfaces, calculated using pwelch command in Matlab.

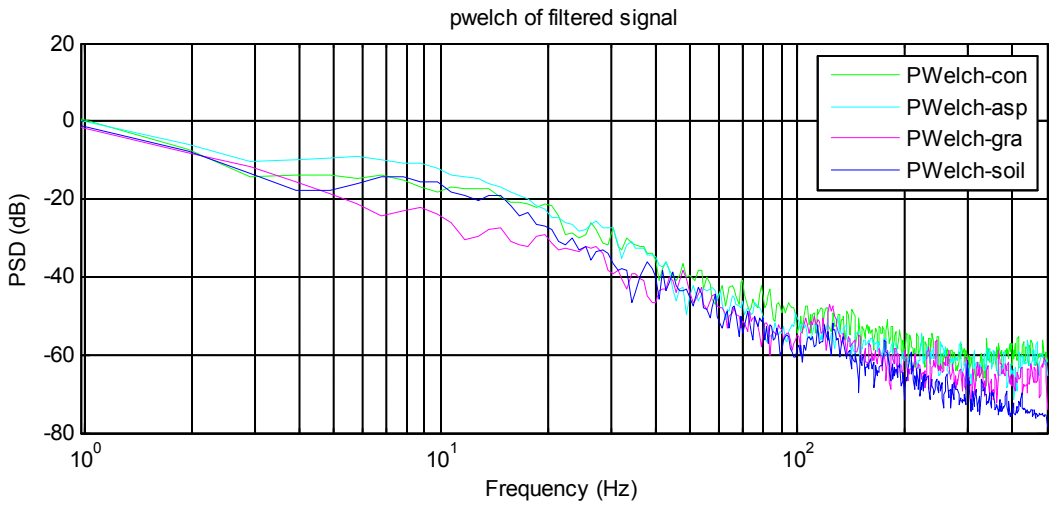


Figure 4-1 power spectral density of the acceleration data on different surfaces

Also, the slip ratio at the beginning of the motion, calculated from the speed of driven and non-driven wheel for a specific speed, is the other parameter which changes on different surfaces and is used to classify different surfaces. Figure 4-2 depicts wheel slip ratio on different surfaces for the same longitudinal speed.

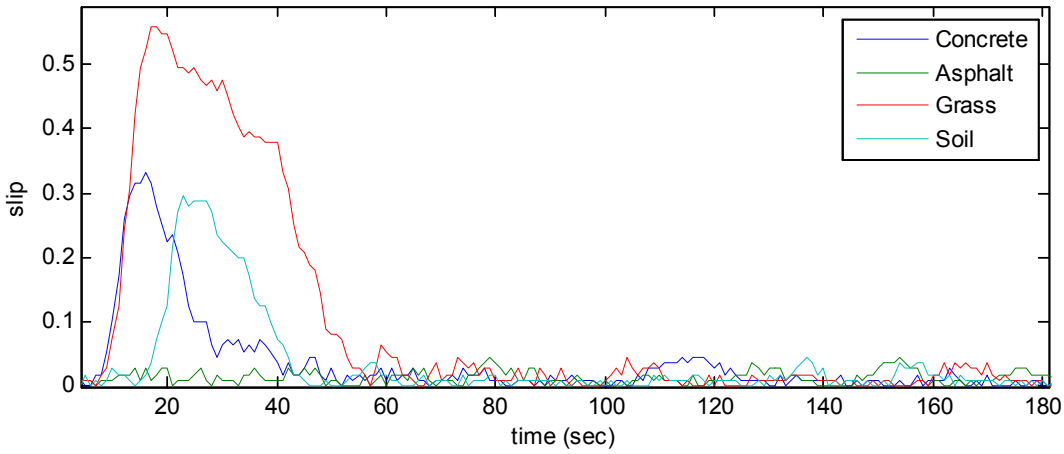


Figure 4-2 slip, calculated from the speed of driven and non-driven wheels on different surfaces

To classify different surfaces, an experiment was setup in the lab which uses four different surfaces of concrete, asphalt, grass and soil. Results were used to define the fuzzy rules. Table 1-1 shows the design of experiment for this study.

Table 4-1 design of experiment for surface classification study

| **Surface type** | **Wheel speed (rpm)** |
|---|---|
| Asphalt | 30 , 50, 70 ,90 |
| Concrete | 30 , 50, 70 ,90 |
| Grass | 30 , 50, 70 ,90 |
| Soil | 30 , 50, 70 ,90 |

Power of acceleration signal and the mean values of slip ratio at the beginning of motion for different robot wheel speeds are shown in Figure 4-3 and Figure 4-4, respectively [215].

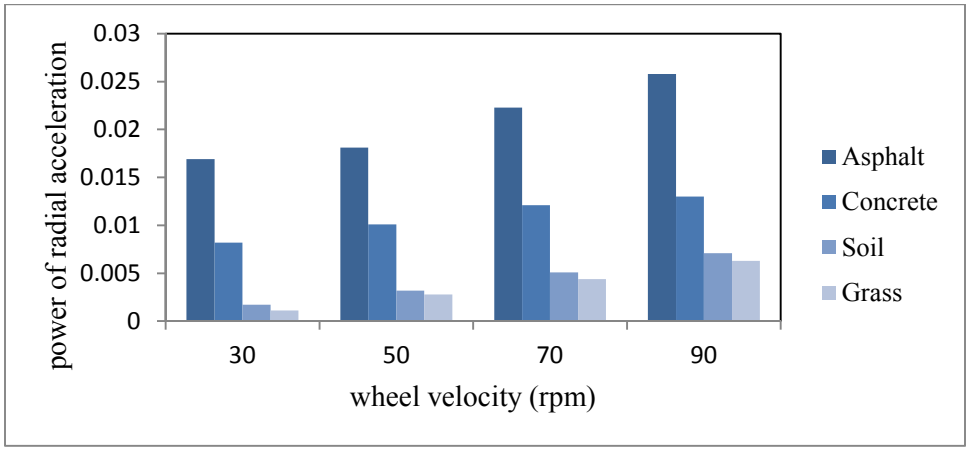


Figure 4-3 power of acceleration signal for different wheel speed on different surfaces

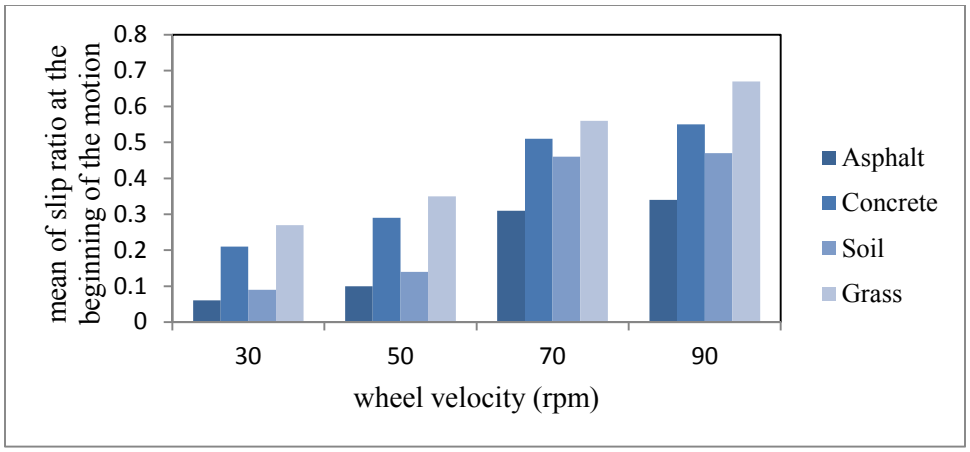

Figure 4-4 mean of slip ratio for different wheel velocities on different surfaces

These two parameters, power of radial component of acceleration signal (below 20 Hz) and the mean of the slip ratio value at the beginning of the motion, along with robot's wheel velocity are considered as the inputs to the fuzzy algorithm and the surface type is the output, Mamdani was used as the implication method. The Fuzzy Logic algorithm used for terrain classification is shown in Figure 4-5 .

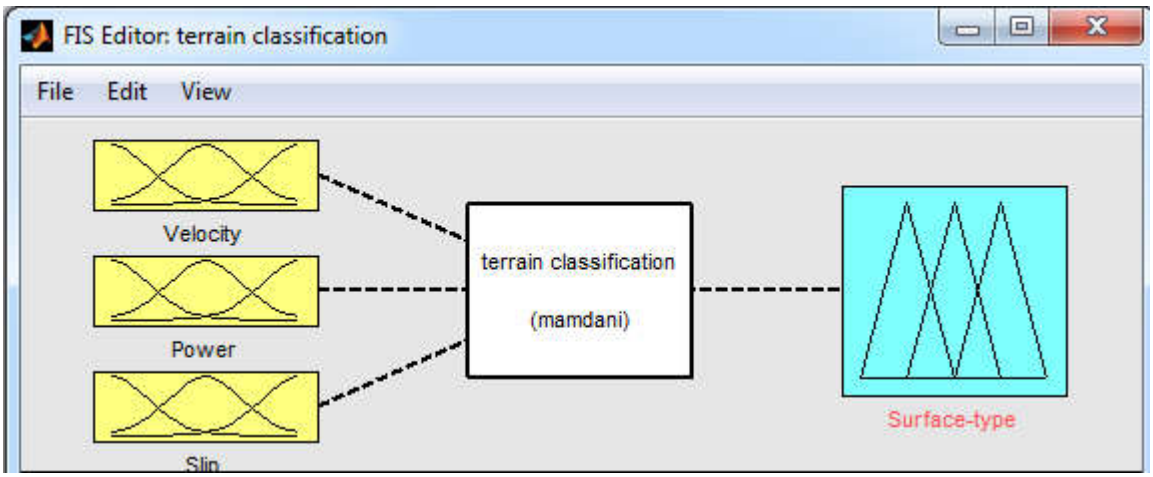

Figure 4-5 fuzzy logic terrain classification algorithm

The fuzzification was done using the collected data; Figure 4-6, Figure 4-7, Figure 4-8, Figure 4-9 show the fuzzy sets selected for the inputs and the output of this fuzzy system [215].

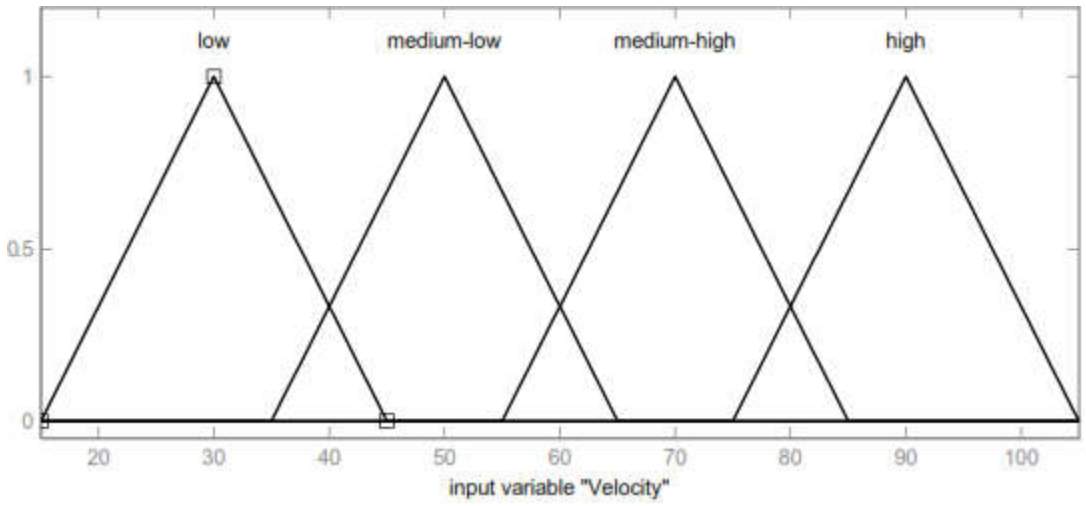


Figure 4-6 Fuzzy set selected for the input variable “velocity”

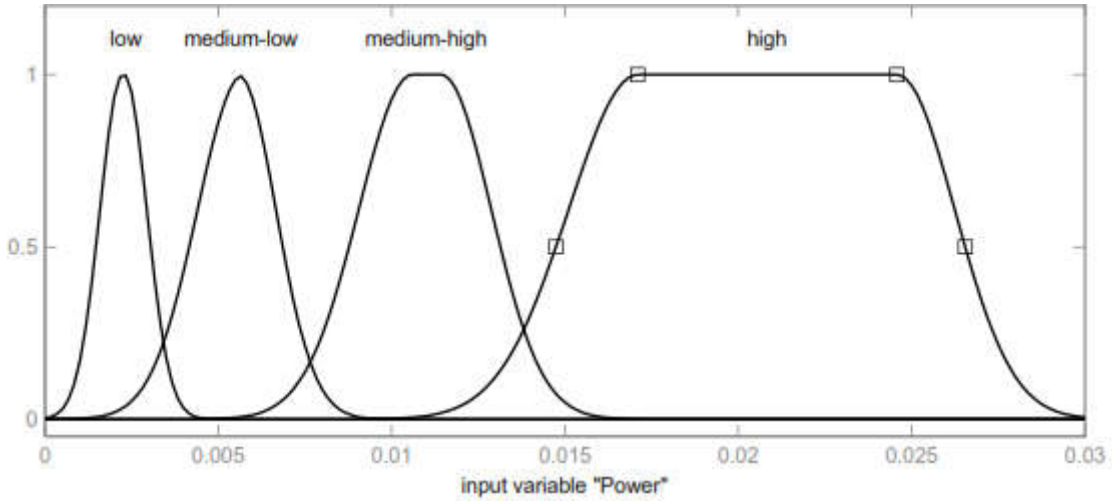


Figure 4-7 Fuzzy set selected for the input variable “power of acceleration”

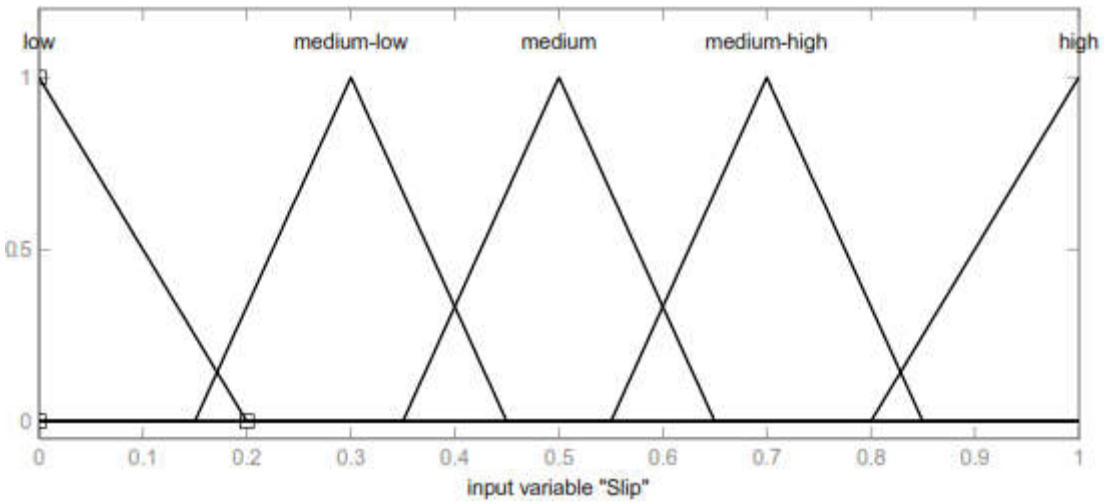


Figure 4-8 Fuzzy set selected for the input variable “wheel slip”

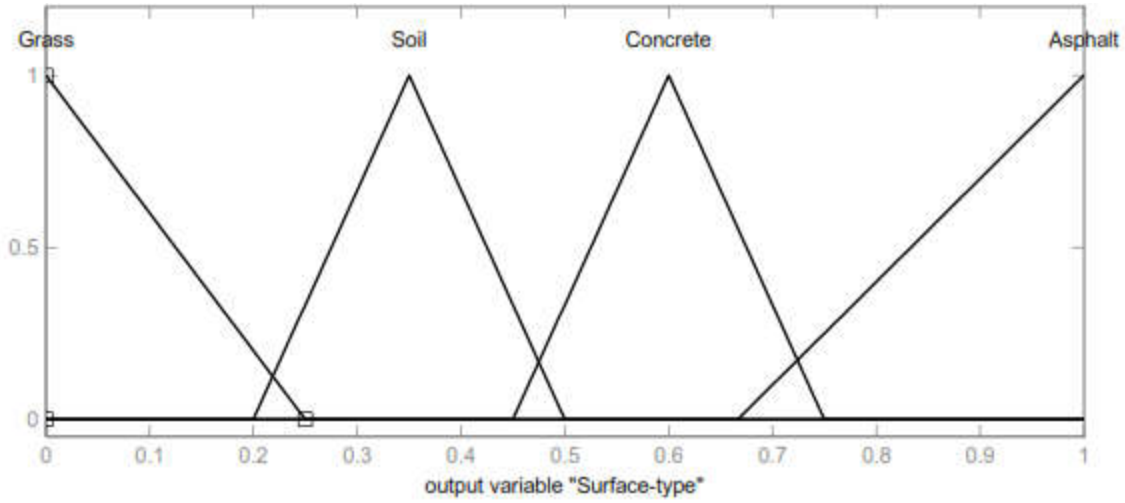


Figure 4-9 Fuzzy set selected for the output variable “surface type”

Figure 4-10 shows the list of fuzzy rules used for this study, the fuzzy rules are defined based on the collected data for instance, for the wheel speed of 30, the power of the signal on the asphalt was 0.0169 and the maximum slip ratio was 0.06 so the following fuzzy rule was defined:

*If the speed is “low” and the power is “high” and the slip is “low” then the surface is “asphalt”*

The surface viewer of terrain classification algorithm is shown in Figure 4-11.

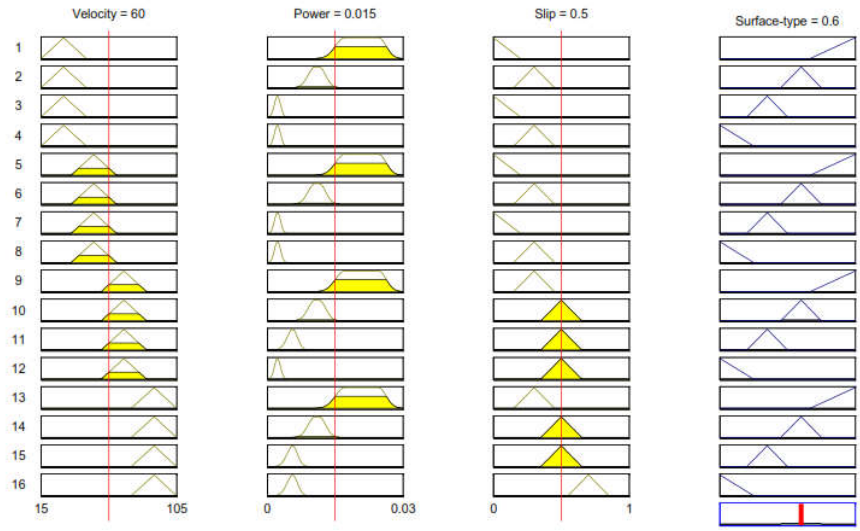


Figure 4-10 Fuzzy rules defined for terrain classification purpose base on collected data

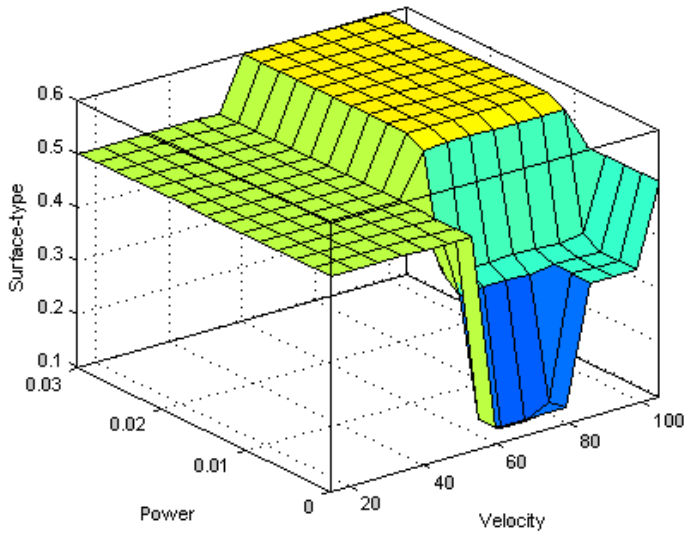


Figure 4-11 the surface viewer of terrain classification algorithm

In order to validate the terrain classification algorithm, another experiment is designed with three different commanded speeds (rather than the ones used to terrain the algorithm) on each of the surfaces. Table 4-2 shows the design of experiment to validate the algorithm.

Table 4-2 Design of experiment for surface classification study

| Surface type | Wheel speed (rpm) |
|---|---|
| Asphalt | 40 , 60 , 80 |
| Concrete | 40 , 60 , 80 |
| Grass | 40 , 60 , 80 |
| Soil | 40 , 60 , 80 |

The output of proposed fuzzy logic based terrain classification algorithm for the validation set is shown in Figure 4-12. As it is observed, the algorithm successfully identified the surfaces for different surfaces.

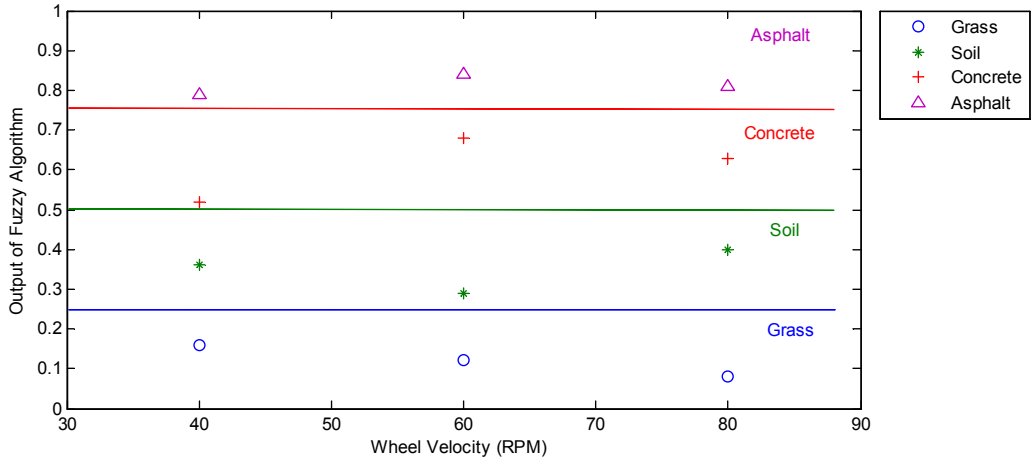


Figure 4-12 The output of terrain classification algorithm for validation set

Moreover, testing the robot on different surfaces, it was observed that power of the radial component of acceleration signal reaches its highest values on asphalt and its lowest values on grass which was predictable since the vibration of the tire, caused by the contact between the tire and the road, is damped on surfaces with softer texture. Also, power of radial vibration is higher when the robot's speed is increased.

Once the surface was identified based on the optimum value of slip ratio on each surface, a desired traction controller can be designed for the robot, a sample algorithm for this purpose is shown in Figure 4-13.

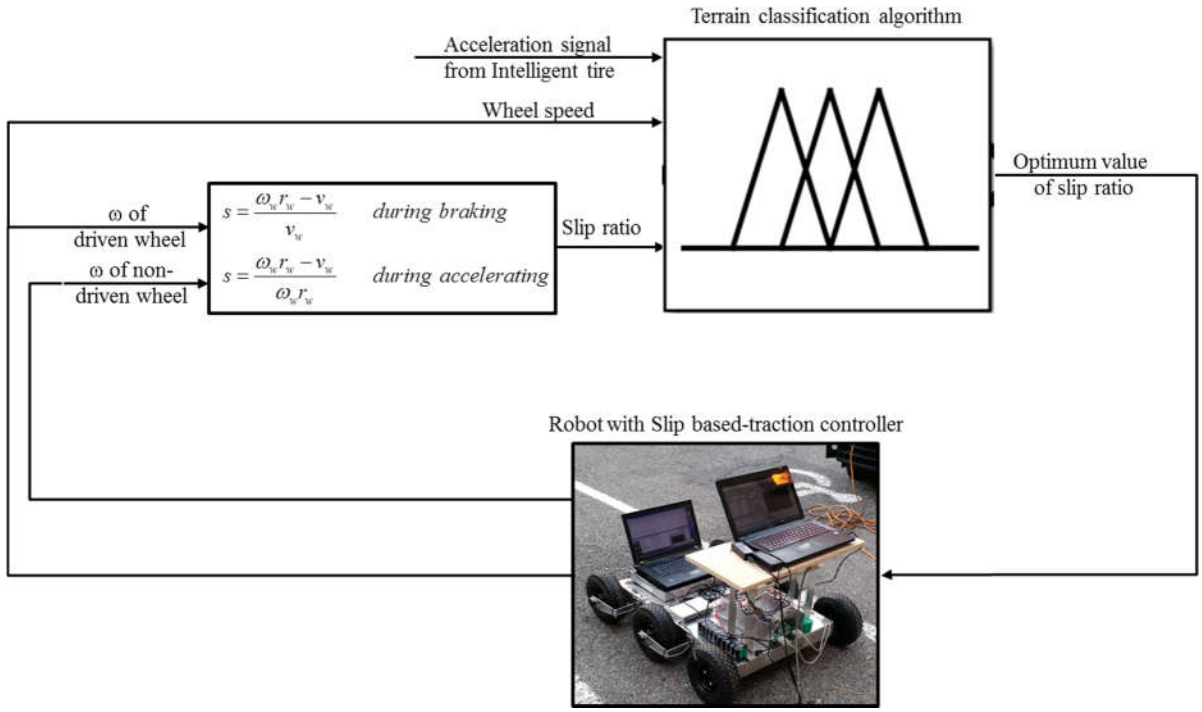


Figure 4-13 sample intelligent tire based traction controller algorithm

## 4.2 Tire Normal Load Estimation Algorithm:

The portable tire testing setup was used to train the normal load estimation algorithm; the encoder signal is used to extract the acceleration signal of each tire revolution. To show the performance of normal load estimation algorithm, two sets of data were collected, one set was used to train the neural network using MATLAB Neural Network Toolbox, and the second data set was used to validate the trained neural network. The second set of data was taken with similar conditions as the training data but because of uncertainty in running the tests, the validation data points are not exactly equal to those of the training data. Table 4-3 shows the test conditions used to terrain the Neural Network algorithm (NN).

Table 4-3 design of experiment to terrain the sample NN for contact patch length

| Trailer Speed | | Normal Load (N) | | |
|---|---|---|---|---|
| (mph) | (km/h) | | | |
| 15 | 24.14 | 2000 | 3000 | 4000 |
| 25 | 40.23 | 2000 | 3000 | 4000 |
| 35 | 56.32 | 2000 | 3000 | 4000 |

Figure 4-14 shows histogram of the error percentages between estimated and measured normal forces for training data points which indicates that the maximum percentage error of the trained data set is below 4%.

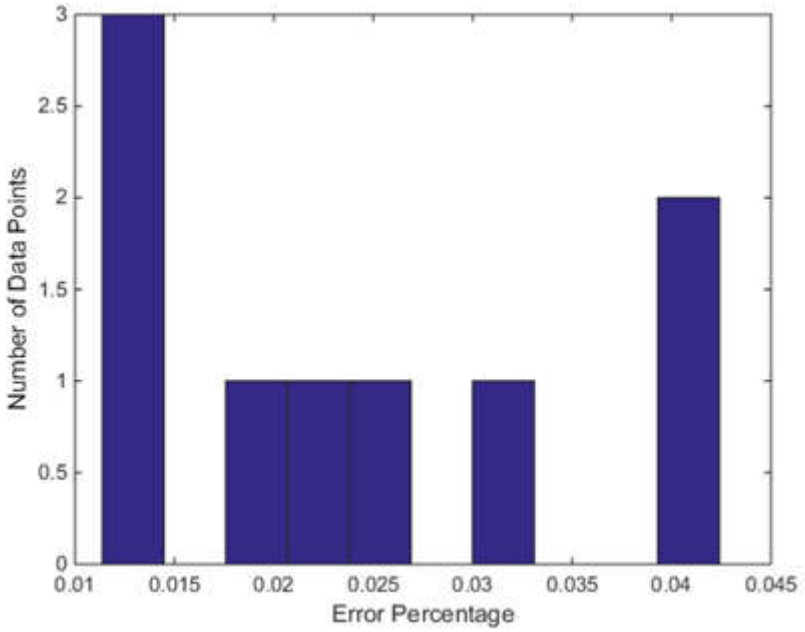


Figure 4-14 histogram of error percentages for the training data set

Figure 4-15 shows the histogram of the error of the validation data points. As seen in the figure, the maximum percentage of error is below 9%. It should be noted that this set of data was not used in the training process of the neural network and was only collected for validation purpose.

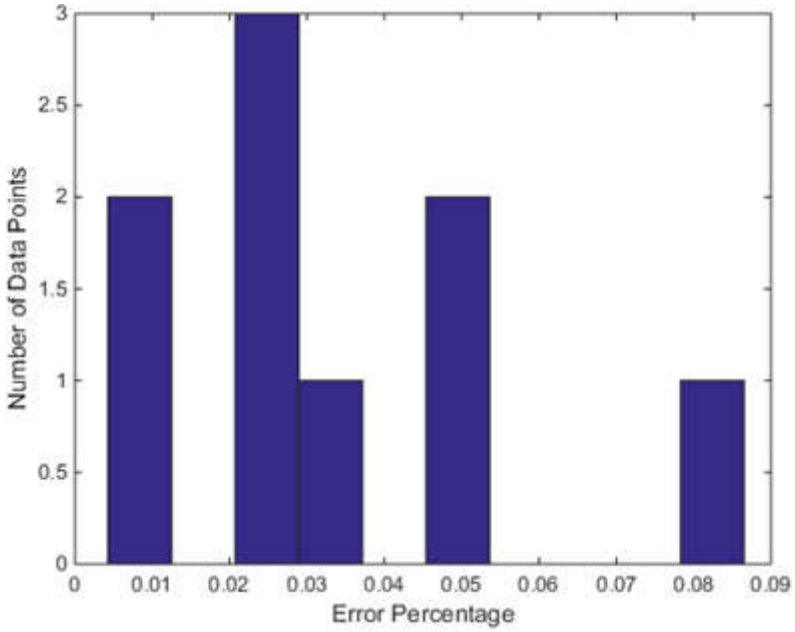

Figure 4-15 histogram of error percentages for the validation data set

It is normal to see larger error percentages with the validation data set compared to the training data set. It should be noted that only one data point of the validation set is close to 9% error and the rest of points are concentrated below 5%. That point could be considered as an outlier. The same situation holds more or less with the training data set. Usually, one or two points have larger error percentages but they are relatively far from the region where the rest of the points are concentrated.

An experiment was designed with the trailer test setup, presented in Table 4-4, to train the general normal load estimation algorithm. The tests were conducted with three different tire pressures (normal, bellow and above normal tire pressure), five different normal loads (2000N – 4000N with the step of 500N) and three different longitudinal speeds on both directions of a 100 m long road. Taking the average of the estimated values for each tire revolution, the overall contact patch length was estimated as follows:

$$2a_{est} = 2\sum_{i=1}^{i=n} a_i \qquad (1)$$

Where $a_{est}$ is half of the overall estimated contact patch length for each testing condition, n is the number of tire revolutions for each experiment, and $a_i$ is half of the contact patch length calculated in each tire revolution using equation (3.2).

Table 4-4 the experiment designed to train the normal load estimation algorithm

| **Tire Inflation Pressure (psi)** | **Tire Longitudinal Speed** | | **Tire Normal Load (N)** |
|---|---|---|---|
| | **(mph)** | **(km/h)** | |
| 25 , 30 , 35 | 15 | 24.14 | 2000 |
| | | | 2500 |
| | | | 3000 |
| | | | 3500 |
| | | | 4000 |
| | 20 | 32.18 | 2000 |
| | | | 2500 |
| | | | 3000 |
| | | | 3500 |
| | | | 4000 |
| | 25 | 40.23 | 2000 |
| | | | 2500 |
| | | | 3000 |
| | | | 3500 |
| | | | 4000 |

As it was stated in Chapter 3, both radial and circumferential components of acceleration can be used to estimate the normal load, however in order to estimate the contact patch length, circumferential acceleration leads to more accurate results [2]. Figure 4-16 shows the contact patch length estimated using circumferential component of acceleration and Equation 1.

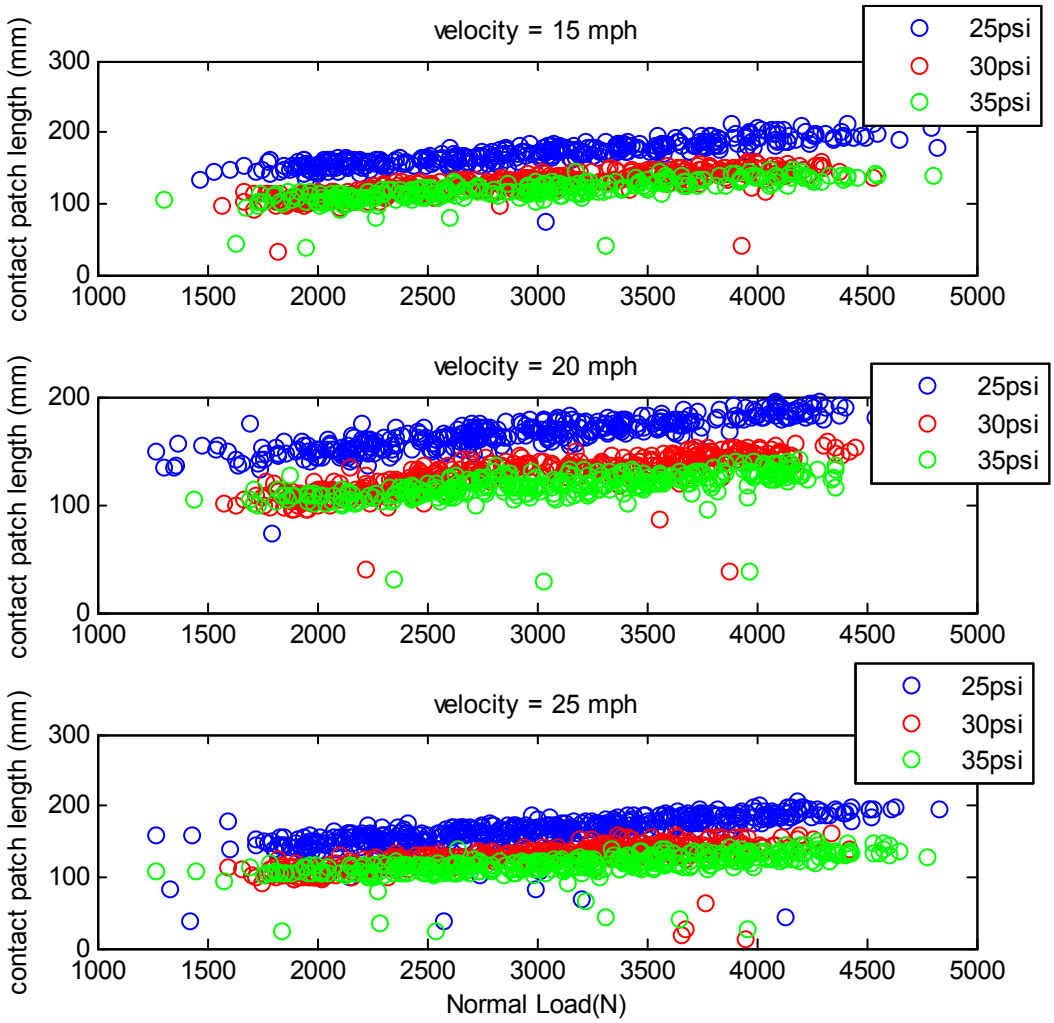


Figure 4-16 the contact patch length estimated using circumferential acceleration

To validate the estimated contact patch length, carbon paper films were placed under the tire in each normal load testing condition to capture the tire footprint; Figure 4-17 shows the tire footprint for different static normal loads. It is observed that the measured contact patch lengths (measured at the center of the tire foot print, where the sensor is attached) are in good agreement with the ones estimated using the circumferential acceleration signal.

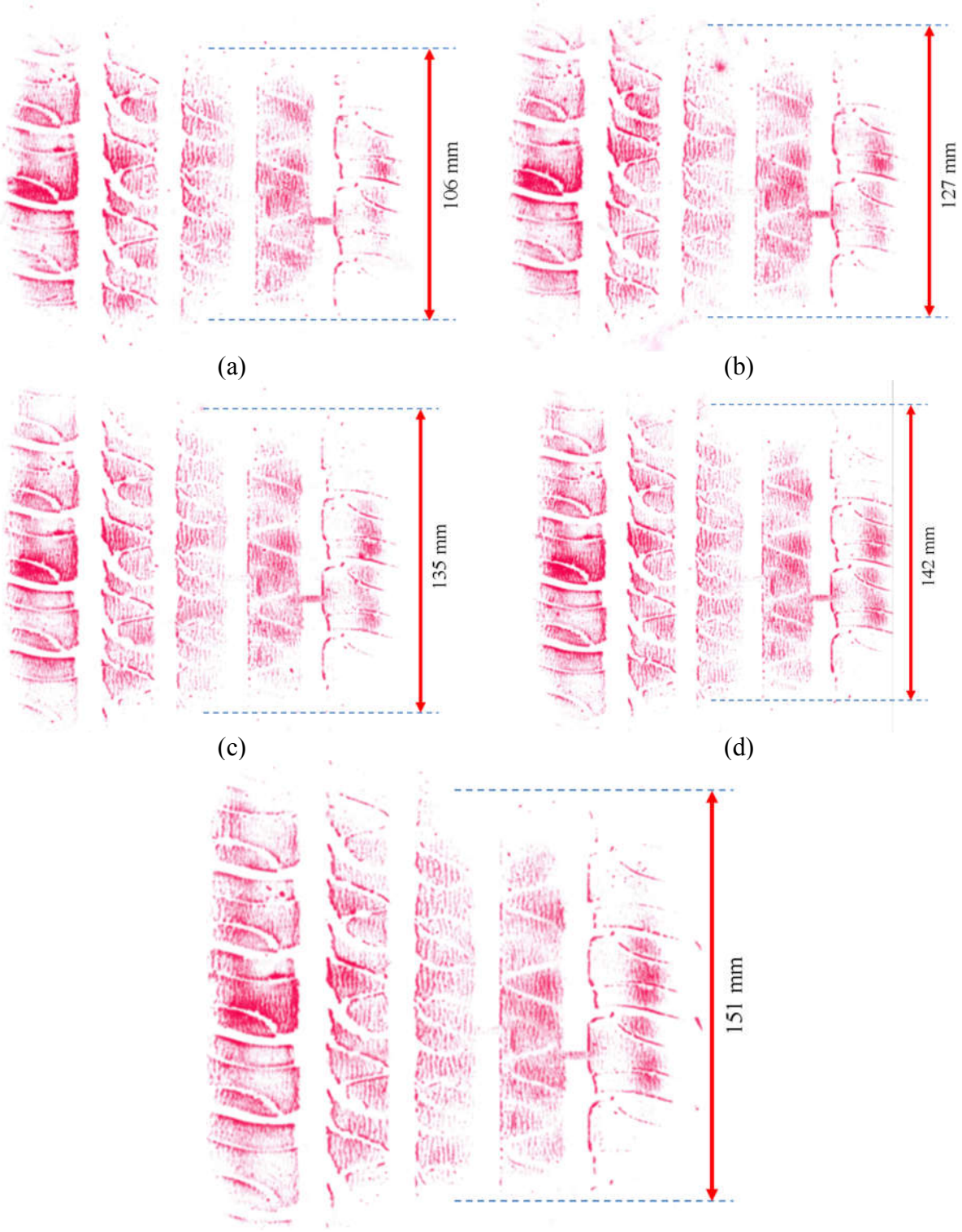


Figure 4-17 The tire foot print captured on carbon paper film in tire pressure of 30 psi and different normal loads (a) 2000N (b) 2500N (c) 3000N (d) 3500N (e) 4000N

Once the contact patch length is estimated, a two-layer feed-forward Neural Network (NN) with sigmoid hidden neurons and linear output neurons [216], which uses thirty five neurons in its hidden layer and also is appropriate for a multi-dimensional mapping problem, shown in Figure 4-18, is used to fit on the data. The inputs of the NN algorithms are tire inflation pressure and circumferential acceleration peaks' time difference and angular velocity of the wheel and the output is the normal load.

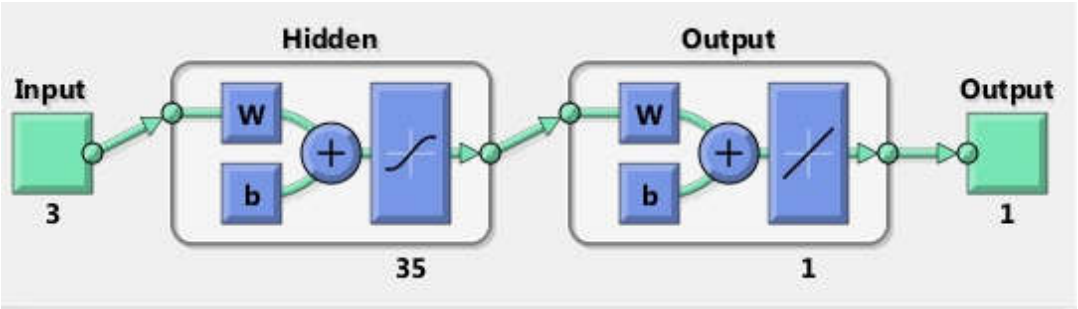

Figure 4-18 two-layer feed-forward NN used to train the normal load estimation algorithm

The data of 3300 tire revolutions for three different longitudinal speeds, three different tire pressures and five different normal loads were selected; 70 percent of the data was selected randomly to train the algorithm, 15 percent for validating and the last 15 percent to test the algorithm. Although it was stated that five normal loads were used to train the algorithm, during the test, the normal load was fluctuating and the average normal load of each tire revolution was used to train the algorithm, this helped improve the performance of the algorithm to cover all the normal loads between the minimum (2000N) and maximum (4000N) normal load values that were used to train the algorithm. Figure 4-19 and Figure 4-20 show the regression performance and the error histogram for the trained algorithm respectively, the error is defined as: the target – the output of trained network.

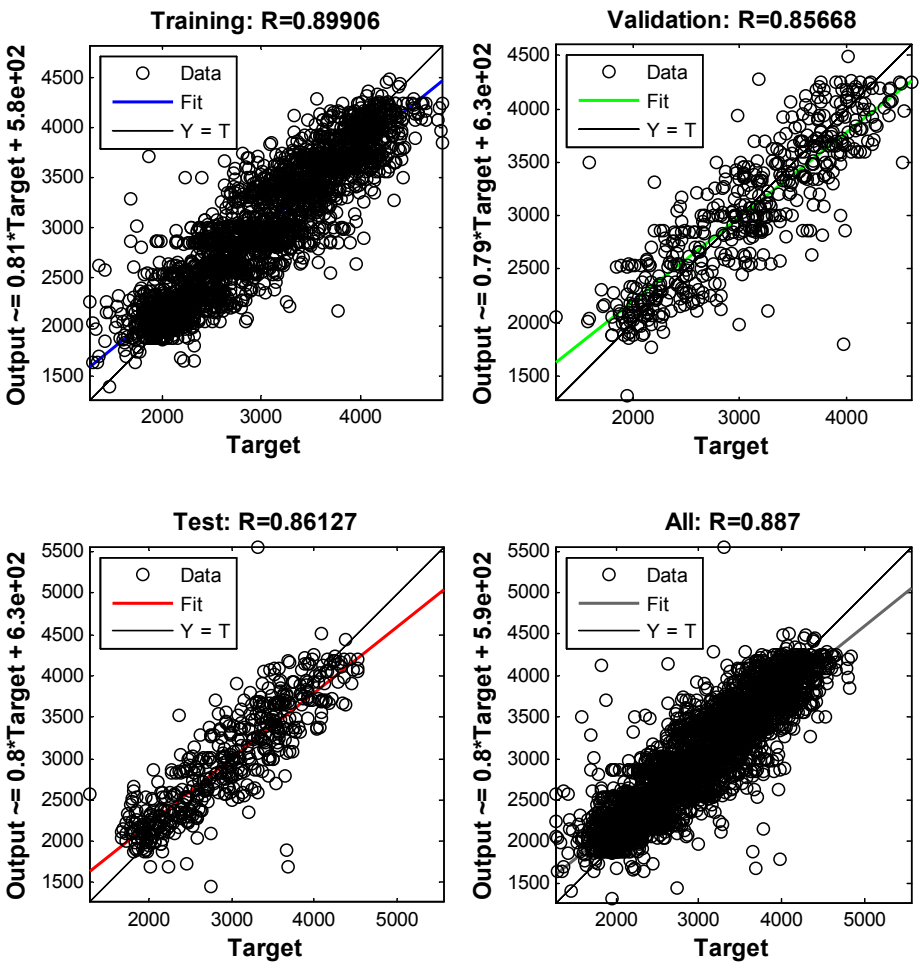


Figure 4-19 The normal load estimation algorithm regression performance

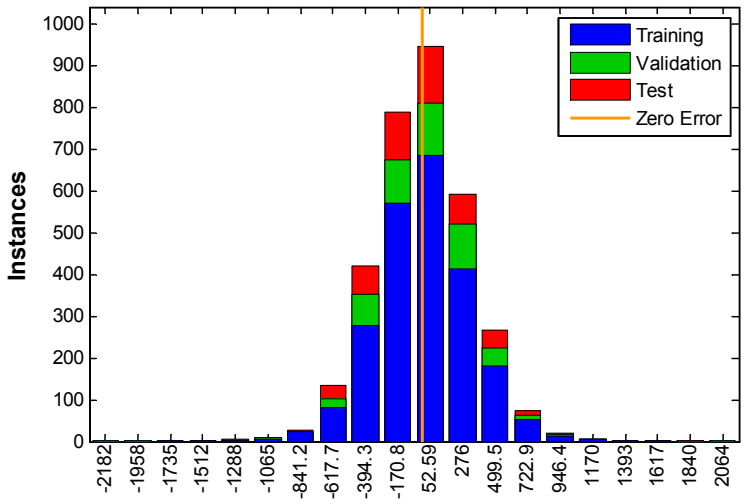


Figure 4-20 The normal load estimation algorithm error histogram

It is observed that in all cases of training, validating and testing, the correlation coefficients vary between 0.89-0.9, which considering the fluctuation in the normal load measurements, they are relatively acceptable. It is believed that this is the worst case scenario and the results would be much better in regular vehicles that have less vertical vibrations. Since the instrumented VW Jatta does not have a force hub, it was not possible to test and validate the algorithm using the vehicle.

### 4.3 Intelligent Tire Based Pressure Monitoring Algorithm

The third algorithm introduced in Chapter 3 was a two-step, pressure monitoring algorithm. In the first step, the wheel angular velocity is estimated through a trained neural network; the inputs are the circumferential acceleration peaks' time difference and radial acceleration peak difference. In order to train the neural network, an experiment was designed with the nominal tire pressure and three different longitudinal speeds, the details are presented in Table 4-5.

Table 4-5 the experiment, designed for the wheel speed estimation algorithm

| **Tire Inflation Pressure (psi)** | **Tire Longitudinal Speed** | |
|---|---|---|
| | **(mph)** | **(km/h)** |
| 30 | 20 | 32.186 |
| | 30 | 48.280 |
| | 40 | 64.373 |

The experimental data of 1317 tire revolutions, collected using the instrumented VW Jetta, was used to study the developed neural network estimation algorithm; 70 percent for training, 15 percent for validation and 15 percent for testing. A two-layer feed-forward Neural Network (NN) with sigmoid hidden neurons that uses ten neurons in its hidden layer was used. The error histogram for the wheel velocity estimation algorithm is shown in Figure 4-21; the correlation coefficient for all cases of training, validating and testing were more than 0.95 that shows there is a good correlation between the inputs and the output of the proposed algorithm.

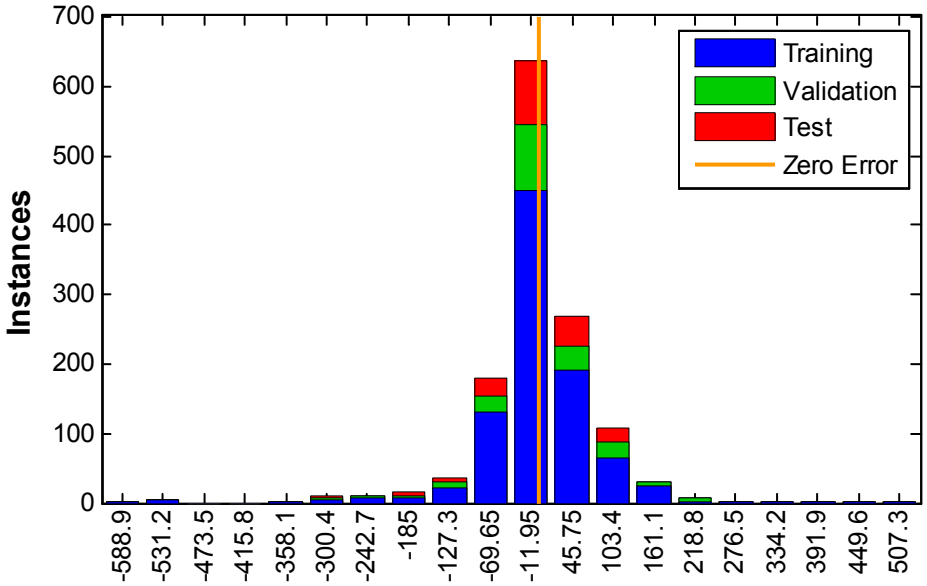

Figure 4-21 the omega estimation algorithm error histogram

In order to evaluate the performance of the wheel velocity estimation algorithm, another experiment is designed with three different longitudinal speeds (20, 30 and 40 mph) and two different tire pressures; first, the nominal tire pressure (in this study is 30 psi), which was used in training the algorithm and second, a tire pressure below the nominal pressure (in this study 25 psi was used). Figure 4-22 and Figure 4-23 show the performance of the algorithm for the tire pressure of 25psi (below nominal pressure) and 30 (nominal tire pressure) respectively.

It is observed that the algorithm performs well to estimate the wheel angular speed for the tire with the nominal pressure (30 psi), however the results of the algorithm for the tire with pressure below the nominal one doesn't give a powerful tool to estimate the tire pressure. In another word, the difference between estimated wheel angular velocity and measured one for the low pressure tire is not high enough. Therefore, in order to estimate the tire pressure the second step of the algorithm was proposed.

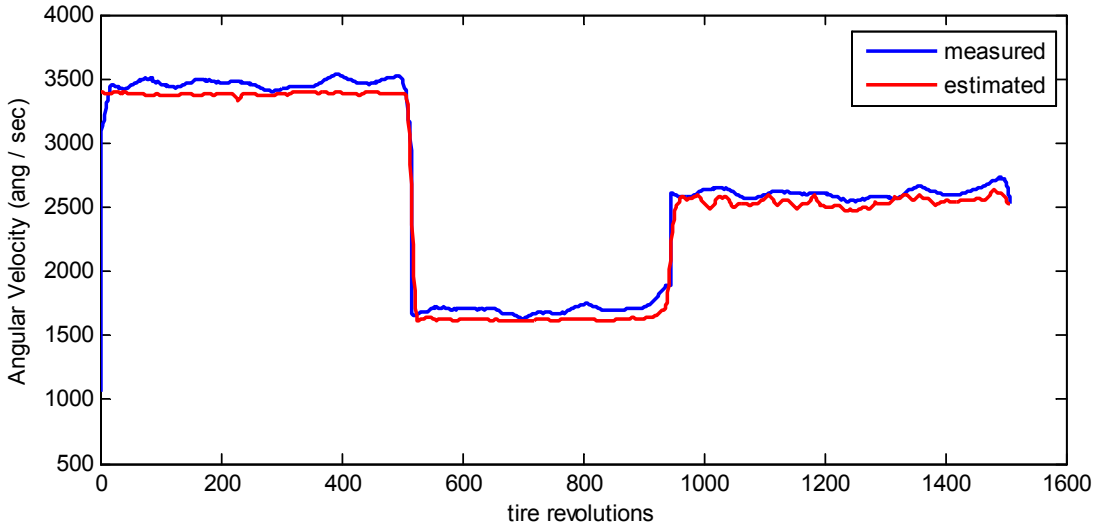


Figure 4-22 the performance of omega estimation algorithm, tire pressure = 25 psi

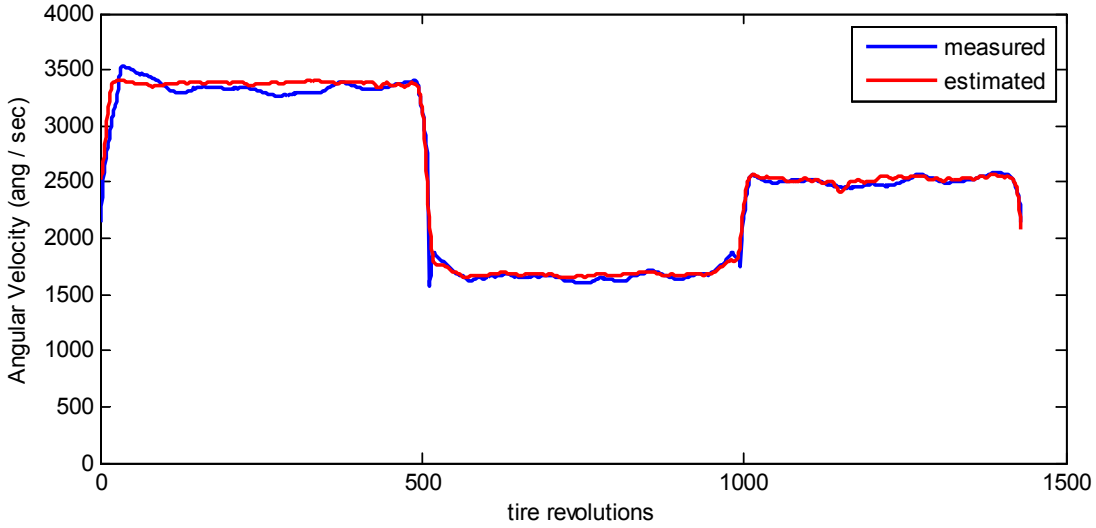


Figure 4-23 the performance of omega estimation algorithm, tire pressure = 30 psi

In the second step, another neural network is trained to estimate the power of radial acceleration signal. The inputs to this algorithm are the estimated wheel velocity from previous step, the circumferential acceleration peaks' time difference and the radial peak difference. Again, the experimental data of 1327 tire revolution, with nominal tire pressure (30 psi) is used through a two-layer feed-forward Neural Network (NN) with sigmoid hidden neurons that uses ten neurons

in its hidden layer to develop the neural network; 70% for training, 15% for validation and 15% for testing. Figure 4-24 shows the error histogram of the radial power estimation algorithm. The correlation coefficient in all cases of training, validation and testing was above 0.91 that shows there was a good correlation between the inputs and the output of the algorithm.

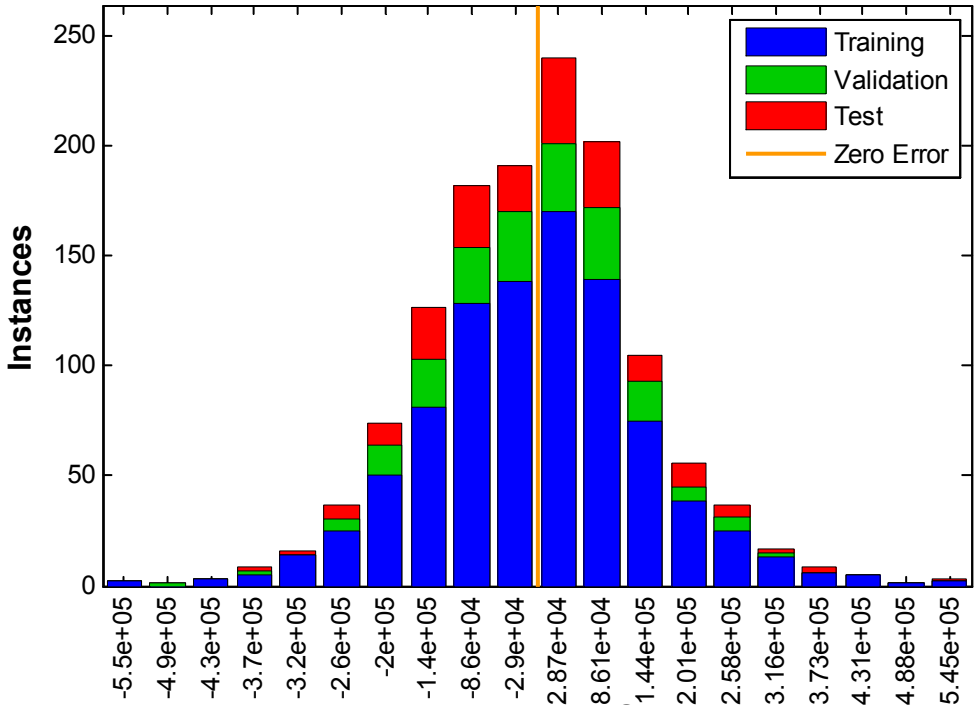


Figure 4-24 The radial acceleration power estimation algorithm's error histogram

In order to evaluate the performance of the second algorithm, the same cases that were used to evaluate the performance of the first step of the algorithm are used. Figure 4-25 and Figure 4-26 show the performance of radial acceleration's power estimation algorithm for the tire with low pressure (25 psi) and with the nominal pressure (30 psi) respectively.

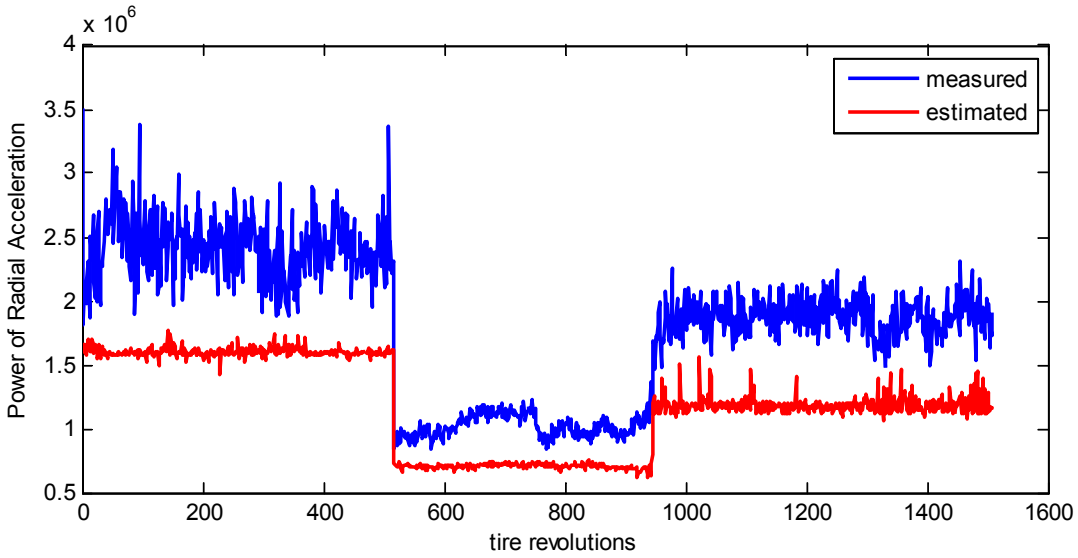


Figure 4-25 the performance of power estimation algorithm, tire pressure = 25 psi

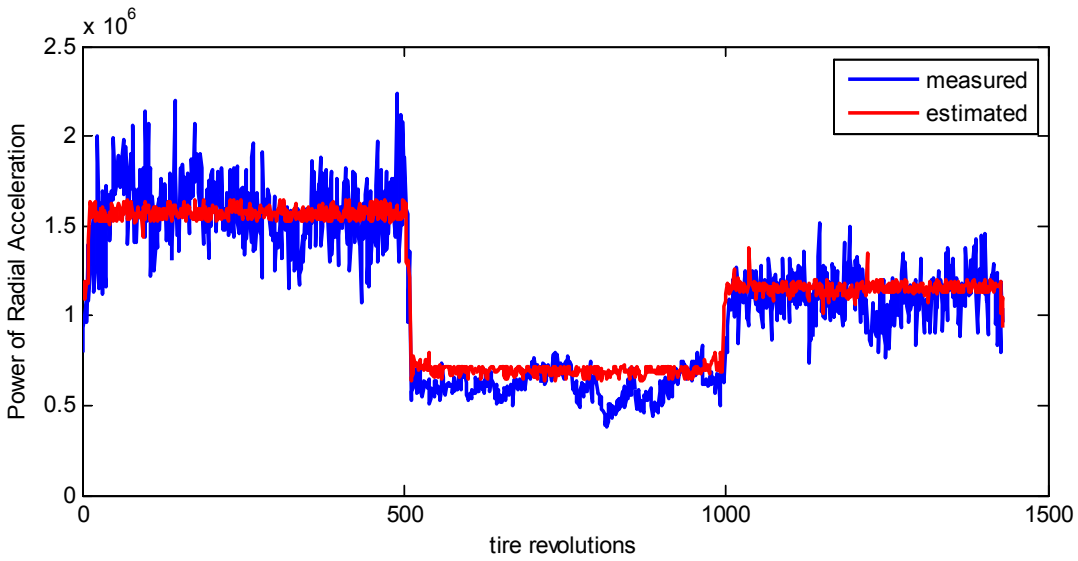


Figure 4-26 the performance of power estimation algorithm, tire pressure = 30 psi

As it is shown, the algorithm performs well for the tire with nominal inflation pressure, and as it was expected, the estimated radial power is smaller than the actual power for the tire with low pressure, since the radial acceleration power increases when the tire pressure drops due to higher deformation, which is not considered in this algorithm. The algorithm can be usedl to warn the driver about the low pressure condition.

## 4.4 Intelligent Tire Base Road Condition Monitoring Algorithm

The other algorithm which was introduced in the previous chapter was a neural network algorithm to classify the road conditions into two categories; wet and dry. To train the algorithm, an experiment was designed with two tire pressures and three different longitudinal speeds on both dry and wet surfaces; the details are presented in Table 4-6.

Table 4-6 the experiment, designed for the road conditions monitoring algorithm

| **Tire Inflation Pressure (psi)** | **Tire Longitudinal Speed** | |
|---|---|---|
| | **(mph)** | **(km/h)** |
| 25 , 30 | 20 | 32.186 |
| | 30 | 48.280 |
| | 40 | 64.373 |

The instrumented VV Jetta 2003 was used to collect the data; all the data was divided into five tire revolutions portions, and the average of the inputs in each portion was used to train the algorithm. It is observed that the circumferential peaks' time difference (represents the contact patch length) and the radial acceleration signal and its power do not change much from the dry surfaces to wet surfaces, however the power of the circumferential acceleration change significantly (especially for the frequencies between 10-100 Hz). Figure 4-27 shows the power spectral density of circumferential acceleration for a selected batch of data for different pressures and speed conditions. The inputs of the algorithm are the power of circumferential acceleration for the frequencies between 10-100 Hz, average of the circumferential acceleration peaks' time difference for each five revolutions of the wheel, average of radial acceleration peak difference and the average of angular velocity of the wheel. The output was set to be 1, for the dry surface and 2 for the wet surfaces. Figure 4-28 shows the power of the circumferential acceleration for the frequencies between 10-100 Hz.

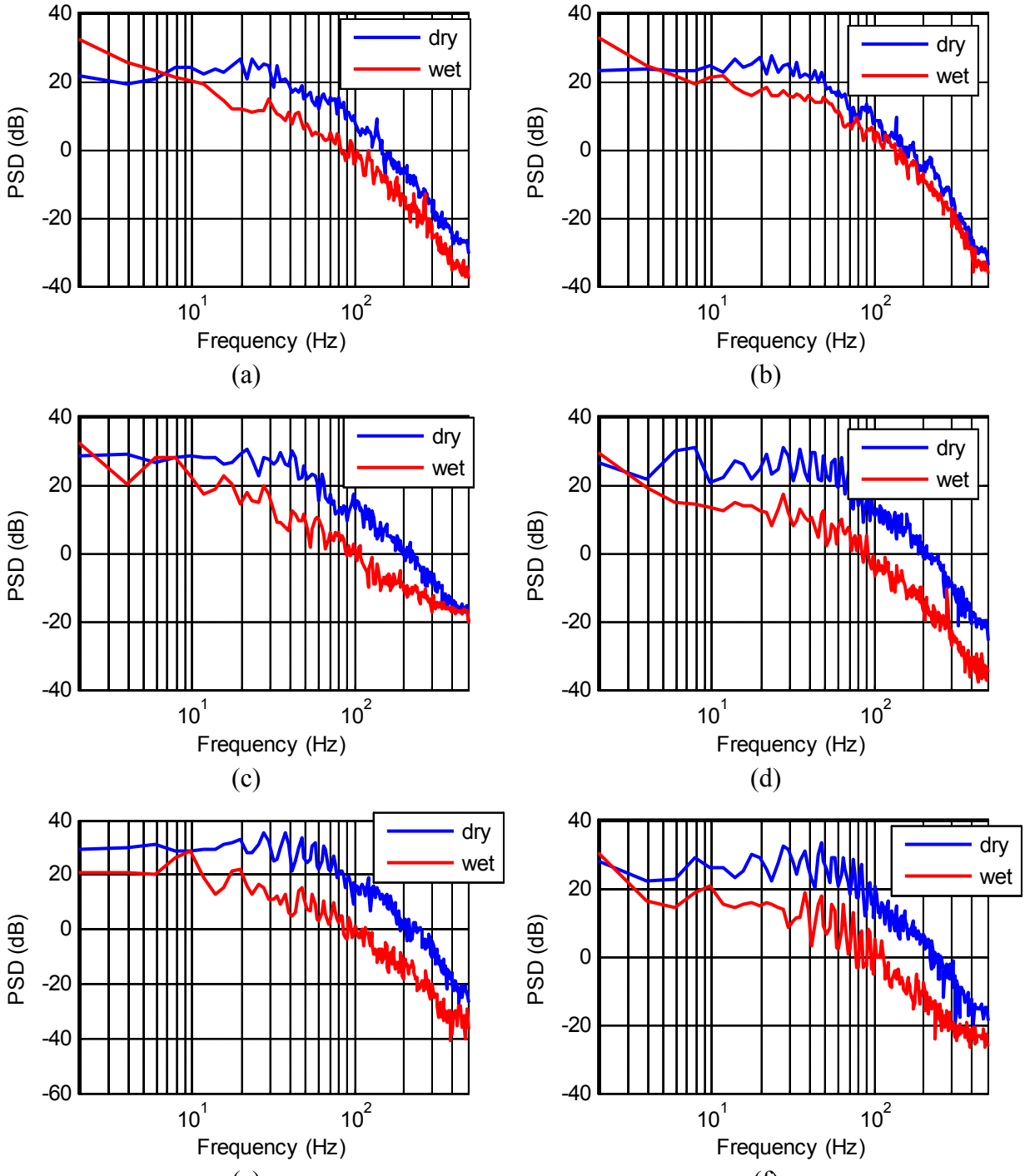


Figure 4-27 power spectral density for a selected batch of data: (a) velocity = 20 mph , tire pressure = 25psi, (b) velocity = 20 mph , tire pressure = 30psi (c) velocity = 30 mph , tire pressure = 25psi (d) velocity = 30 mph , tire pressure = 30psi (e) velocity = 40 mph , tire pressure = 25psi (f) velocity = 40 mph , tire pressure =30psi

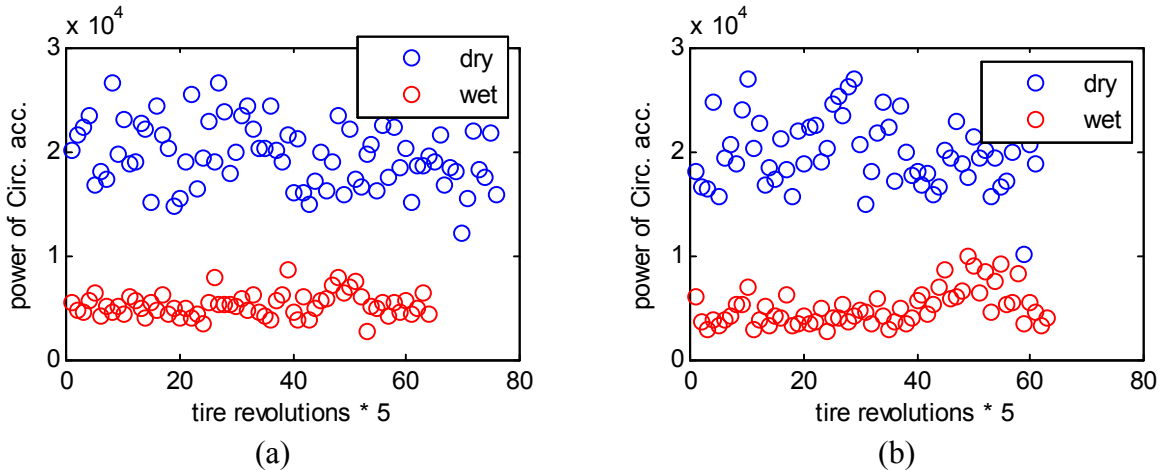


Figure 4-28 Power of circumferential acceleration for a selected batch of data: (a) velocity = 30 mph , tire pressure = 25psi, (b) velocity = 30 mph , tire pressure = 30psi

836 set of data points were used through a two-layer feed-forward Neural Network (NN) with sigmoid hidden neurons that uses ten neurons in its hidden layer to develop the neural network, 70% to train the algorithm, 15% for validating and the last 15% to test the algorithm. The error histogram of the road condition monitoring algorithm is presented in Figure 28; the correlation coefficient between the inputs and the output in all cases of training, validation and testing was above 0.99 that shows the inputs are perfectly correlated to the output of the algorithm.

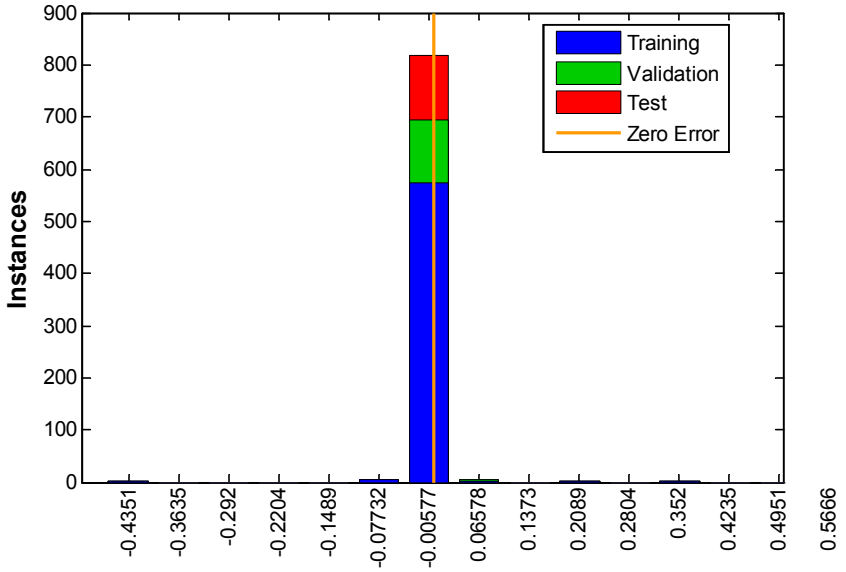


Figure 4-29 the road condition monitoring error histogram

As it was stated before, the output of the algorithm was set to 1 for dry surfaces and 2 for the wet surfaces. A computer code is used along with the algorithm that rounds the outputs within a 20% range of the values 1 or 2 to 1 and 2, respectively. In order to evaluate the performance of the algorithm another set of data is used with different speeds and different tire pressures on both dry and wet surfaces. Figure 4-30and Figure 4-31 show the performance of the algorithm for the low tire pressure and normal tire pressure, respectively.

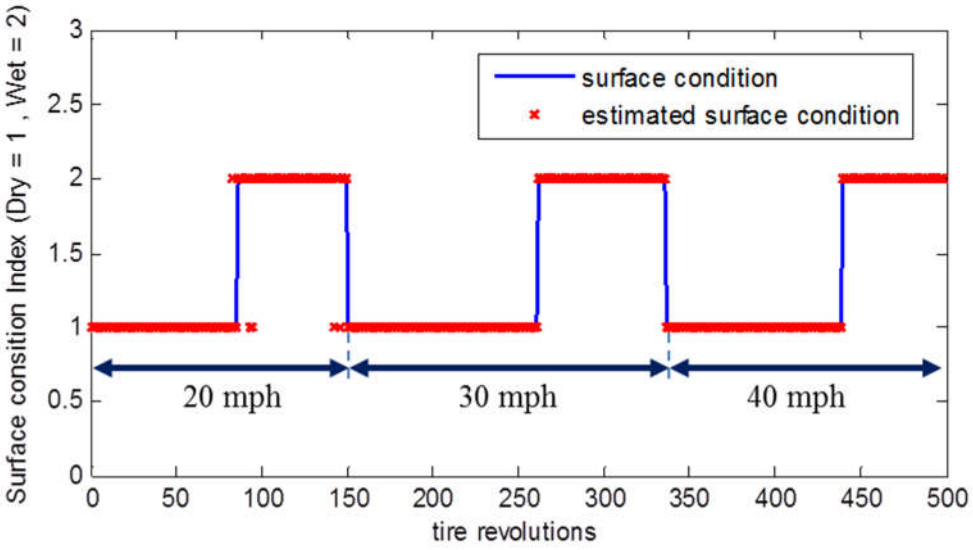


Figure 4-30 the performance of road condition monitoring algorithm, tire pressure = 25 psi

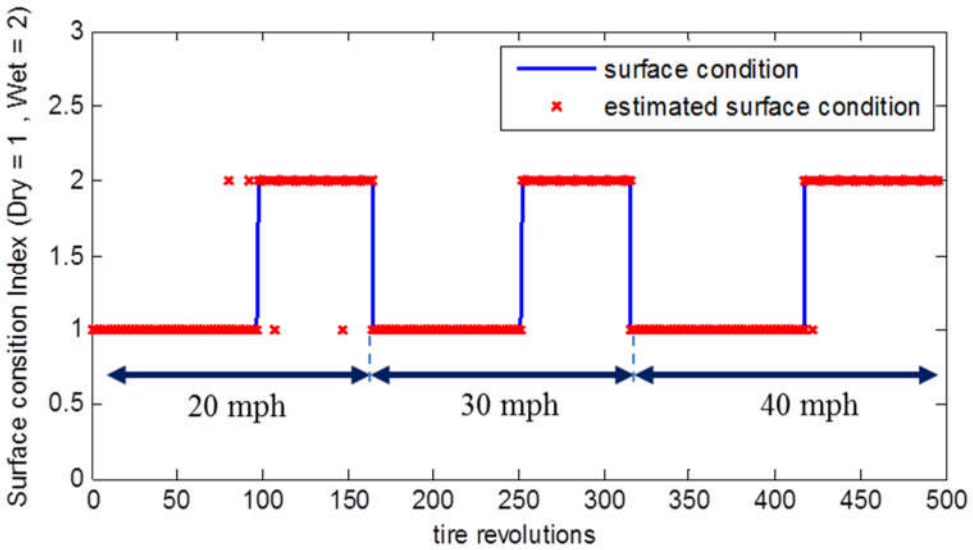


Figure 4-31 the performance of road condition monitoring algorithm, tire pressure = 30 psi

As it is shown, the algorithm can estimate the road condition for the both tires with normal inflation pressure and the low pressure perfectly. The performance of tire-road friction estimation algorithm is discussed next.

### 4.5 Tire-Road Friction Estimation Algorithm:

To evaluate the performance of the Kalman filter and the sliding mode observer CARSIM is used. In both cases, it is assumed that the angular speed is measured and driving and braking torques are known. The information for the vehicle, used for this simulation, is summarized in Table 4-7. The road was divided into three sections with three different coefficients of friction; the initial velocity of the vehicle was 120 km/h and brakes were applied on each surface once. This simulation was designed to evaluate the performance of Kalman filter and SMO during low slip maneuver. The picture of the car which is used for the simulation and the schematic of road sections are shown in Figure 4-32.

Table 4-7 The characteristics of the vehicle, which was used for this study

| **Vehicle Parameter** | **Value** |
|---|---|
| Sprung mass | 1020 (kg) |
| $I_z$<br>Yaw inertia | 1020 (kg-$m^{2)}$ |
| $L_f$ | 1165 (mm) |
| $L_r$ | 865 (mm) |
| t<br>(half of track length) | 587.5 (mm) |
| Tire type | 205/55 R16 |

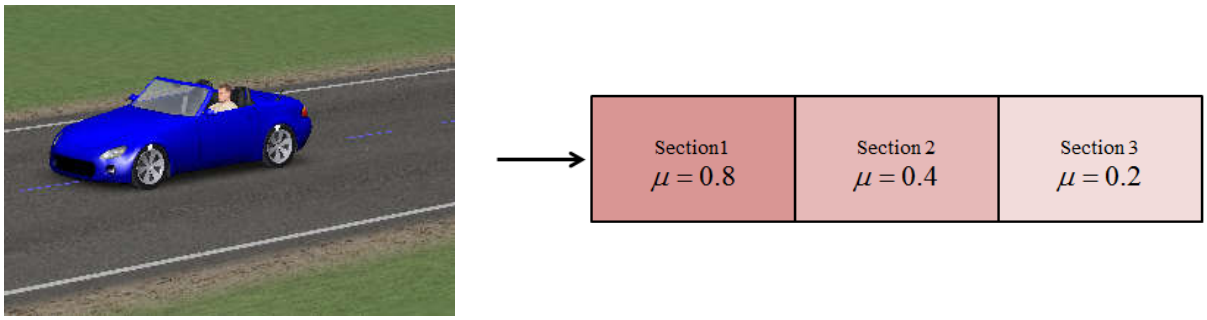


Figure 4-32 The road sections and the vehicle which is used for this simulation.

The values of real longitudinal tire force and estimated one, also real and estimated angular velocity of the wheel are shown in Figure 4-33 and Figure 4-34 for Kalman filter and sliding mode observer, respectively. As it was expected, both estimation algorithms work well for the low slip values and their performance is completely satisfactory. Another simulation is designed to evaluate the performance of these two algorithms during high slip intense maneuvers. For this simulation, the brake is applied to bring the vehicle to a complete stop on a surface with friction coefficient of 0.8. Figure 4-35 and Figure 4-36 show the performance of the Kalman filter and SMO, respectively during high slip maneuver.

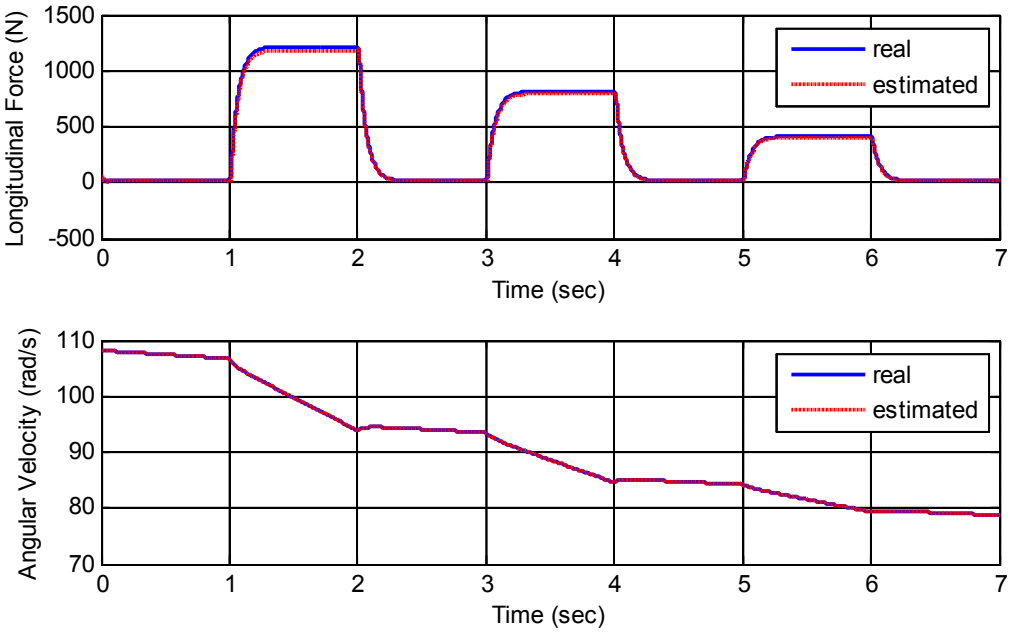


Figure 4-33 performance of Kalman filter estimation algorithm during low slip maneuver

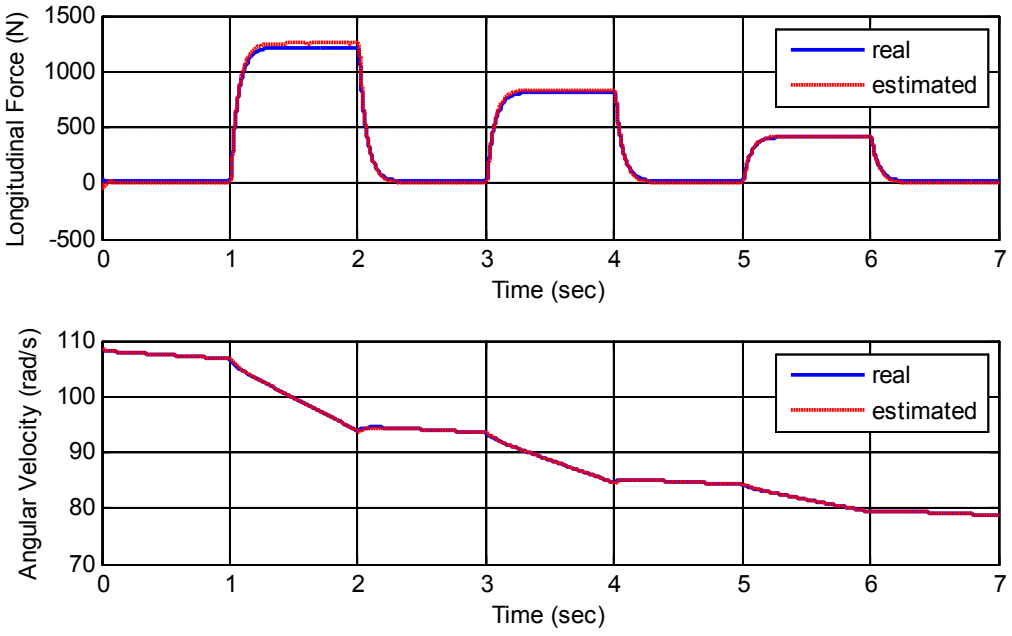


Figure 4-34 performance of Sliding mode observer algorithm during low slip maneuver

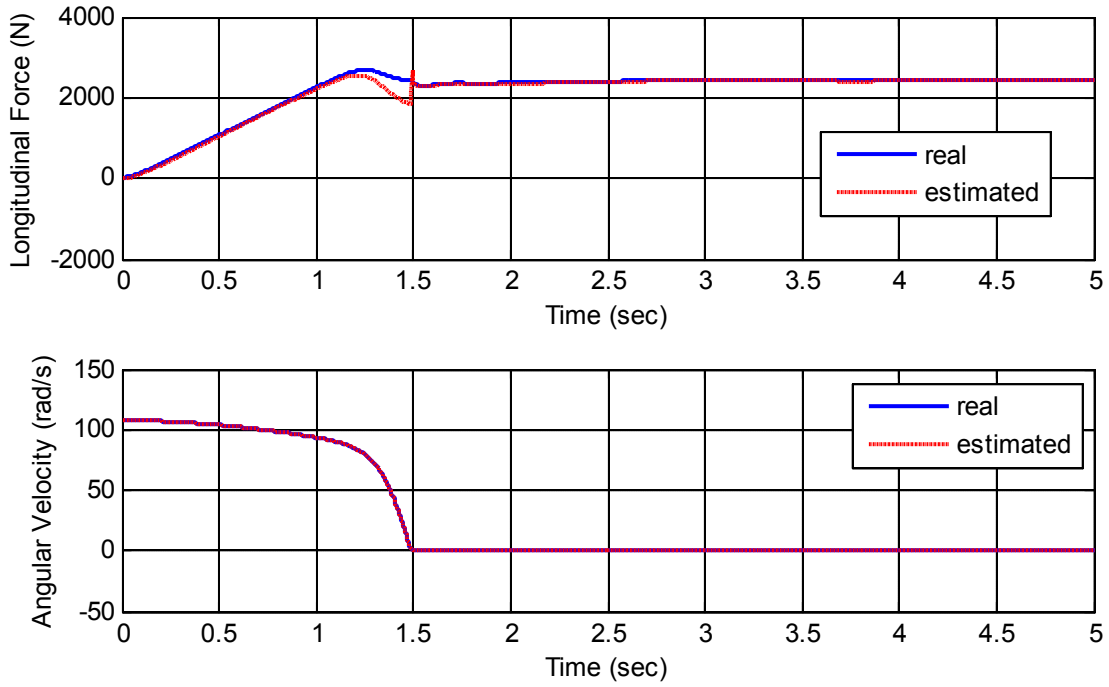


Figure 4-35 performance of Kalman filter estimation algorithm during high slip maneuver

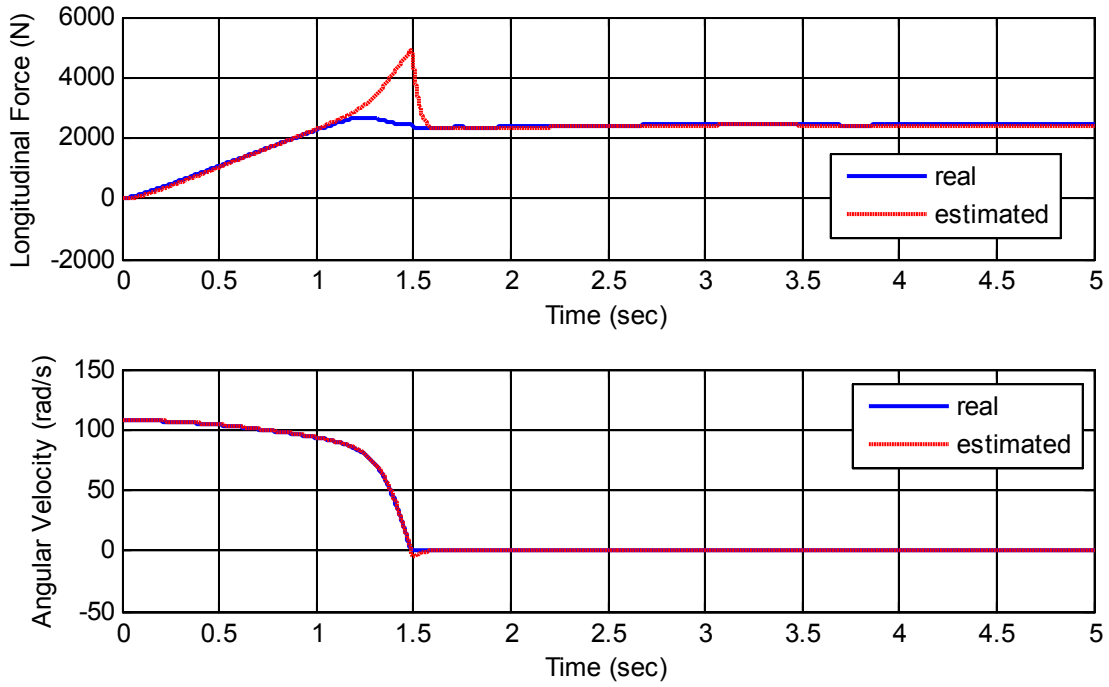


Figure 4-36 performance of Sliding mode observer algorithm during high slip maneuver

As it was expected, the performance of Kalman filter and sliding mode observer is not satisfactory during extreme driving conditions. Therefore, the combined tire-force estimation algorithm is used. To evaluate the performance of the combined tire-force algorithm, a simulation consisting of low and high slip maneuvers, including cornering and turning in both directions (left and right), is designed in Carsim. The schematic of the road which is used for this simulation is shown in Figure 4-37. The vehicle moves forward on section 1 with initial speed of 100 km/h, the brake is applied once on this surface (low slip maneuver), then it negotiates the firs curve (cornering) and enters the second surface, the brake is applied again on the second surface, on the third surface the brake is applied to bring the vehicle to a complete stop (high slip maneuver).

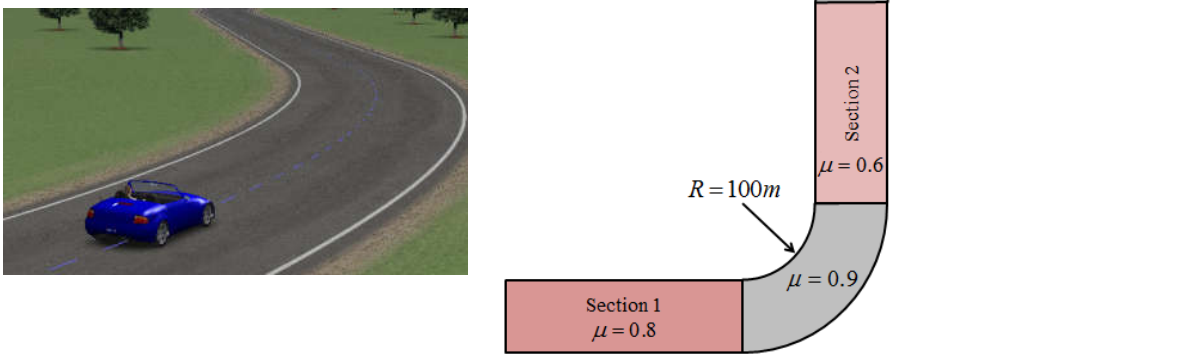


Figure 4-37 the schematic of the road which is used to evaluate combined tire-force algorithm

As it was mentioned in the theory of combined tire-force estimation algorithm, $\hat{F}_{x,i}$ are estimated values obtained using one of the proposed methods (Kalman filter or SMO), here in this study Kalman filter is used to obtain $\hat{F}_{x,i}$ and equation 6 is used to calculate $\hat{F}_{y,f}, \hat{F}_{y,r}$ based on $\hat{F}_{x,i}$.

Figure 4-38 and Figure 4-39 show the performance of combined tire-force algorithm to estimate longitudinal and lateral tire forces, respectively.

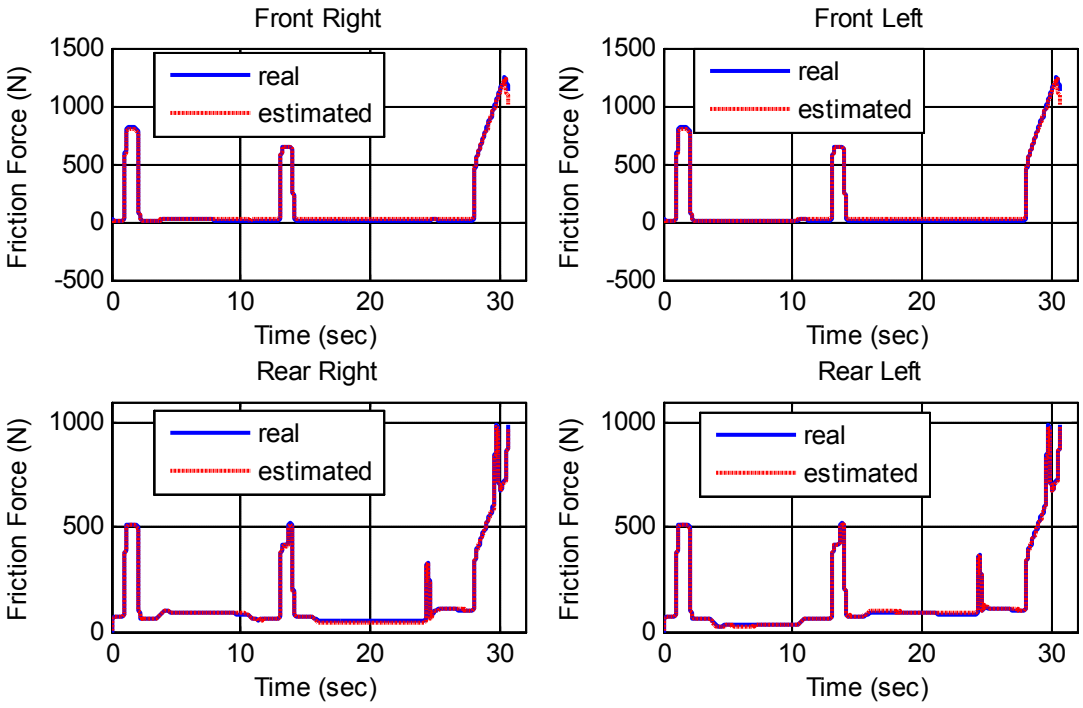


Figure 4-38 the performance of combined tire-force estimation to estimate longitudinal tire force

As it is shown in Figure 4-38, the combined tire-force estimation algorithm works great to estimate the longitudinal force in both low and high slip driving maneuvers, also its performance in estimating tire lateral force is satisfactory, which is shown in Figure 4-39.

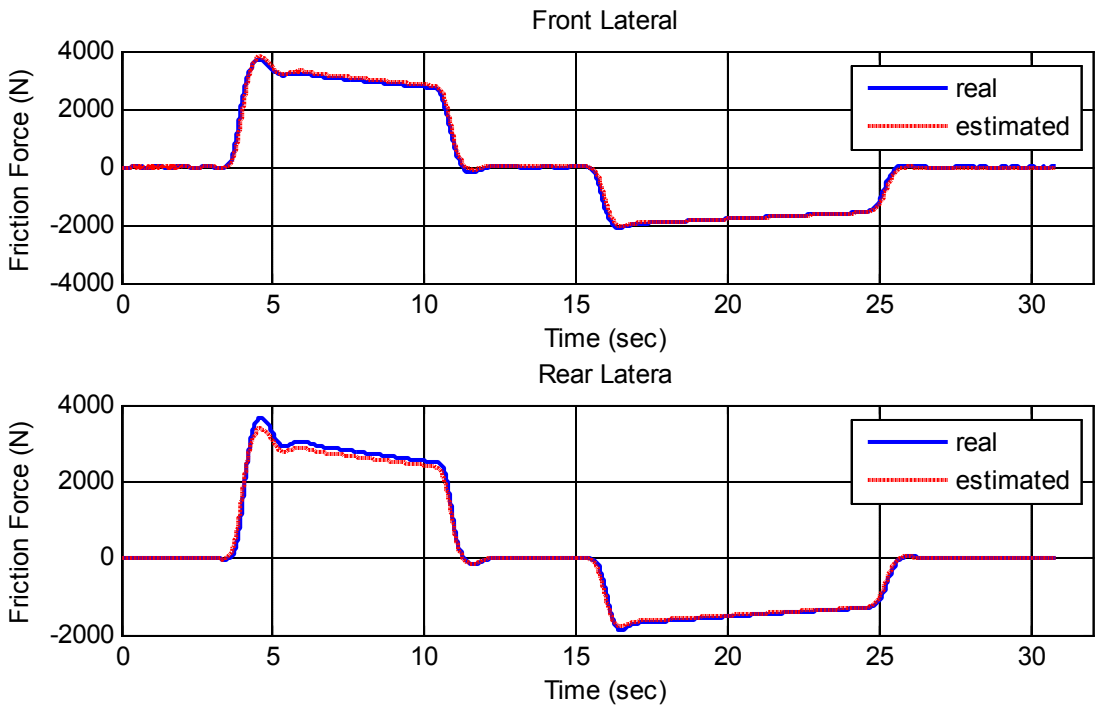


Figure 4-39 the performance of combined tire-force estimation to estimate Lateral tire force

In order to evaluate the performance of the proposed friction estimation algorithm, in which the tire normal load is estimated using the tire acceleration data and the tire forces are estimated through a vehicle dynamic based estimation algorithm, the following experiment was designed. The trailer test setup was used for this purpose. The tire normal load was set to 2000N and the brake was applied to complete wheel lock on a dry asphalt surface at the Virginia Tech Transportation Institute (VTTI) smart road. The first step of the algorithm, used to estimate the normal load, is shown in Figure 4-40. The output of the algorithm is the normal load for each tire revolution which is presented in Figure 4-41 for this experimental data.

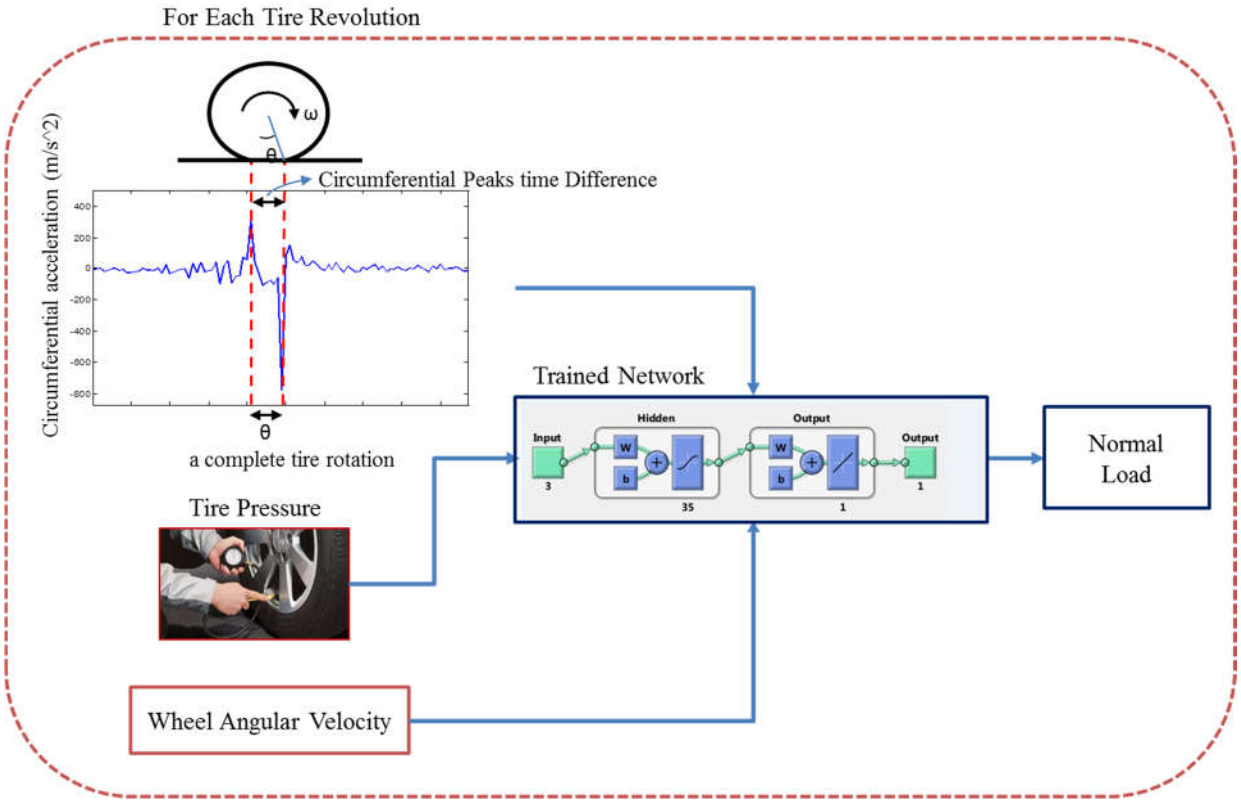


Figure 4-40 Algorithm used in each tire revolution to estimate the tire Normal load

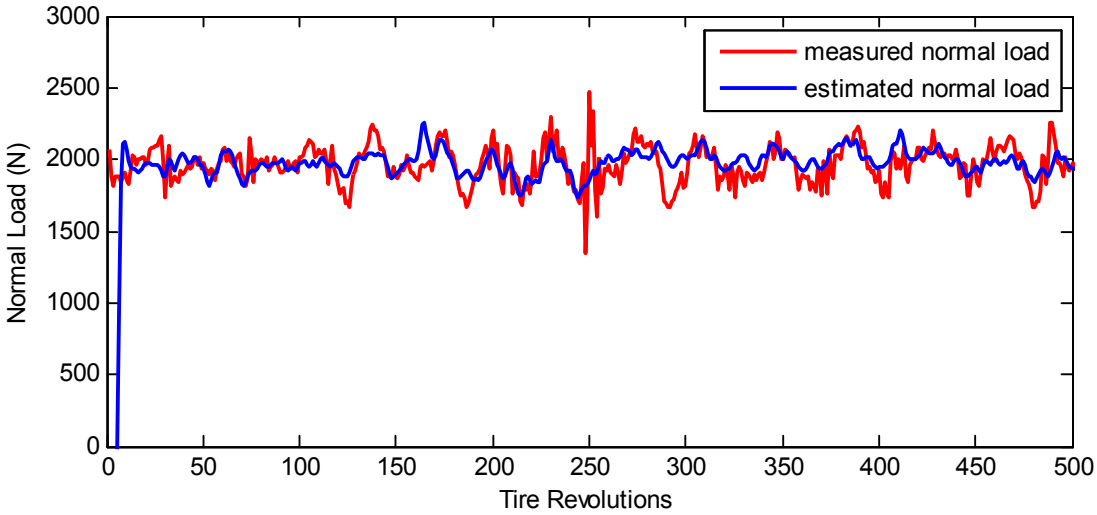


Figure 4-41 the performance of the Normal load estimation algorithm

Since the contact patch length can be obtained from the first algorithm and is an available parameter for each tire revolution, a simple algorithm, shown in Figure 4-42, is used to estimate the dynamic rolling radius of the tire.

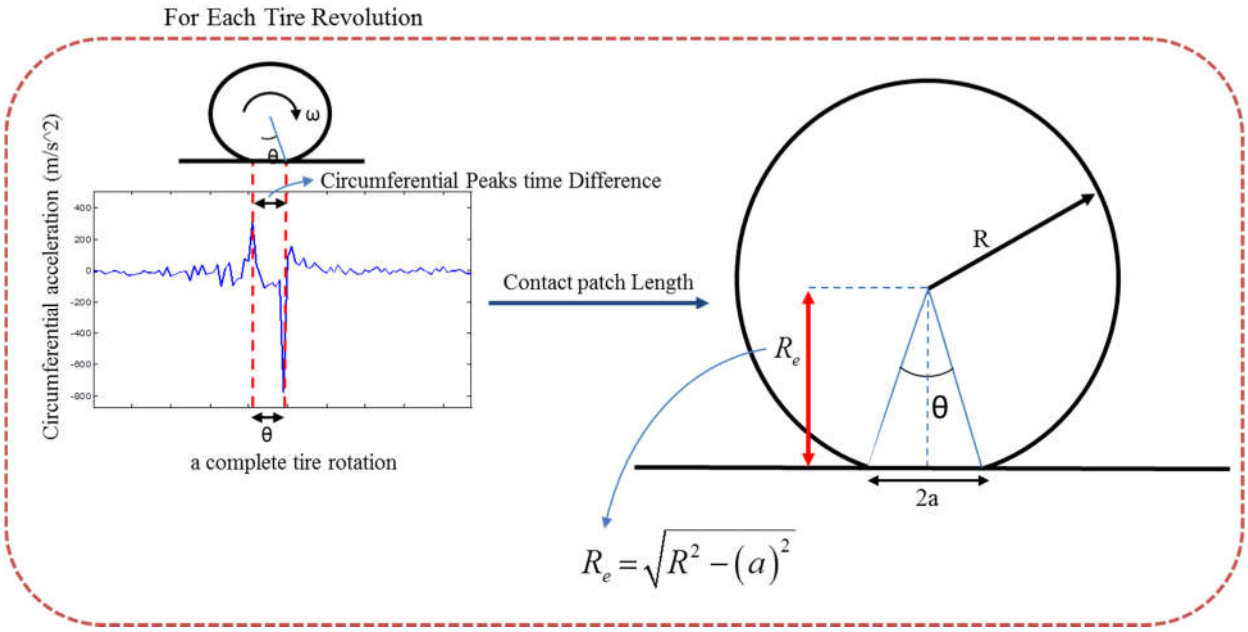


Figure 4-42 Simple algorithm to estimate tire effective radius in each tire revolution

The estimated dynamic rolling radius will be used in the second step to estimate the longitudinal force and to estimate the wheel longitudinal velocity. In the second step of the algorithm, the tire longitudinal force is estimated using a vehicle dynamic based algorithm; single wheel model was used to represent the system and Kalman filter, as explained in section 3.5.1.2, was used as the estimation algorithm. The input to the algorithm is the braking torque (driving torque is zero in this case) and the measured state is the angular velocity of the wheel. The performance of the Kalman filter is shown in Figure 4-43 and Figure 4-44.

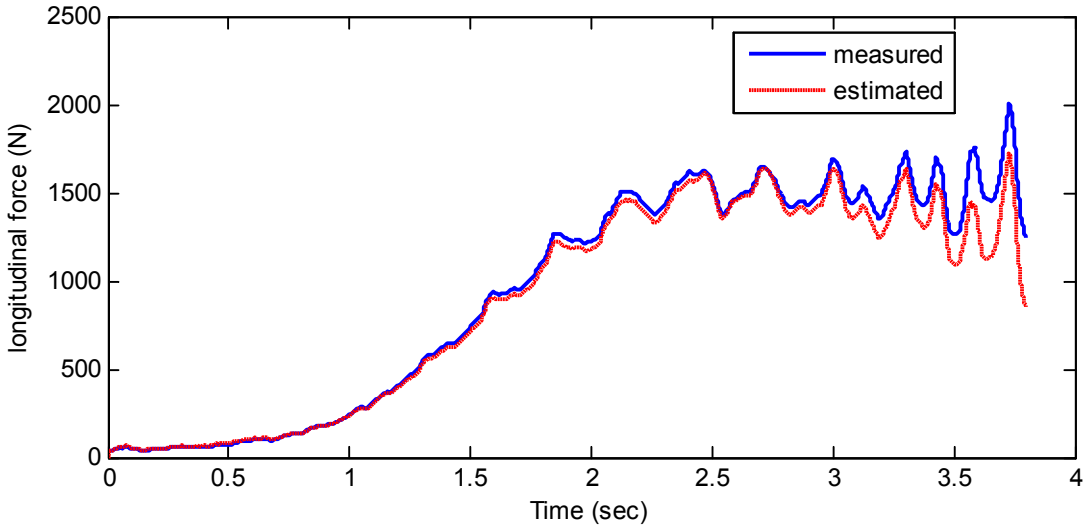


Figure 4-43 the performance of Kalman filter to estimate the longitudinal force

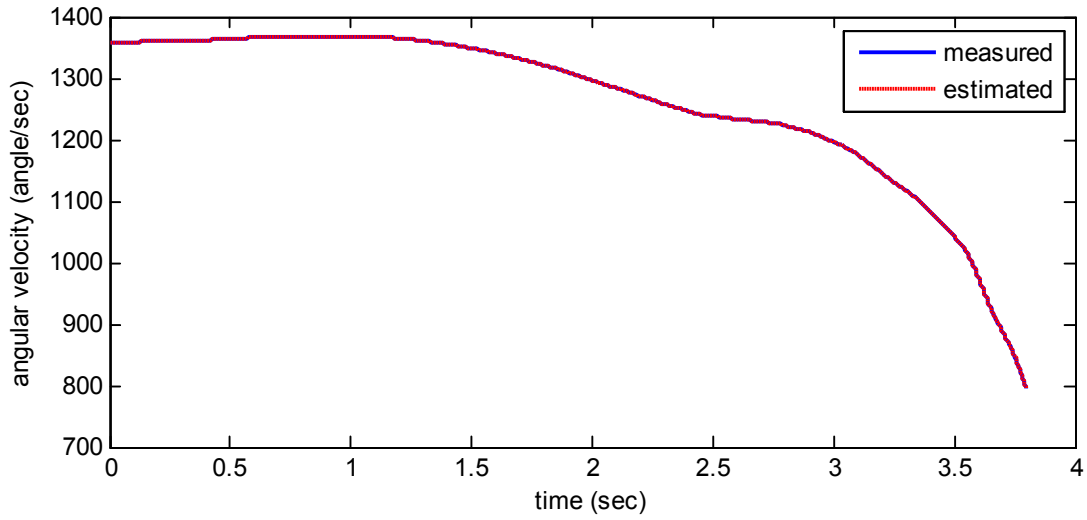


Figure 4-44 the performance of Kalman filter to estimate the wheel angular velocity

The slip ratio is also calculated using the longitudinal velocity of the trailer measured by VBOX, the angular velocity of the wheel and the estimated effective radius of the wheel.

$$s = \frac{v_w - R_e \omega_w}{v_w} \qquad (2)$$

where, $v_w$ is the velocity of the trailer, $\omega_w$ is the angular velocity of the wheel and $R_e$ is the effective radius of the tire. Once the slip ratio is calculated, the normalized longitudinal force

versus the slip ratio is plotted and the friction coefficient is estimated, which is presented in Figure 4-45 for the current case. Using this algorithm, the friction coefficient was estimated to be 0.85 which seems to be reasonable for dry asphalt.

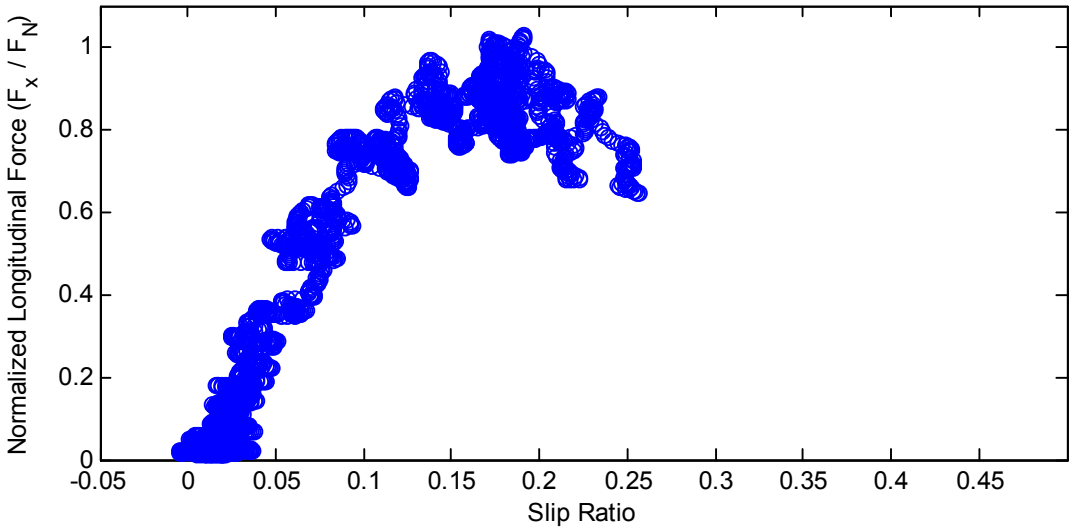


Figure 4-45 the normalized longitudinal force versus slip ratio

## 4.6 Conclusions:

The performances of different algorithms presented in Chapter 3 were evaluated in this chapter. Fist, a Fuzzy Logic based terrain classification algorithm was developed for the wheeled ground robot which categorized all the surfaces into four known surfaces; asphalt, concrete, grass and soil. Second, a Neural Network algorithm was developed and trained to estimate the tire normal load using the data from intelligent tire, and the performance of the algorithm was investigated using a sample set of data collected using the trailer test setup.

Third, a two-step neural network algorithm was trained to monitor the tire pressure. The wheel angular velocity was estimated in the first step of the algorithm using circumferential acceleration peaks' time difference and radial acceleration peak difference. Then, the estimated wheel angular velocity from the first step was used along with circumferential acceleration peaks' time difference

and radial acceleration peak difference to estimate the power of radial acceleration. Comparing the estimated power with the actual one, the tire pressure was estimated. The algorithm was validated using the experimental data collected from the instrumented VW Jetta 2003.

Forth, a road condition monitoring algorithm was trained using Neural Network that classified the road conditions into wet and dry surfaces and works once for every five revolutions of the wheel. The inputs of this algorithm were the average of circumferential acceleration peaks' time difference for each batch of data (five revolutions of the wheel), average of radial acceleration peak difference, average of wheel angular velocity and the power of circumferential acceleration signal for the frequencies between 10-100 Hz. This algorithm also was tested and validate with experimental data collected using the instrumented VV Jetta 2003.

Finally, the performances of different friction estimation algorithms, introduced in previous chapter, were evaluated in both high slip and low slip vehicle maneuvers. Table 4-8 summarizes the performance of the algorithms used in this study.

Table 4-8 the performance of different estimation algorithms during high and low slip maneuvers

| | Kalman Filter | Sliding mode observer | combined force estimation |
|---|---|---|---|
| Low slip maneuvers | ✓ | ✓ | ✓ |
| High slip maneuvers | × | × | ✓ |

# 5 Summary, conclusions and Future Works:

In this study, the application of intelligent tire in tire-road contact characterization was investigated. Five main intelligent tire based algorithms were developed in this study:

1. Fuzzy logic based terrain classification algorithm
2. Neural network algorithm to estimate the tire normal load
3. An intelligent tire based algorithm to monitor the tire pressure
4. An intelligent tire based algorithm to monitor the road surface condition (Dry/Wet)
5. A combined intelligent tire based vehicle dynamic based friction estimation algorithm

To evaluate the performance of proposed algorithms, three different test setup was developed and used in this study:

1. Wheeled ground robot
2. Portable tire testing trailer
3. Instrumented vehicle (VW Jetta 2003)

In all cases of five different algorithms good agreements were observed between the experimental data and the results of proposed algorithms and the algorithm were validated.

## 5.1 Conclusion

Five different algorithms were developed in this study; first, a Fuzzy Logic terrain classification algorithm for wheeled ground robots was developed and validated. The inputs of this algorithm are the wheel velocity, wheel slip and acceleration signals from intelligent tire and the output is the surface type. It classifies all different surfaces into four main categories; asphalt, concrete, grass, and soil.

The second algorithm was a Neural Network normal load estimation algorithm. The inputs of this algorithm are the wheel angular velocity, the tire pressure and the acceleration signal from intelligent tire and the output is the tire normal load. The third algorithm was a two-step pressure monitoring Neural Network algorithm. In the first step, the wheel angular velocity is estimated using acceleration signal from the intelligent tire and feeds into the second step to estimate the power of radial acceleration signal. Comparing the estimate power with the actual one, the tire pressure is estimated.

The fourth algorithm was an intelligent tire based road condition monitoring algorithm to distinguish between dry surfaces and wet surfaces. The algorithm works once for every five revolutions of the wheel and distinguishes between dry and wet surfaces using angular velocity of the wheel and acceleration signal from the intelligent tire. Also, different model based friction estimation algorithms were evaluated, and a combined tire-vehicle dynamic based friction estimation algorithm was proposed.

To evaluate the performance of these algorithms, three different test setups were developed; a six-wheel robot was designed and built for paving the way to developing friction estimation algorithms in a laboratory environment. It was used for terrain classification purposes. The robot was equipped with intelligent tire, accurate encoders to measure the wheel angular speed and a single axis accelerometer to measure the vertical vibration of the chassis. The second test setup was a portable tire test trailer, which was a quarter car test rig installed in a trailer and towed by a truck. The trailer was equipped with different sensors; a force hub to measure the tire forces and moments, an accurate encoder to measure the wheel angular velocity, VBOX to measure the longitudinal speed and an intelligent tire, which has an embedded accelerometer placed on the tire inner-liner, was used in trailer test setup.

The third test setup was an instrumented Volkswagen Jetta with an instrumented steering wheel, an IMU unit to measure roll, pitch, yaw and the acceleration components at the vehicle's Center of Gravity (CG), encoders to measure the wheel angular speed and two intelligent tires (one front and one rear tire). Also, time synchronized data collecting system were developed for all three test setups, which acquired the data of all of the sensors at the same time with the same sample rate.

Through extensive testing on different surfaces, these surfaces were satisfactorily classified using the robot. The portable tire testing trailer was used to design the normal load estimator, which showed satisfactory results to estimate the normal load (the estimation error was always below 10 percent) and to test the new proposed friction estimation algorithm. Also, the performance of the pressure monitoring and road condition monitoring algorithms were evaluated using the experimental data, collected with instrumented VW Jetta 2003 and good agreements were observed between the actual (testing) and estimated conditions. Finally, the performance of different friction estimation algorithms in high slip and low slip maneuvers were evaluated and the combined tire-road friction estimation method showed the best performance.

## 5.2 Future Works:

Some of the works, which are suggested for the continuation of this study are as follows:

- The sensitivity and robustness analysis of the proposed algorithms
- Develop the FE model of intelligent tire and use it as the first step to develop other intelligent tire based algorithms
- Develop an intelligent tire based algorithm to estimate the slip angle
- Develop an intelligent tire based algorithm to estimate the longitudinal and lateral tire forces
- Develop an intelligent tire base algorithm to detect the tire hydroplaning.

## 6 References:


[1] National Highway Traffic Safety Administration, 2012. Fatality analysis reporting system. Retrieved July 3, p.2014

[2] National Highway Traffic Safety Administration, 2010. Fatality analysis reporting system. Retrieved July 3, p.2014

[3] National Highway Traffic Safety Administration, 2011. Fatality analysis reporting system. Retrieved July 3, p.2014

[4] Connelly, L.B. and Supangan, R., 2006. The economic costs of road traffic crashes: Australia, states and territories. *Accident Analysis & Prevention*,*38*(6), pp.1087-1093.

[5] Andreassen, D.C., 1992. Preliminary costs for accident-types, Report ARR-217, ARRB, Victoria, Australia.

[6] Najafi S, Flintsch GW, Khaleghian S. Fuzzy logic inference-based Pavement Friction Management and real-time slippery warning systems: A proof of concept study. Accident Analysis & Prevention. 2016 May 31;90:41-9.

[7] Najafi S, Flintsch GW, Khaleghian S. Pavement friction management–artificial neural network approach. International Journal of Pavement Engineering. 2016 Dec 11:1-1.

[8] Pisano, P.A., Goodwin, L.C. and Rossetti, M.A., 2008, January. US highway crashes in adverse road weather conditions. In *24th Conference on International Interactive Information and Processing Systems for Meteorology, Oceanography and Hydrology, New Orleans, LA*.

[9] Andrey, J., 2010. Long-term trends in weather-related crash risks. *Journal of Transport Geography*, *18*(2), pp.247-258.

[10] Lamm, R., Choueiri, E.M. and Mailaender, T., 1990. Comparison of operating speeds on dry and wet pavements of two-lane rural highways. *Transportation research record*, (1280).

[11] Zhang, L. and Prevedouros, P., 2005. Motorist perceptions on the impact of rainy conditions on driver behavior and accident risk. In *Proceedings of the 84th Annual Meeting of the Transportation Research Board, Washington, DC*.

[12] Satterthwaite, S.P., 1976. An assessment of seasonal and weather effects on the frequency of road accidents in California. *Accident Analysis & Prevention*, *8*(2), pp.87-96.

[13] Andrey, J. and Yagar, S., 1993. A temporal analysis of rain-related crash risk. *Accident Analysis & Prevention*, *25*(4), pp.465-472.

[14] Brodsky, H. and Hakkert, A.S., 1988. Risk of a road accident in rainy weather. *Accident Analysis & Prevention*, *20*(3), pp.161-176

[15] Alvarez, L. and Yi, J., 1999. Adaptive emergency braking control in automated highway systems. In *Decision and Control, 1999. Proceedings of the 38th IEEE Conference on* (Vol. 4, pp. 3740-3745). IEEE.

[16] Schinkel, M. and Hunt, K., 2002. Anti-lock braking control using a sliding mode like approach. In *American Control Conference, 2002. Proceedings of the 2002* (Vol. 3, pp. 2386-2391). IEEE.

[17] Wellstead, P.E. and Pettit, N.B.O.L., 1997, September. Analysis and redesign of an antilock brake system controller. In *Control Theory and Applications, IEE Proceedings*- (Vol. 144, No. 5, pp. 413-426). IET.

[18] Otras, P. and De Wit, C.A., 2000, September. On the optimal braking of wheeled vehicles. In *American Control Conference, 2000. Proceedings of the 2000* (Vol. 1, No. 6, pp. 569-573). IEEE.

[19] Zhang, D., Zheng, H., Sun, J., Wang, Q., Wen, Q., Yin, A. and Yang, Z., 1999. Simulation study for anti-lock braking system of a light bus. In *Vehicle Electronics Conference, 1999.(IVEC'99) Proceedings of the IEEE International* (pp. 70-77). IEEE.

[20] Doumiati, M., Charara, A., Victorino, A. and Lechner, D., 2012. *Vehicle Dynamics Estimation Using Kalman Filtering: Experimental Validation*. John Wiley & Sons.

[21] Eichhorn, U. and Roth, J., 1992. Prediction and monitoring of tyre/road friction. In *XXIV FISITA CONGRESS, 7-11 JUNE 1992, LONDON. HELD AT THE AUTOMOTIVE TECHNOLOGY SERVICING SOCIETY. TECHNICAL PAPERS. SAFETY, THE VEHICLE AND THE ROAD. VOLUME 2 (IMECHE NO C389/321 AND FISITA NO 925226)*.

[22] Breuer, B., Eichhorn, U. and Roth, J., 1992, September. Measurement of tyre/road-friction ahead of the car and inside the tyre. In *International Symposium on Advanced Vehicle Control, 1992, Yokohama, Japan*.

[23] Andersson, M., Bruzelius, F., Casselgren, J., Gäfvert, M., Hjort, M., Hultén, J., Håbring, F., Klomp, M., Olsson, G., Sjödahl, M. and Svendenius, J., 2007. Road friction estimation. *Saab Automobile AB, Trollhättan, Sweden*.

[24] Tuononen, A.J., 2008. Optical position detection to measure tyre carcass deflections. *Vehicle System Dynamics*, *46*(6), pp.471-481.

[25] Tuononen, A. and Hartikainen, L., 2008. Optical position detection sensor to measure tyre carcass deflections in aquaplaning. *International Journal of Vehicle Systems Modelling and Testing*, *3*(3), pp.189-197.

[26] Tuononen, A., 2009. Optical position detection to measure tyre carcass deflections and implementation for vehicle state estimation.

[27] Howard, A. and Seraji, H., 2001. Vision-based terrain characterization and traversability assessment. *Journal of Robotic Systems*, *18*(10), pp.577-587.

[28] Kuno, T. and Sugiura, H., 1999. Detection of road conditions with CCD cameras mounted on a vehicle. *Systems and Computers in Japan*, *30*(14), pp.88-99.

[29] Holzmann, F., Bellino, M., Siegwart, R. and Bubb, H., 2006, October. Predictive estimation of the road-tire friction coefficient. In *Computer Aided Control System Design, 2006 IEEE*

*International Conference on Control Applications, 2006 IEEE International Symposium on Intelligent Control, 2006 IEEE* (pp. 885-890). IEEE.

[30] Jokela, M., Kutila, M. and Le, L., 2009, August. Road condition monitoring system based on a stereo camera. In *Intelligent Computer Communication and Processing, 2009. ICCP 2009. IEEE 5th International Conference on*(pp. 423-428). IEEE.

[31] Alonso, J., López, J.M., Pavón, I., Recuero, M., Asensio, C., Arcas, G. and Bravo, A., 2014. On-board wet road surface identification using tyre/road noise and Support Vector Machines. *Applied Acoustics*, *76*, pp.407-415.

[32] Kongrattanaprasert, W., Nomura, H., Kamakura, T. and Ueda, K., 2009. Automatic detection of road surface conditions using tire noise from vehicles. *Inst Electron Inform Commun Eng*, *108*(411), pp.55-60.

[33] Kongrattanaprasert, W., Nomura, H., Kamakura, T. and Ueda, K., 2009. Detection of Road Surface Conditions using Tire noise from vehicles. *電気学会論文誌 D (産業応用部門誌)*, *129*(7), pp.761-767.

[34] Kongrattanaprasert, W., Nomura, H., Kamakura, T. and Ueda, K., 2010. Detection of road surface states from tire noise using neural network analysis. *電気学会論文誌 D (産業応用部門誌)*, *130*(7), pp.920-925.

[35] Kongrattanaprasert, W., Nomura, H., Kamakura, T. and Ueda, K., 2010. Automatic detection of road surface states from tire noise using neural network analysis. In *Proceeding of 20 th International Congress on Acoustics, ICA2010*.

[36] Erdogan, G., Alexander, L. and Rajamani, R., 2011. Estimation of tire-road friction coefficient using a novel wireless piezoelectric tire sensor. *Sensors Journal, IEEE*, *11*(2), pp.267-279.

[37] Breuer, B., Bill, K., Gruber, S., Semsch, M., Strothjohann, T. and Xie, C., 2002. The mechatronic vehicle corner of Darmstadt University of technology-interaction and cooperation of a sensor tire, new low-energy disc brake and smart wheel suspension. *International journal of automotive technology*, *3*(2), pp.63-70.

[38] Bachmann, T., 1995, September. The importance of the integration of road, tyre, and vehicle technologies. In *FISITA XXth World Congress, Montreal, Canada*.

[39] Hollingum, J., 2001. Autonomous radio sensor points to new applications.*Sensor Review*, *21*(2), pp.104-107.

[40] Singh, K.B., Arat, M.A. and Taheri, S., 2013. An Intelligent Tire Based Tire-Road Friction Estimation Technique and Adaptive Wheel Slip Controller for Antilock Brake System. *Journal of Dynamic Systems, Measurement, and Control*, *135*(3), p.031002.

[41] Matilainen, M.J. and Tuononen, A.J., 2011, June. Tire friction potential estimation from measured tie rod forces. In *Intelligent Vehicles Symposium (IV), 2011 IEEE* (pp. 320-325). IEEE.

[42] Matilainen, M.J. and Tuononen, A.J., 2012. Intelligent tire to measure contact length in dry asphalt and wet concrete conditions. In *Int. Symp. Adv. Veh. Control*.

[43] Khaleghian, S., Ghasemalizadeh, O., and Taheri, S., ‘‘Estimation of the Tire Contact Patch Length and Normal Load Using Intelligent Tires and Its Application in Small Ground Robot to Estimate the Tire-Road Friction,’’ Tire Science and Technology, TSTCA, Vol. 44, No. 4, October–December 2016, pp. 248–261.

[44] Niskanen, A.J. and Tuononen, A.J., 2014, September. Three 3-Axis Accelerometers on the Inner Liner of a Tyre for Finding the Tyre-Road Contact Friction Indicators. In *Proc. of AVEC International Symposium on Advanced Vehicle Control, Tokyo, Japan*.

[45] Niskanen, A.J. and Tuononen, A.J., 2014. Three 3-axis accelerometers fixed inside the tyre for studying contact patch deformations in wet conditions.*Vehicle System Dynamics*, *52*(sup1), pp.287-298.

[46] Niskanen, A.J. and Tuononen, A.J., 2015, June. Accelerometer tyre to estimate the aquaplaning state of the tyre-road contact. In *Intelligent Vehicles Symposium (IV), 2015 IEEE* (pp. 343-348). IEEE.

[47] Klein, S.D., Gm Global Technology Operations, Inc., 2010. *Friction estimation and detection for an electric power steering system*. U.S. Patent Application 12/755,526.

[48] Patel, A., Fenkanyn, J.M., Singh, K.B. and Suh, P.J.M., 2012. *Load estimation system and method for a vehicle tire*. U.S. Patent Application 13/534,043.

[49] Singh, K.B., The Goodyear Tire & Rubber Company, 2015. *Road friction estimation system and method*. U.S. Patent 8,983,749.

[50] Singh KB, inventor; The Goodyear Tire & Rubber Company, assignee. Road friction estimation system and method. United States patent US 8,983,749. 2015 Mar 17.

[51] Singh, K.B., Parsons, A.W. and Engel, M., The Goodyear Tire & Rubber Company, 2015. *Tire slip angle estimation system and method*. U.S. Patent 8,983,716.

[52] Singh, K.B., Parsons, A.W., Engel, M. and Suh, P.J.M., The Goodyear Tire & Rubber Company, 2014. *Tire load estimation system using road profile adaptive filtering*. U.S. Patent 8,844,346.

[53] Miyazaki, N., Japan Electronics Industry, Limited, 1999. *Road surface friction sensor and coefficient detector*. U.S. Patent 5,892,139.

[54] Giustino, J.M., Bichler, A.R., Goslar, M., Liu, R.Y. and Becherer, T., Continental Tire North America, Inc., 2007. *Tire status detection system and method*. U.S. Patent 7,171,848.

[55] Hattori, Y., Yokohama Rubber Company, 2007. *Method for detecting strain state of tire, device for detecting strain state, and the tire*. U.S. Patent 7,302,836.

[56] Hillenmayer, F. and Kuchler, G., Siemens Aktiengesellschaft, 2006. *System for monitoring a vehicle with pneumatic tires, signal analysis method, and vehicle tire*. U.S. Patent 7,000,462.

[57] Chen, Y.Y., Industrial Technology Research Institute, 2012. *Tire and detection-alarm mechanism thereof*. U.S. Patent 8,302,469.

[58] Neugebauer, J., Grubisic, V. and Diefenbach, W., Fraunhofer-Gesellschaft Zur Forderung Der Angewandten Forschung EV, 1988. *Measuring the overall deformation of a tire*. U.S. Patent 4,724,703.

[59] Becherer, T., Continental Aktiengesellschaft, 1999. *Vehicle tire with a device for determining tire-road adhesion*. U.S. Patent 5,964,265.

[60] Miyoshi, A. and Nakano, K., Sumitomo Rubber Industries, Ltd. and Advics Co., Ltd., 2007. *Method of detecting longitudinal force of tire and longitudinal force detecting apparatus used therein*. U.S. Patent 7,257,997.

[61] Miyoshi, A., Tsurita, T. and Kunii, M., Sumitomo Rubber Industries, Ltd. and Sumitomo Electric Industries, Ltd., 2007. *System and method for determining tire force*. U.S. Patent 7,249,498.

[62] Carcaterra, A., Platini, M. and Roveri, N., Ace SRL and Universita'Degli Studi Di Roma" La Sapienza", 2012. *Method and device for optical measuring of tyre adhesion and tyre suitable said measurement*. U.S. Patent Application 14/235,137.

[63] Sistonen, M., 1990. *Device for measuring the friction on a surface*. U.S. Patent 4,955,933.

[64] Bell, L.D. and Bell, C.D., Bell, Larry D. and Christopher D., 1999. *Method and apparatus for monitoring the coefficient of friction between a tire and rolling surface, particularly to provide the vehicle operator with coefficient of friction, tire tread wear out and skid warning indications*. U.S. Patent 5,864,056.

[65] Wilson, K., Wilson Kitchener C., 2002. *Vehicle and vehicle tire monitoring system, apparatus and method*. U.S. Patent Application 10/143,312.

[66] Abe, Y. and Sawa, T., Nippo Sangyo Co. Ltd., 1986. *Dynamic friction coefficient measuring apparatus*. U.S. Patent 4,594,878.

[67] Mancosu, F., Brusarosco, M. and Arosio, D., Pirelli Pneumatici SPA, 2009.*Method and system for determining a cornering angle of a tyre during the running of a vehicle*. U.S. Patent 7,552,628.

[68] T.D. Gillespie, *Fundamentals of Vehicle Dynamics*, Society of Automotive Engineers, Warrendale, PA, 1992.

[69] Singh, K.B., 2012. Development of an Intelligent Tire Based Tire-Vehicle State Estimator for Application to Global Chassis Control. *Mechanical Engineering Dept, Virginia Tech, Blacksburg*.

[70] Canudas-de-Wit, C., Petersen, M.L. and Shiriaev, A., 2003, December. A new nonlinear observer for tire/road distributed contact friction. In *Decision and Control, 2003. Proceedings. 42nd IEEE Conference on* (Vol. 3, pp. 2246-2251). IEEE.

[71] De Wit, C.C., Horowitz, R. and Tsiotras, P., 1999. Model-based observers for tire/road contact friction prediction. In *New Directions in nonlinear observer design* (pp. 23-42). Springer London.

[72] Claeys, X., Yi, J., Alvarez, L., Horowitz, R. and De Wit, C.C., 2001. A dynamic tire/road friction model for 3D vehicle control and simulation. In*Intelligent Transportation Systems, 2001. Proceedings. 2001 IEEE* (pp. 483-488). IEEE.

[73] Hsiao, T., Liu, N.C. and Chen, S.Y., 2011, June. Robust estimation of the friction forces generated by each tire of a vehicle. In *American Control Conference (ACC), 2011* (pp. 5261-5266). IEEE.

[74] Rajamani, R., Phanomchoeng, G., Piyabongkarn, D. and Lew, J.Y., 2012. Algorithms for real-time estimation of individual wheel tire-road friction coefficients. *Mechatronics, IEEE/ASME Transactions on*, *17*(6), pp.1183-1195.

[75] Cho, W., Yoon, J., Yim, S., Koo, B. and Yi, K., 2010. Estimation of tire forces for application to vehicle stability control. *Vehicular Technology, IEEE Transactions on*, *59*(2), pp.638-649.

[76] Rabhi, A., M'Sirdi, N.K. and Elhajjaji, A., 2007, July. Estimation of contact forces and tire road friction. In *2007 Mediterranean Conference on Control&Automation*.

[77] M'sirdi, N.K., Rabhi, A., Ouladsine, M. and Fridman, L., 2006, June. First and high-order sliding mode observers to estimate the contact forces. In*International Workshop on Variable Structure Systems, 2006. VSS'06.*

[78] Hac, A., Brown, T. and Martens, J., 2004. *Detection of vehicle rollover* (No. 2004-01-1757). SAE Technical Paper.

[79] Tsourapas, V., Piyabongkarn, D., Williams, A. and Rajamani, R., 2009, June. New method of identifying real-time predictive lateral load transfer ratio for rollover prevention systems. In *American Control Conference, 2009. ACC'09.* (pp. 439-444). IEEE.

[80] Grip, H.F., Imsland, L., Johansen, T., Kalkkuhl, J.C. and Suissa, A., 2009, June. Estimation of road inclination and bank angle in automotive vehicles. In *American Control Conference, 2009. ACC'09.* (pp. 426-432). IEEE.

[81] Chen, S.K., Moshchuk, N., Nardi, F. and Ryu, J., 2010. Vehicle rollover avoidance. *Control Systems, IEEE*, *30*(4), pp.70-85.

[82] Ryu, J., Moshchuk, N.K. and Chen, S.K., 2007, July. Vehicle state estimation for roll control system. In *American Control Conference, 2007. ACC'07* (pp. 1618-1623). IEEE.

[83] Cho, K., Son, H., Choi, S.B. and Kang, S., 2010, September. Lateral acceleration compensation of a vehicle based on roll angle estimation. In*Control Applications (CCA), 2010 IEEE International Conference on* (pp. 1363-1368). IEEE.

[84] Wang, J., Alexander, L. and Rajamani, R., 2004. GPS based real-time tire-road friction coefficient identification.

[85] Hahn, J.O., Rajamani, R. and Alexander, L., 2002. GPS-based real-time identification of tire-road friction coefficient. *Control Systems Technology, IEEE Transactions on*, *10*(3), pp.331-343.

[86] Gustafsson, F., 1997. Slip-based tire-road friction estimation. *Automatica*,*33*(6), pp.1087-1099.

[87] Doumiati, M., Victorino, A., Charara, A. and Lechner, D., 2011, June. Estimation of road profile for vehicle dynamics motion: experimental validation. In *American Control Conference (ACC), 2011* (pp. 5237-5242). IEEE.

[88] Doumiati, M., Charara, A., Victorino, A. and Lechner, D., 2012. Road safety: embedded observers for estimation of vehicle's vertical tyre forces.*International Journal of Vehicle Autonomous Systems*, *10*(1-2), pp.117-143.

[89] Samadi, B., Kazemi, R., Nikravesh, K.Y. and Kabganian, M., 2001. Real-time estimation of vehicle state and tire-road friction forces. In *American Control Conference, 2001. Proceedings of the 2001* (Vol. 5, pp. 3318-3323). IEEE.

[90] Baffet, G., Charara, A., Lechner, D. and Thomas, D., 2008. Experimental evaluation of observers for tire–road forces, sideslip angle and wheel cornering stiffness. *Vehicle System Dynamics*, *46*(6), pp.501-520.

[91] Shim, T. and Margolis, D., 2004. Model-based road friction estimation.*Vehicle system dynamics*, *41*(4), pp.249-276.

[92] Shim, T. and Margolis, D., 2004. An analytical tyre model for vehicle simulation in normal driving conditions. *International journal of vehicle design*, *35*(3), pp.224-240.

[93] Doumiati, M., Victorino, A., Charara, A. and Lechner, D., 2009, June. Unscented Kalman filter for real-time vehicle lateral tire forces and sideslip angle estimation. In *Intelligent Vehicles Symposium, 2009 IEEE* (pp. 901-906). IEEE.

[94] Doumiati, M., Victorino, A., Charara, A. and Lechner, D., 2010, June. A method to estimate the lateral tire force and the sideslip angle of a vehicle: Experimental validation. In *American Control Conference (ACC), 2010* (pp. 6936-6942). IEEE.

[95] Doumiati, M., Victorino, A.C., Charara, A. and Lechner, D., 2011. Onboard real-time estimation of vehicle lateral tire–road forces and sideslip angle.*Mechatronics, IEEE/ASME Transactions on*, *16*(4), pp.601-614.

[96] Doumiati, M., Victorino, A., Charara, A. and Lechner, D., 2009, August. Estimation of vehicle lateral tire-road forces: a comparison between extended and unscented Kalman filtering. In *Control Conference (ECC), 2009 European* (pp. 4804-4809). IEEE.

[97] Doumiati, M., Victorino, A., Lechner, D., Baffet, G. and Charara, A., 2010. Observers for vehicle tyre/road forces estimation: experimental validation.*Vehicle System Dynamics*, *48*(11), pp.1345-1378.

[98] Ghandour, R., Victorino, A., Doumiati, M. and Charara, A., 2010, June. Tire/road friction coefficient estimation applied to road safety. In *Control & Automation (MED), 2010 18th Mediterranean Conference on* (pp. 1485-1490). IEEE.

[99] Ghandour, R., Victorino, A., Charara, A. and Lechner, D., 2011, August. A vehicle skid indicator based on maximum friction estimation. In *Proceedings of the 18th IFAC World Congress* (Vol. 18, pp. 2272-2277).

[100] Ghandour, R., da Cunha, F.H., Victorino, A., Charara, A. and Lechner, D., 2011, June. Risk indicators prediction based on the estimation of tire/road forces and the maximum friction coefficient: Experimental validation. In*Control & Automation (MED), 2011 19th Mediterranean Conference on* (pp. 700-705). IEEE.

[101] Dakhlallah, J., Glaser, S., Mammar, S. and Sebsadji, Y., 2008, June. Tire-road forces estimation using extended Kalman filter and sideslip angle evaluation. In *American Control Conference, 2008* (pp. 4597-4602). IEEE.

[102] Sebsadji, Y., Glaser, S., Mammar, S. and Dakhlallah, J., 2008, June. Road slope and vehicle dynamics estimation. In *American Control Conference, 2008* (pp. 4603-4608). IEEE.

[103] Cheng, Q., Correa-Victorino, A. and Charara, A., 2011, June. A new nonlinear observer using unscented Kalman filter to estimate sideslip angle, lateral tire road forces and tire road friction coefficient. In *Intelligent Vehicles Symposium (IV), 2011 IEEE* (pp. 709-714). IEEE.

[104] Ray, L.R., 1997. Nonlinear tire force estimation and road friction identification: simulation and experiments. *Automatica*, *33*(10), pp.1819-1833.

[105] Ray, L.R., 1998, June. Experimental determination of tire forces and road friction. In *American Control Conference, 1998. Proceedings of the 1998*(Vol. 3, pp. 1843-1847). IEEE.

[106] Jin, X. and Yin, G., 2015. Estimation of lateral tire–road forces and sideslip angle for electric vehicles using interacting multiple model filter approach.*Journal of the Franklin Institute*, *352*(2), pp.686-707.

[107] Rajamani, R., Piyabongkarn, D., Lew, J.Y., Yi, K. and Phanomchoeng, G., 2010. Tire-road friction-coefficient estimation. *Control Systems, IEEE*, *30*(4), pp.54-69.

[108] Baffet, G., Charara, A. and Lechner, D., 2008. *Estimation of tire-road forces and vehicle sideslip angle*. INTECH Open Access Publisher.

[109] Baffet, G., Charara, A. and Lechner, D., 2009. Estimation of vehicle sideslip, tire force and wheel cornering stiffness. *Control Engineering Practice*, *17*(11), pp.1255-1264.

[110] Zhang, W., Ding, N., Yu, G. and Zhou, W., 2009, August. Virtual sensors design in vehicle sideslip angle and velocity of the centre of gravity estimation. In *Electronic Measurement & Instruments, 2009. ICEMI'09. 9th International Conference on* (pp. 3-652). IEEE.

[111] Baffet, G., Charara, A. and Dherbomez, G., 2007. An observer of tire–road forces and friction for active security vehicle systems. *Mechatronics, IEEE/ASME Transactions on*, *12*(6), pp.651-661.

[112] Ahn, C.S., 2011. Robust estimation of road friction coefficient for vehicle active safety systems [Ph. D. thesis]. *Ann Arbor, MI: The University of Michigan*.

[113] Zhang, H., Huang, X., Wang, J. and Karimi, H.R., 2014. Robust energy-to-peak sideslip angle estimation with applications to ground vehicles.*Mechatronics*.

[114] Zhu, T. and Zheng, H., 2008, August. Application of unscented Kalman filter to vehicle state estimation. In *Computing, Communication, Control, and Management, 2008. CCCM'08. ISECS International Colloquium on* (Vol. 2, pp. 135-139). IEEE.

[115] Pan, Z., Zong, C., Zhang, J., Xie, X. and Dong, Y., 2009, August. UKF and EKF estimator design based on a nonlinear vehicle model containing UniTire model. In *Mechatronics and Automation, 2009. ICMA 2009. International Conference on* (pp. 4780-4784). IEEE.

[116] Chu, L., Shi, Y., Zhang, Y., Liu, H. and Xu, M., 2010, August. Vehicle lateral and longitudinal velocity estimation based on Adaptive Kalman Filter. In*Advanced Computer Theory and Engineering (ICACTE), 2010 3rd International Conference on* (Vol. 3, pp. V3-325). IEEE.

[117] Chu, L., Zhang, Y. and Shi, Y., 2010. Vehicle Lateral and Longitudinal Velocity Estimation Based on Unscented Kalman Filter [C]. In *2nd International Conference on Education Technology and Computer* (Vol. 427).

[118] Hsu, Y.H.J., Laws, S.M. and Gerdes, J.C., 2010. Estimation of tire slip angle and friction limits using steering torque. *Control Systems Technology, IEEE Transactions on*, *18*(4), pp.896-907.

[119] Ray, L.R., 1995. Nonlinear state and tire force estimation for advanced vehicle control. *Control Systems Technology, IEEE Transactions on*, *3*(1), pp.117-124.

[120] Gao, X., Yu, Z., Neubeck, J. and Wiedemann, J., 2010. Sideslip angle estimation based on input–output linearisation with tire–road friction adaptation. *Vehicle System Dynamics*, *48*(2), pp.217-234.

[121] Pacejka, H.B. and Bakker, E., 1992. The magic formula tyre model. *Vehicle system dynamics*, *21*(S1), pp.1-18.

[122] Pacejka, H.B. and Besselink, I.J.M., 1997. Magic formula tyre model with transient properties. *Vehicle system dynamics*, *27*(S1), pp.234-249.

[123] Bakke, E., Nyborg, L. and Pcejka, H.B., 1987. *Tyre modeling for Use in Vehicle Dynamic Studies*. Technical Report 870421, Society of Automotive Engineers, Warrendale PA.

[124] Pacejka, H.B. and Sharp, R.S., 1991. Shear force development by pneumatic tyres in steady state conditions: a review of modelling aspects.*Vehicle system dynamics*, *20*(3-4), pp.121-175.

[125] van Oosten, J.J. and Bakker, E., 1992. Determination of magic tyre model parameters. *Vehicle System Dynamics*, *21*(S1), pp.19-29.

[126] Kim, C.S., Hong, K.S., Yoo, W.S. and Park, Y.W., 2007, October. Tire-road friction estimation for enhancing the autonomy of wheel-driven vehicles. In*Control, Automation and Systems, 2007. ICCAS'07. International Conference on* (pp. 273-277). IEEE.

[127] Yi, K., Hedrick, K. and Lee, S.C., 1999. Estimation of tire-road friction using observer based identifiers. *Vehicle System Dynamics*, *31*(4), pp.233-261.

[128] Jayachandran, R., Ashok, S.D. and Narayanan, S., 2013. Fuzzy Logic based Modelling and Simulation Approach for the estimation of Tire Forces.*Procedia Engineering*, *64*, pp.1109-1118.

[129] Svendenius, J., 2007. *Tire modeling and friction estimation* (Doctoral dissertation, Lund University).

[130] Ghandour, R., Victorino, A., Doumiati, M. and Charara, A., 2010, June. Tire/road friction coefficient estimation applied to road safety. In *Control & Automation (MED), 2010 18th Mediterranean Conference on* (pp. 1485-1490). IEEE.

[131] Villagra, J., D'Andréa-Novel, B., Fliess, M. and Mounier, H., 2011. A diagnosis-based approach for tire–road forces and maximum friction estimation. *Control engineering practice*, *19*(2), pp.174-184.

[132] Patra, N. and Datta, K., 2012. Observer Based Road-Tire Friction Estimation for Slip Control of Braking System. *Procedia Engineering*, *38*, pp.1566-1574.

[133] Doumiati, M., Victorino, A.C., Charara, A. and Lechner, D., 2011. Onboard real-time estimation of vehicle lateral tire–road forces and sideslip angle.*Mechatronics, IEEE/ASME Transactions on*, *16*(4), pp.601-614.

[134] Svendenius, J., Gäfvert, M., Bruzelius, F. and Hultén, J., 2009. Experimental Validation of the Brush Tire Model 5. *Tire Science and Technology*, *37*(2), pp.122-137.

[135] Pacejka, H., 2005. *Tire and vehicle dynamics*. Elsevier.

[136] Erdogan, G., 2009, Tire Modeling lecture, Lateral and longitudinal tire forces

[137] Chen, Y. and Wang, J., 2011. Adaptive vehicle speed control with input injections for longitudinal motion independent road frictional condition estimation. *Vehicular Technology, IEEE Transactions on*, *60*(3), pp.839-848.

[138] Svendenius, J., 2007. *Tire modeling and friction estimation* (Doctoral dissertation, Lund University).

[139] Andersson, M., Bruzelius, F., Casselgren, J., Hjort, M., Löfving, S., Olsson, G. and Yngve, S., 2010. Road friction estimation, Part II–IVSS project report.

[140] Nishihara, O. and Masahiko, K., 2011. Estimation of road friction coefficient based on the brush model. *Journal of Dynamic Systems, Measurement, and Control*, *133*(4), p.041006.

[141] Matilainen, M.J. and Tuononen, A.J., 2011, June. Tire friction potential estimation from measured tie rod forces. In *Intelligent Vehicles Symposium (IV), 2011 IEEE* (pp. 320-325). IEEE.

[142] Yamazaki, S., Furukawa, O. and Suzuki, T., 1997. Study on real time estimation of tire to road friction. *Vehicle System Dynamics*, *27*(S1), pp.225-233.

[143] De Wit, C.C., Olsson, H., Astrom, K.J. and Lischinsky, P., 1995. A new model for control of systems with friction. *Automatic Control, IEEE Transactions on*, *40*(3), pp.419-425.

[144] ENSIEG-INPG, B.P. and ST Martin d'lieres, F.R.A.N.C.E., 1999. Dynamic tire friction models for vehicle traction control.

[145] Canudas-de-Wit, C., Petersen, M.L. and Shiriaev, A., 2003, December. A new nonlinear observer for tire/road distributed contact friction. In *Decision and Control, 2003. Proceedings. 42nd IEEE Conference on* (Vol. 3, pp. 2246-2251). IEEE.

[146] Alvarez, L., Yi, J., Horowitz, R. and Olmos, L., 2005. Dynamic friction model-based tire-road friction estimation and emergency braking control.*Journal of dynamic systems, measurement, and control*, *127*(1), pp.22-32.

[147] Matuško, J., Petrović, I. and Perić, N., 2008. Neural network based tire/road friction force estimation. *Engineering Applications of Artificial Intelligence*,*21*(3), pp.442-456.

[148] Breuer, B., Eichhorn, U. and Roth, J., 1992, September. Measurement of tyre/road-friction ahead of the car and inside the tyre. In *International Symposium on Advanced Vehicle Control, 1992, Yokohama, Japan*.

[149] Dieckmann, T., 1992. Assessment of road grip by way of measured wheel variables. In *XXIV FISITA CONGRESS, 7-11 JUNE 1992, LONDON. HELD AT THE AUTOMOTIVE TECHNOLOGY SERVICING SOCIETY. TECHNICAL PAPERS. SAFETY, THE VEHICLE AND THE ROAD. VOLUME 2 (IMECHE NO C389/349 AND FISITA NO 925227)*.

[150] Gustafsson, F., 1997. Slip-based tire-road friction estimation. *Automatica*,*33*(6), pp.1087-1099.

[151] Hwang, W. and Song, B.S., 2000. Road condition monitoring system using tire-road friction estimation. *Proceedings of AVEC 2000, Ann Arbor, Michigan*, pp.437-442.

[152] Yi, K., Hedrick, K. and Lee, S.C., 1999. Estimation of tire-road friction using observer based identifiers. *Vehicle System Dynamics*, *31*(4), pp.233-261.

[153] Fischlein, H., Gnadler, R. and Unrau, H.J., 2001. The influence of the track surface structure on the frictional force behaviour of passenger car tyres in dry and wet track surface conditions. *ATZ worldwide*, *103*(10), pp.20-24.

[154] Germann, S. and Daiß, A., 1994, August. Monitoring of the friction coefficient between tyre and road surface. In *Control Applications, 1994., Proceedings of the Third IEEE Conference on* (pp. 613-618). IEEE.

[155] Muller, S., Uchanski, M. and Hedrick, K., 2003. Estimation of the maximum tire-road friction coefficient. *Journal of dynamic systems, measurement, and control*, *125*(4), pp.607-617.

[156] Wang, J., Alexander, L. and Rajamani, R., 2004. Friction estimation on highway vehicles using longitudinal measurements. *Journal of dynamic systems, measurement, and control*, *126*(2), pp.265-275.

[157] Lee, C., Hedrick, K. and Yi, K., 2004. Real-time slip-based estimation of maximum tire-road friction coefficient. *Mechatronics, Ieee/Asme Transactions On*, *9*(2), pp.454-458.

[158] Shayang Ye Industrial Co. Ltd. IG52GM 01&02 Type, 2011

[159] Shayang Ye Industrial Co. Ltd. Magnetic Encoders, 2010.

[160] Northern Tool and Equipment. Knobby Tire on Wheel, 2013, URL http://www.northerntool.com/shop/tools/product_18845_18845

[161] Moog Components Group. Slip Rings With Through-Bores, 2012. URL http://www.moog.com/products/slip-rings/commercial-industrial-slip-rings/slip-rings-with-through-bores/sra-73683/.

[162] Singh, Kanwar B., Mustafa Ali Arat, and Saied Taheri. "An Intelligent Tire Based Tire-Road Friction Estimation Technique and Adaptive Wheel Slip Controller for Antilock Brake System." Journal of Dynamic Systems, Measurement, and Control 135 (2013): 031002-1.

[163] Singh, Kanwar Bharat, Mustafa Ali Arat, and Saied Taheri. "Enhancement of Collision Mitigation Braking System Performance Through Real-Time Estimation of Tire-road Friction Coefficient by Means of Smart Tires." SAE International Journal of Passenger Cars-Electronic and Electrical Systems 5.2 (2012): 607-624.

[164] Dytran, 3023A5 Tri-axial accelerometer, URL http://www.dytran.com/Model-3023A-Triaxial-Accelerometer-P1361.aspx

[165] Encoder Product Company, Model 15s incremental shaft encoder, URL http://www.encoder.com/literature/datasheet-15s.pdf

[166] Kistler forcehub, type 9295A, URL

https://kistler-embedded.partcommunity.com/3d-cad-models/FileService/File/kistler/02_force/05_special_sensors_and_dynamometer/04_wheel_force_measurement/9295_english.pdf/

[167] Encoder Product Company, Model 755A incremental shaft encoder, URL

http://encoder.com/core/files/encoder/products/72b19e6bf8ad1b1ea2b906dadb104dba.pdf

[168] Emerson process management company, model TESCOM ER3000 Electopneumatic controller, URL

http://www.documentation.emersonprocess.com/groups/public/documents/data_sheets/der301767x012.pdf

[169] DATRON sensor system, measuring steering wheel system (MSW/S), URL:

http://www.measure.com.au/tiny_mce_gallery/files/measurement_steering_wheel_brochure.pdf

[170] Michigan Scientific Corporation, SR10AW/PE512 slip ring, URL:

http://www.michsci.com/Products/sliprings/eos/sr10a_pe512_specs.htm

[171] Texnese sensors by TEXYS, IB6-XY3-Z5-GX100-GY100-GZ100 accelerometer inertial measurement unit, URL:

http://www.texense.com/en/produits/controls_3/ib-6-imu-6-axis-imu-inertial-box-6-axis-measurement_145.html?PHPSESSID=jao693ocrhojasa05r2fo97jo2

[172] Ojeda, L., Borenstein, J., Wits, G., Karlsen, R., Terrain characterization and classification with a mobile robot, journal of field robotics 23(2), 103-122 (2006)

[173] Parka, B., Kimb, J., Lee, J., Terrain Feature Extraction and Classification for Mobile Robots Utilizing Contact Sensors on Rough Terrain, International Symposium on Robotics and Intelligent Sensors 2012 (IRIS 2012)

[174] Brooks, C., Iagnemma, K., and Dubowsky, S., Vibration-based Terrain Analysis for Mobile Robots, Proceedings of the 2005 IEEE, International Conference on Robotics and Automation Barcelona, Spain, April 2005

[175] Christopher Brooks, Karl Iagnemma, and Steven Dubowsky, "Vibration-based Terrain Analysis for Mobile Robots" IEEE International Conference on Robotics and Automation, April, 2005

[176] Weiss, C., Frohlich, H., Zell, A., Vibration-based Terrain Classification Using Support Vector Machines, Proceedings of the 2006 IEEE/RSJ, International Conference on Intelligent Robots and Systems, October 9 - 15, 2006, Beijing, China

[177] Christian Weiss, Holger Frojlich and Andeas Zell, "Vibration-based Terrain Classification Using Support Vector Machines" IEEE/RSJ International Conference on Intelligent Robots and Systems, October, 2006

[178] Christian Weiss, Nikolas Fechner, Matthias Stark, Andreas Zell, "Comparison of Different Approaches to Vibration-based Terrain Classification" Conference on Mobile Robots, September, 2007

[179] E.M. DuPont, R.G. Roberts, C.A. Moore, M.F. Selekwa, E.G. Collins, Online terrain classification for mobile robots, in: Proceedings of IMECE 2005 ASME 2005 International Mechanical Engineering Congress and Exposition Conference, Orlando, FL, November 2005.

[180] E.M. Dupont, C.A. Moore, J.E.G. Collins, E. Coyle, Frequency response method for terrain classification in autonomous ground vehicles, Autonomous Robots 24 (4) (2008) 337–347.

[181] E.M. DuPont, E.G. Collins, E.J. Coyle, R.G. Roberts, New Research on Mobile Robotics. Nova Science Publishers, Terrain Classification using Vibration Sensors: Theory and Methods, 2008, Chapter 3.

[182] E.G. Collins Jr., E. Coyle, Vibration-based terrain classification using surface profile input frequency responses, in: IEEE International Conference on Robotics and Automation, May 2008, pp. 3276–3283.

[183] R. Manduchi, A. Castano, A. Talukder, and L. Matthies, "Obstacle detection and terrain classification for autonomous off-road navigation," *Robotics And Automation*, vol. 18, pp. 81 – 102, 2005.

[184] P. Bellutta, L. Manduchi, K. Matthies, K. Owens, and A. Rankin, "Terrain perception for demo III," in *Proc. IEEE Intelligent Vehicles Symposium*, Dearborn, MI, 2000, pp. 326 – 332.

[185] R. Castano, R. Manduchi, and J. Fox, "Classification experiments on real-world textures," in *Workshop on Empirical Evaluation in Computer Vision*, Kauai, HI, 2001.

[186] Talukder, A., Manduchi, R., Castano, R., Owens, K., Matthies, L., Castano, A., & Hogg, R. Autonomous terrain characterization and modelling for dynamic control of unmanned vehicles _2002, September_. IEEE Conference on Intelligent Robots and Systems _IROS_, Lausanne, Switzerland.

[187] Larson, A., Voyles, R., & Demir, G. _2004, April–May_. Terrain classification through weakly structured vehicle/ terrain interaction. IEEE International Conference on Robotics and Automation, New Orleans, LA, Vol. 1, pp. 218–224.

[188] Vandapel, N., Huber, D., Kapuria, A., & Hebert, M. _2004, April–May_. Natural terrain classification using 3D Ladar data. IEEE International Conference on Robotics and Automation, New Orleans, LA, pp. 5117–5122.

[189] Seung-Youn Lee, Dong-Min Kwak, "A Terrain Classification Method for UGV Autonomous Navigation Based on SURF" International Conference on Ubiquitous Robots and Ambient Intelligence (URAI), November, 2011

[190] Lua, L., Ordonezb, C., Collins Jr., E., Coyle, E., , Palejiya, D., Terrain surface classification with a control mode update rule using a 2D laser stripe-based structured light sensor, Robotics and Autonomous Systems 59 (2011) 954–965

[191] L. Ojeda, J. Borenstein, G. Witus, R. Karlesen, Terrain characterization and classification with a mobile robot, Journal of Field Robotics 23 (2) (2006) 103–122.

[192] Lauro Ojeda, Johann Borenstein, Gary Witus, Robert Karlsen, “Terrain Characterization and Classification with a Mobile Robot” Jounal of Field Robotics, 2006

[193] Bekker, G. _1956_. Theory of land locomotion. Ann Arbor, MI: University of Michigan Press.

[194] Bekker, G. _1960_. Off the road locomotion. Ann Arbor, MI: University of Michigan Press.

[195] Bekker, G. _1969_. Introduction to terrain-vehicle systems. Ann Arbor, MI: University of Michigan Press.

[196] Howard, A., Seraji, H., Vision-Based Terrain Characterization and Traversability Assessment, Journal of Robotic System, 18(10), 557-587 (2001)

[197] Cuong, D., Zhu, C. , Thi, N., Study on the variation characteristics of vertical equivalent damping ratio of tire–soil system using semi-empirical model, Journal of Terramechanics 51 (2014) 67–80

[198] Pinnington, R., A particle-envelope surface model for road–tire interaction, international journal of solid and structures, 49 (2012) 546-555

[199] Zadeh LA. Fuzzy sets as a basis for a theory of possibility. Fuzzy sets and systems. 1978 Jan 31;1(1):3-28.

[200] Hájek P. Metamathematics of fuzzy logic. Springer Science & Business Media; 1998 Aug 31.

[201] - Yilmazoglu, O., et al. "Integrated InAs/GaSb 3D magnetic field sensors for “the intelligent tire”." *Sensors and Actuators A: Physical* 94.1 (2001): 59-63.

[202] - Zhang, Xiangwen, et al. "Intelligent tires based on wireless passive surface acoustic wave sensors." *Intelligent Transportation Systems, 2004. Proceedings. The 7th International IEEE Conference on*. IEEE, 2004.

[203] - Pohl, Alfred, Reinhard Steindl, and Leonhard Reindl. "The “intelligent tire” utilizing passive SAW sensors measurement of tire friction." *Instrumentation and Measurement, IEEE Transactions on* 48.6 (1999): 1041-1046.

[204] - KB Singh, MA Arat, S Taheri, “Development of a Smart Tire System and its Use in Improving the Performance of a Collision Mitigation Braking System”, ASME International Mechanical Engineering Congress and Exposition, 2012 ,77-87

[205] - MA Arat, KB Singh, S Taheri ,“An intelligent tire based adaptive vehicle stability controller”, MA Arat, KB Singh, S Taheri, International Journal of Vehicle Design 65 (2-3), 2014, 118-143

[206] - Ray, Laura R. "Nonlinear tire force estimation and road friction identification: simulation and experiments." *Automatica* 33.10 (1997): 1819-1833.

[207] - Li, Li, Fei-Yue Wang, and Qunzhi Zhou. "Integrated longitudinal and lateral tire/road friction modeling and monitoring for vehicle motion control." *Intelligent Transportation Systems, IEEE Transactions on* 7.1 (2006): 1-19.

[208] Behroozinia, P., Khaleghian, S., Taheri, Mirzaeifard, R., "An Investigation of Intelligent Tires Using Finite Element Analysis", submitted to the International Journal of Pavement Engineering, In Press.

[209] Duda, Richard O., Peter E. Hart, and David G. Stork. *Pattern classification*. John Wiley & Sons, 2012.

[210] Omid Ghasemalizadeh, Seyedmeysam Khaleghian and Saied Taheri. (2016); A REVIEW OF OPTIMIZATION TECHNIQUES IN ARTIFICIAL NETWORKS. Int. J. of Adv. Res. 4(9). 1668-1686] (ISSN 2320-5407).

[211] C. Wanki, J. Yoon, S. Yim, B. Koo, K. Yi, Estimation of Force for Application to Vehicle Stability Control, IEEE Transaction on Vehicular Technology, Vol 59, No. 2 , 2010

[212] – Doumiati, Moustapha, Ali Charara, Alessandro Victorino, and Daniel Lechner.*Vehicle Dynamics Estimation Using Kalman Filtering: Experimental Validation*. John Wiley & Sons, 2012

[213] Rajamani,R., Piyabongkarn,D., Lew,J.Y., & Grogg,J.A. (2006). Algorithms for real- time estimation of individual wheel tire-road friction coefficients. In Proceedings of the 2006 American control conference (pp.4682–4689).

[214] Khaleghian, S., Emami, A., Taheri, S., A Technical Survey on Tire-Road Friction, Friction, 2017

[215] Khaleghian, S., Taheri, S., Terrain Classification Using Intelligent Tire, Journal of Terramechanics, Vol 71, (pp.14-24) 2017

[216] Duda, Richard O., Peter E. Hart, and David G. Stork. *Pattern classification*. John Wiley & Sons, 2012.